Progressive Damage and Failure Analysis of Composite Laminates

Ashith P. K. Joseph

A dissertation
submitted in partial fulfillment of the
requirements for the degree of

Doctor of Philosophy

University of Washington

2017

Reading Committee:

Anthony M. Waas, Chair

Marco Salviato

Jinkyu Yang

Program Authorized to Offer Degree:
Aeronautics & Astronautics

University of Washington

Abstract

Progressive Damage and Failure Analysis of Composite Laminates

Ashith P. K. Joseph

Chair of the Supervisory Committee:
Boeing-Egtvedt Chair Anthony M. Waas
William E Boeing Department of Aeronautics and Astronautics

Composite materials are widely used in various industries for making structural parts due to higher strength to weight ratio, better fatigue life, corrosion resistance and material property tailorability. To fully exploit the capability of composites, it is required to know the load carrying capacity of the parts made of them. Unlike metals, composites are orthotropic in nature and fails in a complex manner under various loading conditions which makes it a hard problem to analyze. Lack of reliable and efficient failure analysis tools for composites have led industries to rely more on coupon and component level testing to estimate the design space. Due to the complex failure mechanisms, composite materials require a very large number of coupon level tests to fully characterize the behavior. This makes the entire testing process very time consuming and costly. The alternative is to use virtual testing tools which can predict the complex failure mechanisms accurately. This reduces the cost only to its associated computational expenses making significant savings. Some of the most desired features in a virtual testing tool are (1) Accurate representation of failure mechanism: Failure progression predicted by the virtual tool must be same as those observed in experiments. A tool has to be assessed based on the mechanisms it can capture. (2) Computational efficiency: The greatest advantages of a virtual tools are the savings in time and money and hence computational efficiency is one of the most needed features. (3) Applicability to a wide range of problems: Structural parts are subjected to a variety of loading conditions including

static, dynamic and fatigue conditions. A good virtual testing tool should be able to make good predictions for all these different loading conditions. The aim of this PhD thesis is to develop a computational tool which can model the progressive failure of composite laminates under different quasi-static loading conditions. The analysis tool is validated by comparing the simulations against experiments for a selected number of quasi-static loading cases.

TABLE OF CONTENTS

LIST OF FIGURES

LIST OF TABLES

GLOSSARY

:

ACKNOWLEDGMENTS

I would like to express my gratitude to Prof. Anthony Waas for the valuable guidance provided throughout the course of my PhD program. His passion and enthusiasm towards the subject has always been a great motivation. The opportunity he provided allowed me to work on various challenging problems which are of relevance to the industry. The lessons I learned from him is going to help immensely in the rest of my professional carrier and life.

I would like to thank the Boeing company for providing financial support for the work described in the appendices of this thesis and giving me opportunity to work on challenging projects. Technical discussions with Salvatore Liguore, Mostafa Rassaian, Joe Schaefer and Brian Justusson are gratefully acknowledged.

I would like to thank Jonathan Bartely-Cho of Northrop Grumman Corporation and Padmasiri Vipul Ranatunga of Air Force Research Laboratory for giving the opportunity to be a part of the project which forms the basis of this thesis. Technical feedbacks and suggestions I received from Jonathan Bartley-Cho have helped in shaping the work presented here.

I enjoyed the technical discussions with my colleagues at the composite structures laboratory and it helped me in understanding the subject better. I am thankful to Paul Davidson, Wooseok Ji, Nhung Nguyen, Dianyun Zhang, Wu Xu, Royan D'Mello, Jiawen Xie and all the other lab-mates for their valuable help and guidance.

I would like to thank the William E. Boeing Aeronautics and Astronautics department at University of Washington and Aerospace Engineering department at University of Michigan for all the facilities provided. Special thanks to Ed Connery for facilitating my transfer from University of Michigan to University of Washington. Help from Dzung Tran (A&A machine

shop) in getting the test fixtures and specimens ready in time is also greatly appreciated.

I also thank my family and close friends for their constant encouragement and support.

DEDICATION

To my family

Chapter 1

INTRODUCTION

Computational modeling of composite laminates for assessing stiffness and strength is a subject of contemporary interest to airframe manufacturers, such as the Boeing company. Progressive damage and failure analysis of composite laminates is complex and developing a robust computational model is the subject of this dissertation.

The finite element (FE) method and computational studies using FE are mainstays in structural analysis and design. Virtual testing is a subject where the requirements of carrying out several laboratory tests can be partially replaced through validated computational models so that the number of laboratory tests and hence costs associated with the tests, can be reduced without sacrificing accuracy.

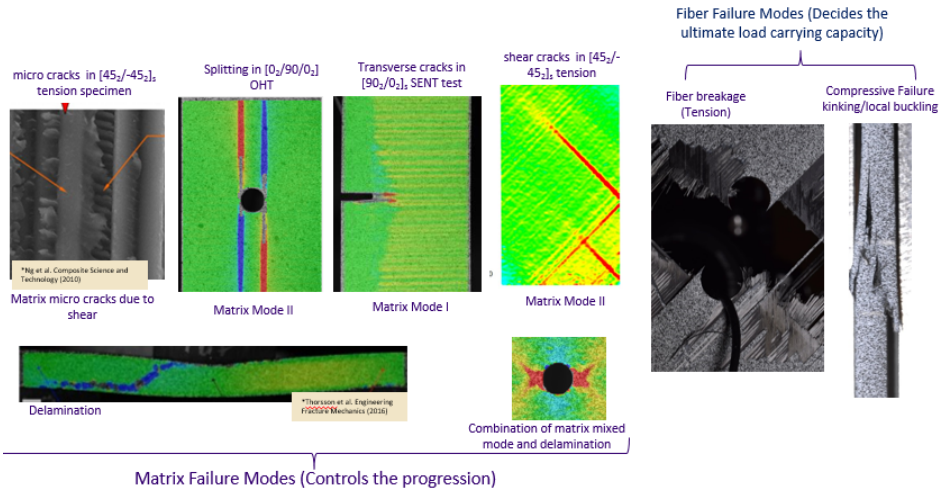

Figure 1.1: Damage and failure events observed in experiments

The first step to fulfilling the goal of developing a virtual testing tool is understanding

various important failure modes observed in the composite laminate experiments. Figure 1.1 presents some of these mechanisms including damage and failure events. Intralaminar and interlaminar matrix macrocracks can occur under pure mode I (referred to as transverse cracks), pure mode II (referred to as splitting) or mixed mode conditions. Since the matrix is a continuous medium from the plies to the ply interfaces, intralaminar and interlaminar failure modes do interact with each other. Explicit modeling of fibers and matrix, known as the microscale model, can automatically capture this mechanism correctly but the homogenized macroscopic approaches will be limited in capturing the interactions correctly. Damage/Failure events alter the stress fields around the damaged/failed region and cause subsequent failure events to occur in a progressive manner. For most of the laminates with 0 plies, various matrix damage and failure mechanisms discussed above control the progression of failure. But the ultimate load carrying capacity is usually determined by the strength of the fibers under tension and compression. Under tension the fibers eventually break and this failure of the main load carrying member causes additional intralaminar and interlaminar matrix failure leading to a two piece failure. Under compression fiber failure occurs due to kink band formation or local buckling mechanism. Fiber compressive failure is highly influenced by initial fiber misalignment and the non-linear response of the matrix material.

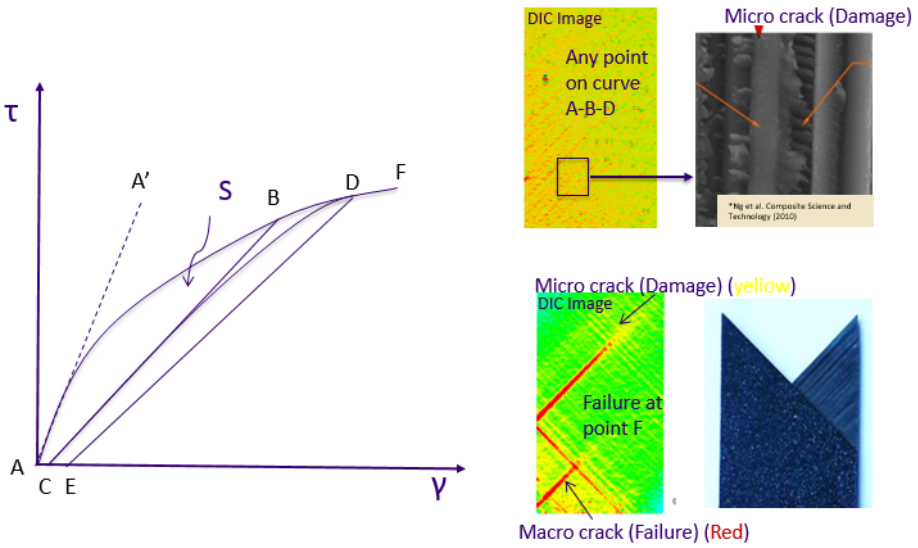

Figure 1.2: Damage and failure definitions with $[+45/-45]_s$ tension test

For the clarity of further discussions in this work, it is required to define the difference between damage and failure. Figure 1.2 shows the typical behavior of a $[+45/-45]_s$ coupon under tensile loading. The lamina shear response for the coupon undergoing cycle loading is shown with the curve A-B-C-D-E-F in the figure. Initial stiffness of the coupon is represented with the line A-A. Unloading of the coupon at point B causes the coupon to reach point C corresponding to the zero stress state. At point C there is a small amount of plastic strain present which can be ignored for practical purposes. Further loading to point D has a lower initial stiffness compared to A-B. Similar behavior continues for the further loading cycles until it reaches point F when the coupon loses its load carrying capacity. At any point on the curve A-B-D, non-linearity in the shear stress-strain response is caused by the development of microcracks as shown in the figure. These cracks are visible only under a microscope and primarily occur due to the local shear state in the matrix material. These micro cracks form at an angle to the fiber direction and reduce the effective stiffness in the transverse and shear responses of the lamina. Energy dissipated due to the microcrack formation is shown as S in the figure formed by the curve A-B-C. Formation of microcrack is defined as damage and

it causes pre-peak non-linear behavior in the stress-strain response. At point F macrocracks visible to bare eyes form and they cause a post peak softening behavior or a catastrophic stress drop in some cases. These macrocracks are formed as a result of the coalescence of the microcracks and releases energy corresponding to the formation of new surfaces in the material. Macrocrack formation resulting in the creation of new surfaces and a post peak softening behavior is defined as failure. Macrocracks can also form directly without the gradual microcrack development under certain loading conditions including pure tension in transverse direction.

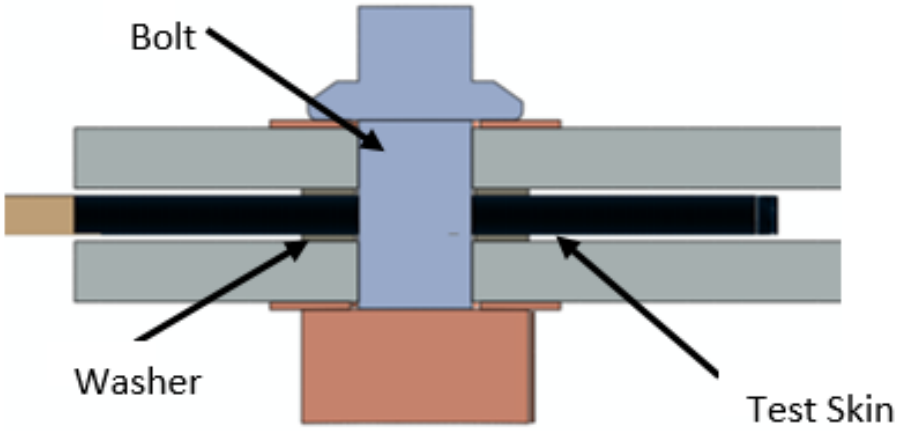

Figure 1.3: Double shear bolted joint configuration

While shell element based formulation is widely used for the failure analysis of materials, the limitations of a 2D formulation are clearly visible in problems such as composite bolted joints. Figure 1.3 shows the sectional view of a double shear bolted joint. A pretension load is applied to the bolt in all the applications and experimental studies have shown that the pretension value can affect the peak load and failure mechanisms significantly [10]. A 2D representation of composite laminates cannot capture any of these effects. 3D model can capture ply scaling/stacking effects and the influence of adjacent plies on the failure. Since

applicability to a wide range of problems is of interest in this study, 3D failure model is considered.

Micromechanics models and multiscale approaches makes the failure analysis computationally expensive and hence not considered here as computational efficiency is a requirement. At the macroscale level damage is usually modeled using curve fitting functions, as a function of the strain or the energy dissipated to microcrack formation. An example for the former is the commonly used Ramberg-Osgood fit [27]. The limitation associated with this approach is that it the curves are calibrated for a pure shear response case and hence does not take the effect of multi axial loading into account. Schapery theory [29, 31] is a homogenized damage modeling approach which represents the non-linear response as a function of the total energy dissipated due to the formation of microcracks and hence can account for complex loading cases in a thermodynamically accurate way. Homogenized approaches for failure or macrocrack modeling in a finite element frame work can be broadly categorized into continuum approaches and discrete crack approaches. Continuum crack approaches such as crack band [4] models crack of finite width corresponding to the element size. Energy dissipated during the crack formation is effectively smeared over the entire element in this case, making it a computationally efficient and reliable method. Discrete crack can be further subdivided into nodal/shape functions enrichment methods and interface methods. XFEM [21] and VMCM [28] are examples for the nodal/shape function enrichment methods and the computational cost associated with these methods are usually very high. Interface methods are used for cases in which crack path is known in advance. Hence this is particularly suitable for delamination modeling and for modeling intralaminar failure when the crack path is known. Inserting interface elements at every possible interface can make it computationally expensive.

Based on the existing models, Schapery Theory and crack band methods are chosen in this study for the progressive damage and failure analysis of composite laminates because of its computational efficiency, successful applications demonstrated in the literature [26, 11, 17] and simplicity in theory and implementation. The model developed in this work is collectively

called intra-inter crack band model (I2CBM).

The thesis is organized as follows; In chapter 1, a general introduction regarding mechanisms of observed damage and failure progression in composite laminates are described. In chapter 2, all the relevant details of the I2CBM formulation and implementation are discussed. Chapter 3 compares the open hole and filled hole simulation results with the experimental data. Sensitivity of the filled hole simulation results withe bolt pretension are also discussed in the same chapter. Chapter 4 demonstrates the applicability of the model to different bolted joint configurations and compared with experiments. Original contributions from this thesis work and plans for the future research are listed in chapter 5. Appendix A of this thesis contains the open hole tension and compression simulations results obtained using the 2D progressive damage and failure analysis code known as Enhanced Schapery Theory (EST) [26]. Open hole bending bending simulations with EST are presented in Appendix B. I2CBM was developed to overcome the limitations of this 2D model as described earlier in this chapter.

Chapter 2

INTRA-INTER CRACK BAND MODEL (I2CBM)

The Intra-Inter Crack Band Model is based on combining a pre-failure continuum model that includes micro-damage, with a post-peak non continuum model that captures macro-cracks. Pre-peak lamina response, which dictates the overall composite material response is non-linear owing to formation of micro cracks in the matrix [23] (mostly due to shear, figure 2.1), which is captured in I2CBM using *Schapery Theory* of micro damage [29]. Post-peak behavior of macroscopic fracture evolution is incorporated using a modified *Crack Band Model*. When an appropriate transition criterion is met (from pre-peak damage to post-peak failure), post peak softening region begins and the area enclosed by the post peak response is the fracture toughness scaled by the element characteristic length[4, 26]. Typical response of a stress-strain work conjugate pair implemented in I2CBM is shown in figure 2.2.

In addition to the above feature, additional important characteristics of the I2CBM model are as follows;

1. A coupled failure mechanism which links in-plane (intra-ply) failure to inter-ply failure is used. This is based on the experimental observation that shows during in-plane loading of laminates, delamination due to failure of interface layer between two plies can only initiate if a crack forms within one of the plies. 2. To ensure correct energy dissipation, matrix normal and shear surface tractions must vanish simultaneously at failure through cracking since a crack must have zero tractions on its surface. A novel mixed mode evolution law has been implemented incrementally to achieve this. 3. The strength values are statistically distributed over the geometry of the test coupon. This approach takes the strength variation measured in the experiments, and helps to model localization of the failure events. 4. Residual strength approach is used to account for post-kink strength retention under confined compression of

0 plies. When the residual compressive strength level is reached, the stress state is fixed at that value for further increments of loading. The value of the residual strength is dependent on the material and can be affected by geometric features such as spatial constraints and bolt pretension. 5. Accurate calculation of element characteristic length for various failure modes. Since I2CBM is implemented as a user subroutine in the commercial finite element code, the average characteristic lengths provided by the FE solver need not be correct and can lead to incorrect energy dissipation. The correct choice for characteristic lengths for each mode is calculated separately. 6. A global crack spacing method is used which ensures that a certain spacing in maintained between adjacent cracks as observed in experiments. 7. Fiber fracture toughness corrections are modified as a function of the transverse normal stresses. This is an indirect way to account for the spatial constraints while modeling the failure.

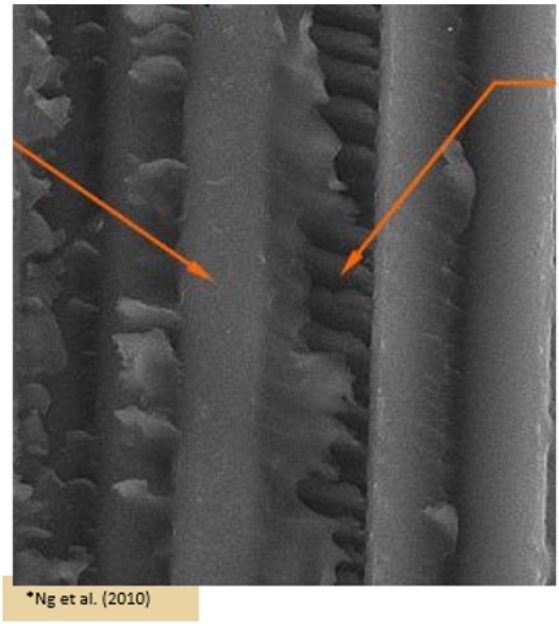

Figure 2.1: Microcracks in $[+45/-45]_s$ tension test specimen

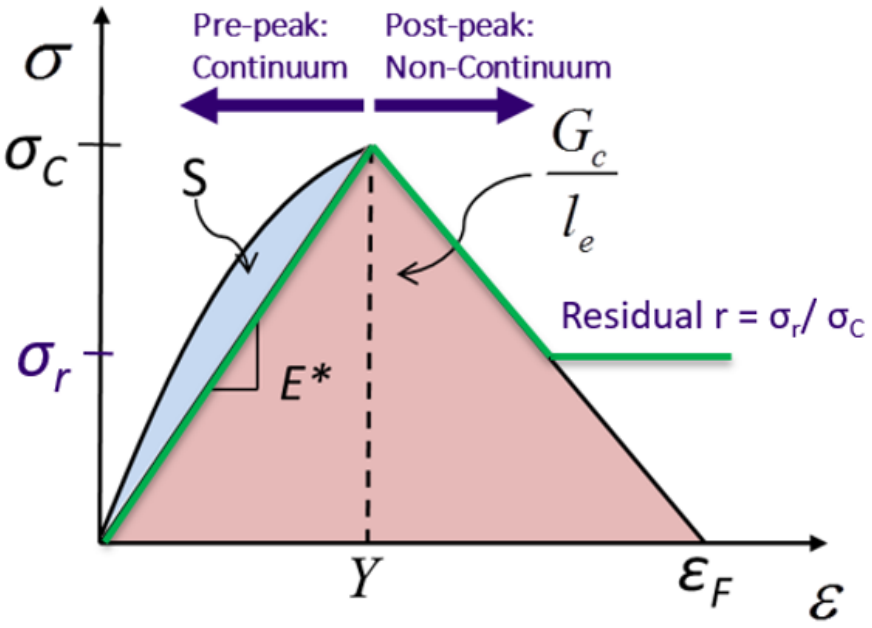

Figure 2.2: Generalized element stress-strain response

2.1 Schapery Theory for 3D Stress State

Schapery theory (ST) is an energy based approach for modeling the transverse and shear moduli degradation [29, 31]. It allows to characterize the non-linear curves as a function of the energy dissipated during the micro crack formation. The assumption that the fiber direction stiffness is unaffected by the microcrack formation is valid as the fibers are unaffected by microcracks. The approach is extended from plane stress state to 3D state of stress in this current work. Transverse and shear moduli degradation with microcracks is modeled using polynomial functions of the dissipated energy as shown in equation 2.1. ST has been combined with the Bazant-Oh crack band model in a 2D setting as reported in Pineda and Waas[26]. Here, a 3D characterization of the lamina in the pre-peak regime, which is an essential feature of I2CBM, is adopted.

$$\begin{aligned} E_{22} &= E_{220} e_s(S) \\ G_{12} &= G_{120} g_s(S) \end{aligned} \tag{2.1}$$

With the transversely isotropic assumption of the lamina, out of plane stiffness properties are degraded as shown below.

$$\begin{aligned} E_{33} &= E_{220} e_s(S) \\ G_{13} &= G_{120} g_s(S) \\ G_{23} &= G_{230} e_s(S) \end{aligned} \tag{2.2}$$

The total energy of the system can be written as a sum of the elastic, microdamage and macroscopic failure components

$$W_T = W_E + S + \sum S_i \tag{2.3}$$

Finally the microdamage evolution equation is obtained using the condition that the total energy is stationary with respect to microdamage energy Sr = $S^{1/3}$

$$\begin{aligned} [2(\alpha_{12}^2 + \alpha_{12}^3)\varepsilon_{11}\varepsilon_{22} + 2\alpha_{23}\varepsilon_{22}\varepsilon_{33} + 2(\alpha_{13}^2 + \alpha_{13}^3)\varepsilon_{11}\varepsilon_{33} \\ +\alpha_{22}\varepsilon_{22}^2 + \alpha_{33}\varepsilon_{33}^2]E_{22}^0 \tfrac{de_s}{dS_r} \\ +G_{23}^0\gamma_{23}^2 \tfrac{de_s}{dS_r} + G_{12}^0(\gamma_{12}^2 + \gamma_{13}^2)\tfrac{dg_s}{dS_r} = -6S_r^2 \end{aligned} \tag{2.4}$$

Where coefficient α's are

$$\begin{aligned} \alpha_{11} &= \tfrac{(1-\nu_{23}\nu_{32})}{(1-\nu_{12}\nu_{21}-\nu_{23}\nu_{32}-\nu_{13}\nu_{31}-2\nu_{21}\nu_{32}\nu_{13})} \\ \alpha_{12}^2 &= \tfrac{\nu_{12}}{(1-\nu_{12}\nu_{21}-\nu_{23}\nu_{32}-\nu_{13}\nu_{31}-2\nu_{21}\nu_{32}\nu_{13})} \\ \alpha_{12}^3 &= \tfrac{\nu_{23}\nu_{13}}{(1-\nu_{12}\nu_{21}-\nu_{23}\nu_{32}-\nu_{13}\nu_{31}-2\nu_{21}\nu_{32}\nu_{13})} \\ \alpha_{13}^2 &= \tfrac{\nu_{32}\nu_{12}}{(1-\nu_{12}\nu_{21}-\nu_{23}\nu_{32}-\nu_{13}\nu_{31}-2\nu_{21}\nu_{32}\nu_{13})} \\ \alpha_{13}^3 &= \tfrac{\nu_{13}}{(1-\nu_{12}\nu_{21}-\nu_{23}\nu_{32}-\nu_{13}\nu_{31}-2\nu_{21}\nu_{32}\nu_{13})} \\ \alpha_{23} &= \tfrac{\nu_{32}+\nu_{12}\nu_{31}}{(1-\nu_{12}\nu_{21}-\nu_{23}\nu_{32}-\nu_{13}\nu_{31}-2\nu_{21}\nu_{32}\nu_{13})} \\ \alpha_{22} &= \tfrac{(1-\nu_{13}\nu_{31})}{(1-\nu_{12}\nu_{21}-\nu_{23}\nu_{32}-\nu_{13}\nu_{31}-2\nu_{21}\nu_{32}\nu_{13})} \\ \alpha_{33} &= \tfrac{(1-\nu_{12}\nu_{21})}{(1-\nu_{12}\nu_{21}-\nu_{23}\nu_{32}-\nu_{13}\nu_{31}-2\nu_{21}\nu_{32}\nu_{13})} \end{aligned} \tag{2.5}$$

2.2 Crack Band Model

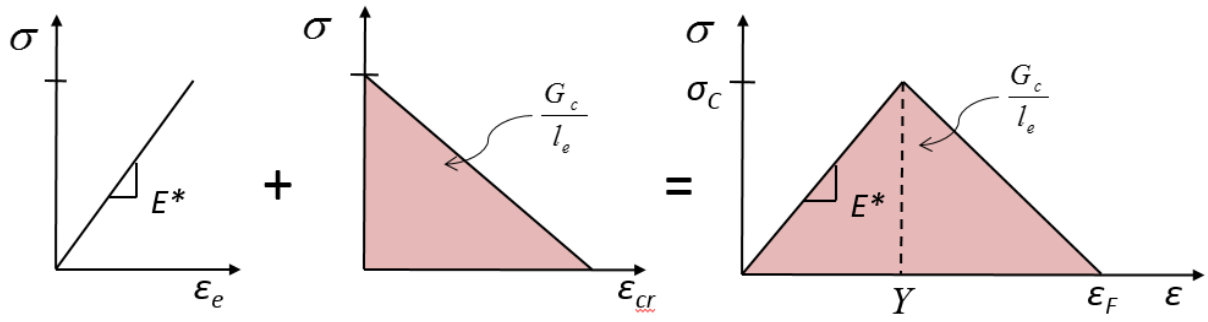

Figure 2.3: Crack band stress strain response

Crack band theory is an effective, element level approach to model the onset and propagation of macroscopic cracks in a mesh objective manner. The theory is a two parameter failure model which requires the strength and fracture toughness parameters as input,[4]. Stress-based initiation criteria define various failure mode initiations in I2CBM. Upon the initiation of failure, the crack band model acts like entities in series with one representing the elastic part and the other representing the cracking mechanism. The total strain in the element is a sum of the elastic strain and the crack strain as shown in equation 2.6. This idea is effectively summarized in the figure 2.3. The area indicated by S in the figure accounts for the energy dissipated due to microdamage evolution. G_c/l_e term shows the energy dissipated in the case of failure, where G_c is the fracture toughness of the material and l_e is the element characteristic length perpendicular to the crack direction. Element characteristic length is accurately calculated for each failure mode using the commercial FE solver's subroutine for characteristic length calculation.

$$\varepsilon = \varepsilon_e + \varepsilon_{cr} \tag{2.6}$$

A limitation of the crack band model is the maximum element size which can be used

for producing mesh objective results. This correspond to the element size for which the stress-strain response in figure 2.3 shows a vertical stress drop after the peak stress. Element sizes larger than this lead to physically incorrect snap-back behavior. The critical element length to prevent this behavior is given by,

$$l_e < \min\left\{\frac{2G^f_{IC}E_{110}}{X^2_{T/C}}, \frac{2G^m_{IC}E^*_{22}}{Y^2_{T/C}}, \frac{2G^m_{IIC}G^*_{12}}{S^2}\right\} \tag{2.7}$$

2.2.1 Fiber Failure Plane

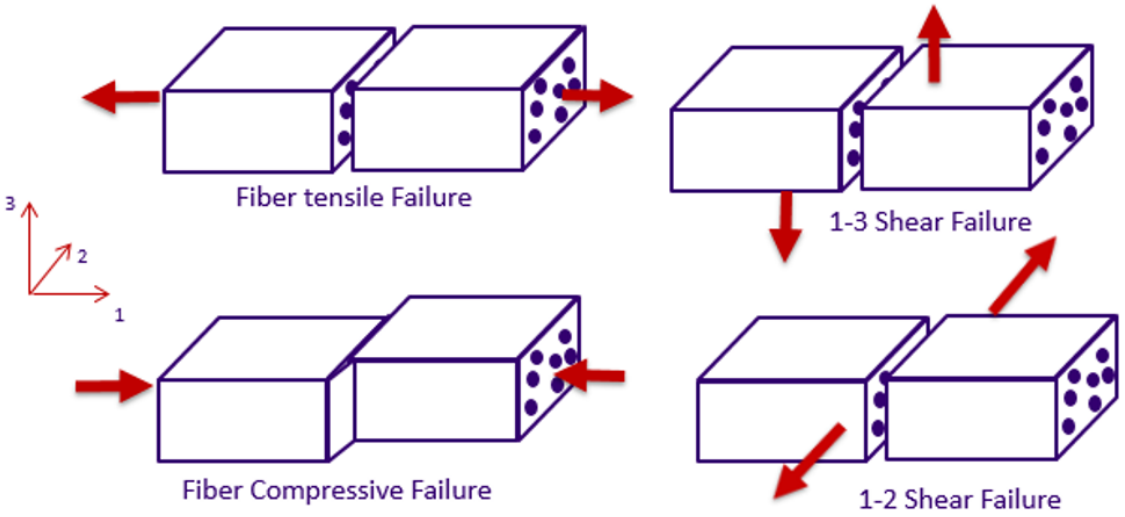

Figure 2.4: Failure modes in 2-3 plane

Failure plane whose normal is defined by direction 1, includes fiber failure modes (figure 2.4). The shear modes 1-2 and 1-3 involves significant fiber rotations and it's strength values can be very high compared to the shear strength measured using standard experiments where fiber rotations are not significant. With the standard symmetric stress tensor finite element implementation, it is not possible to model these shear modes accurately and hence are not considered in the current implementation. Therefore the only failure modes considered

in this plane are the fiber tensile and compressive failure modes. Fiber failure modes are triggered when the fiber direction stress reaches a critical value.

2.2.2 Transverse Failure Plane

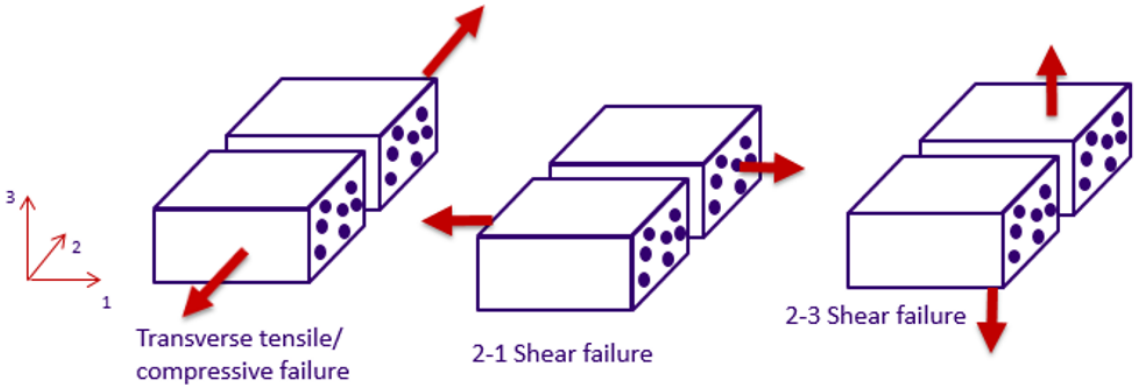

Figure 2.5: Failure modes in 1-3 plane

Transverse failure modes shown in figure 2.4 are characterized by macro cracks in the matrix and hence appropriate mixed mode laws are to be used in their modeling. Hashin criteria is used for the failure initiation under the general combined loading situation and it is given by

$$\frac{\sigma_{22}^2}{Y_{T/C}^2} + \frac{\tau_{12}^2}{S_{12}^2} + \frac{\tau_{23}^2}{S_{23}^2} \geq 1 \tag{2.8}$$

The model can use both stress and strain based criteria as appropriate for the specific problem. Current work uses stress based criteria and additional failure initiation criteria can be easily incorporated into the model as needed. Final failure state is achieved when the mixed mode evolution criteria is met

$$\frac{G_{22}}{G_{22c}} + \frac{G_{12}}{G_{12c}} + \frac{G_{23}}{G_{23c}} \geq 1 \tag{2.9}$$

2.2.3 Delamination Failure Plane

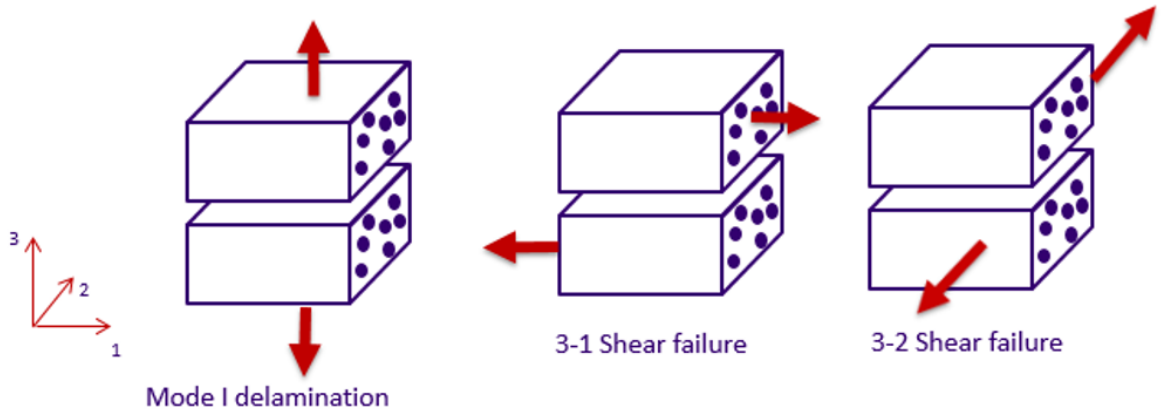

Figure 2.6: Failure modes in 1-2 plane

Similar to the transverse failure modes, delamination modes are also caused by macroscopic failure in the matrix. Hence a mixed mode failure initiation criteria is used.

$$\frac{\sigma_{33}^2}{X_{33T/C}^2} + \frac{\tau_{23}^2}{S_{23}^2} + \frac{\tau_{13}^2}{S_{13}^2} \geq 1 \tag{2.10}$$

It is also assumed that mode I delamination does not occur under compression. This is a valid assumption as the compressive strength in 3 direction is usually very high and hence it does not occur the loading conditions which are of interest here. Final failure is achieved when the mixed mode evolution criteria is met.

$$\frac{G_{33}}{G_{33c}} + \frac{G_{23}}{G_{23c}} + \frac{G_{13}}{G_{13c}} \geq 1 \tag{2.11}$$

Multiple failure modes can coexist in the same element. Transverse and delamination failure modes are linked to each other as they both are associated with matrix cracks. Therefore initiation of one of those failure planes causes the initiation in other failure plane as well. The fiber mode is treated independent of the other modes. The stiffness matrix is treated as a diagonal matrix when any of the failure criteria are met. This is different from the standard implementation of crack band/smeared crack model which has coupling terms in the stiffness matrix after the failure initiation. The material is in non-continuum state after the failure initiation and this model assumes that coupling terms do not carry much meaning in a non-continuum state and also simplifies the implementation. Delamination is initiated in the interface layers when the adjacent ply undergoes an in-plane failure mode. This communication between in-plane failure and delamination allows to capture complex intra-inter failure mechanisms effectively.

2.3 Novel Mixed Mode Evolution Scheme

The need for a correct mixed mode evolution is scheme can be explained with a 2D element example where two modes of failure mode I and mode II can exist together.

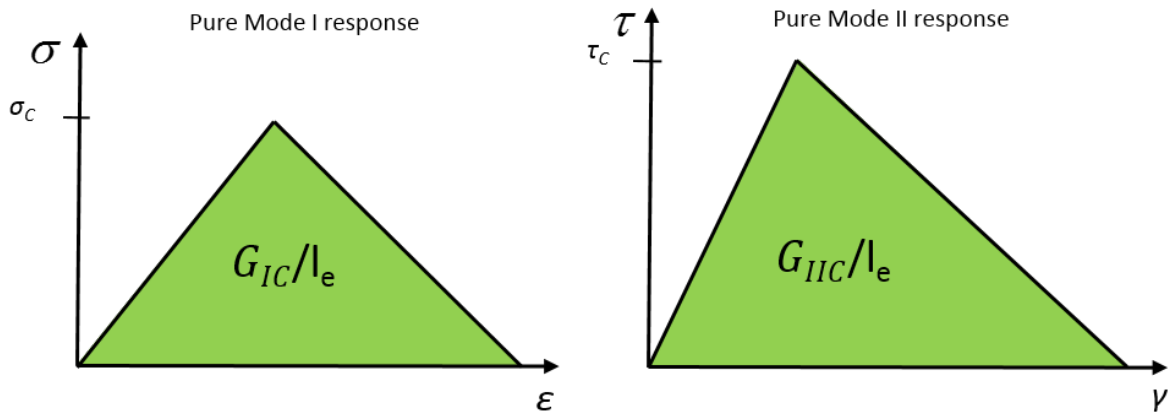

Figure 2.7: Response of pure modes

Stress strain responses of pure mode I and mode II cases in a continuum failure mechanics

frame work are shown in figure 2.7. Pure mode I and mode II strengths σ_c and τ_c, and fracture toughness values G_{Ic} and G_{IIc} are considered to be material properties which can be measured experimentally. Fracture toughness values correspond to the energy dissipated per unit area of the crack formed and when this idea is implemented in a continuum finite element framework, area under the stress-strain response corresponds to the ratio of fracture toughness to element characteristic length l_e. Element characteristic length can be visualized as the dimension of the element normal to the crack plane. Scaling of the fracture energy with respect to element characteristic length allows sharp crack to be modeled using standard continuum finite element framework by effectively smearing the crack plane on the entire element.

In a general loading scenario, material points in a body experience a combination of mode I and mode II loading. Hashin-Rotem failure criteria (equation 2.12) is a failure criteria commonly used to determine the failure initiation under mixed-mode loading condition.

$$\frac{\sigma^{*2}}{\sigma_c^2} + \frac{\tau^{*2}}{\tau_c^2} = 1 \tag{2.12}$$

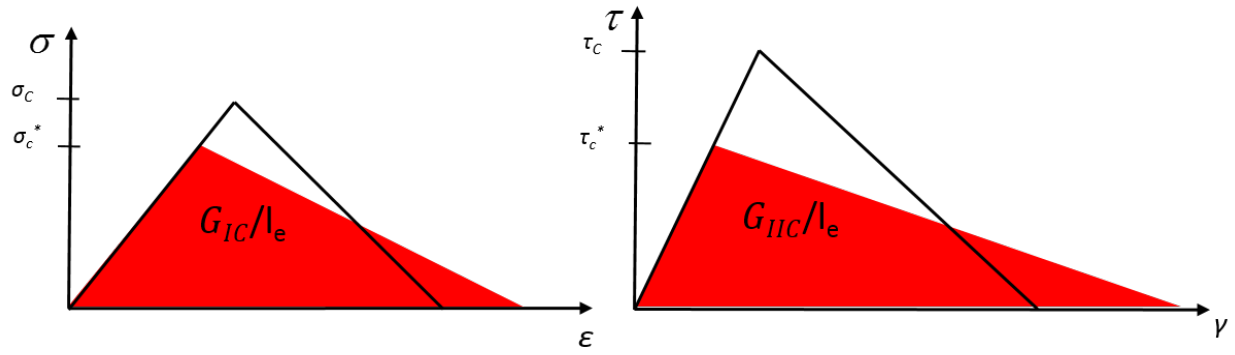

Figure 2.8: Mixed mode response with Hashin failure initiation criteria

When equation 2.12 is satisfied, individual modes have to start unloading at stress states lower than the pure mode strength values as shown in figure 2.8. To ensure that each mode

dissipates energy corresponding to the fracture toughness values the unloading curves have to form the area shown by red region in the figure. Each mode can unload at different rates and final failure criteria such as a simple power law (equation 2) can be used to decide the point at which mixed-mode crack is completely formed. G_I^* and G_{II}^* indicate the energy dissipated so far by mode I and mode II respectively.

$$\frac{G_I^*}{G_{Ic}} + \frac{G_{II}^*}{G_{IIc}} = 1 \tag{2.13}$$

When equation 2.13 is satisfied, the individual stress-strain states of the modes can be at points A and B as shown in figure 2.9. This means that under the standard implementation of mixed mode law, final failure state is achieved with non-zero tractions on the crack plane. This is physically incorrect as the tractions have to vanish simultaneously in a crack plane.

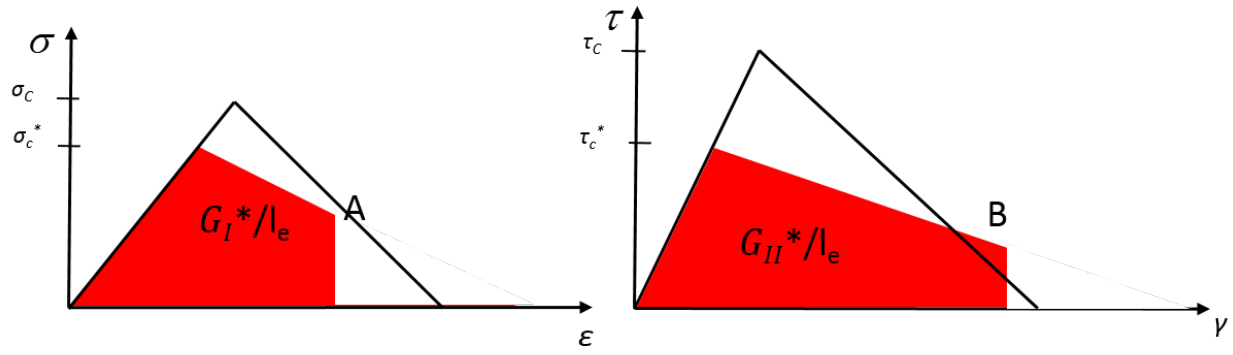

Figure 2.9: Final failure state under standard mixed mode implementation

The main issues which prevents from determining an unloading path such that it satisfies equation 2.13 and also ensure that tractions vanish simultaneously at the crack plane are as follows 1.G_I^* and G_{II}^* values are unknown at the final failure 2. Unloading rates of the individual modes can vary as the failure evolution progresses and hence it is impossible to predetermine the final failure strain values or work with a prescribed unloading curve.

2.3.1 Incremental Mixed Mode Evolution Scheme

An incremental mixed-mode evolution law is developed such that it satisfies the following conditions 1. Failure initiation is determined by any criteria of choice (such as equation 2.12) 2. Any mixed mode final failure criteria (such as equation 2.13) 3. Surfaces tractions vanish simultaneously on the crack plane when mixed mode final failure criteria is satisfied Since all the finite element solvers used for solving continuum failure analysis use an incremental solution approach, it is very practical to develop an incremental formulation which can be incorporated into them easily.

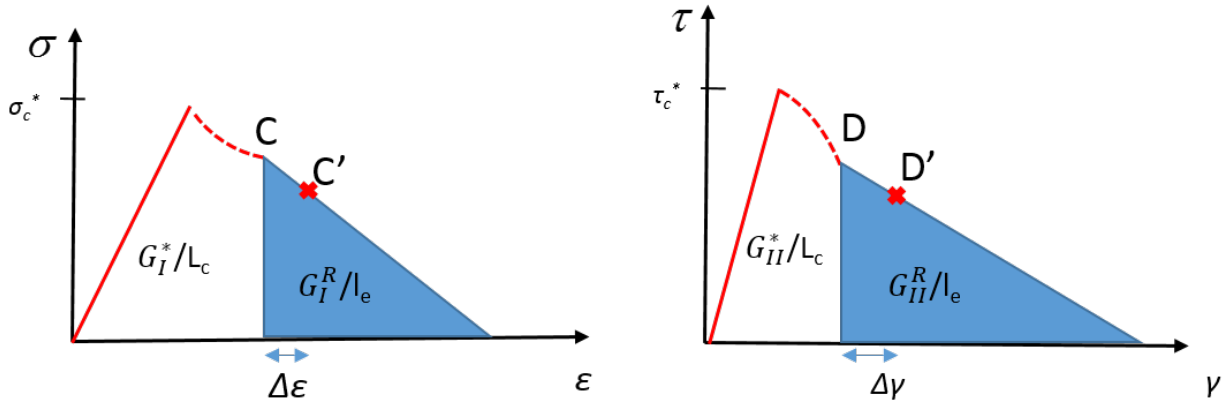

Figure 2.10: Incremental mixed mode evolution law : A point on the post-peak path

We can consider two post-peak path points C and D for mode I and mode II respectively as shown in figure 2.10 to illustrate the incremental mixed mode evolution methodology. C and D could be the points of failure initiation or any point reached after that. At this stage energy dissipated so far G_I^* and G_{II}^* can easily be calculated from the area under the stress-strain curves. Stress-strain values at C and D are also known. Finite element solver also provides the incremental strains and at that increment. Stress values at C and D are the unknowns which need to be determined. This can be easily estimated if the energy remaining to be dissipated G_I^R and G_{II}^R are known. This means that at any given point on

the post-peak curve, G_I^R and G_{II}^R are the unknowns which needs to be solved. If power law shown in equation 2.13 is the final failure criteria used, it can be rewritten as below

$$\frac{G_I^* + G_I^R}{G_{Ic}} + \frac{G_{II}^* + G_{II}^R}{G_{IIc}} = 1 \tag{2.14}$$

Now we need an additional equation to solve for the G_I^R and G_{II}^R. In-order to construct a second equation, the following assumption is made *'Ratio of energy remaining to be dissipated for the modes is proportional to the ratio of energy dissipated by the modes so far'* . This can be represented using the equation below

$$G_I^* : G_{II}^* :: G_I^R : G_{II}^R \tag{2.15}$$

Equations 2.14 and 2.15 can easily be solved for G_I^R and G_{II}^R as below

$$\begin{aligned} G_I^R &= \tfrac{g1 G_{IC}}{g1+g2} - G_I^* \\ G_{II}^R &= \tfrac{g2 G_{IIC}}{g1+g2} - G_{II}^* \end{aligned} \tag{2.16}$$

Where $g1 = \frac{G_I^*}{G_{Ic}}$ and $g2 = \frac{G_{II}^*}{G_{IIc}}$ This procedure can be repeated until the final failure criterion (equation 2.13) is satisfied. In the case of a 3D elements, traction on the crack plane consists of a normal component and two shear components. In this case equations 2.15 and 2.16 become equations 2.17 and 2.18 respectively.

$$G_I^* : G_{II1}^* : G_{II2}^* :: G_I^R : G_{II1}^R : G_{II2}^R \tag{2.17}$$

$$\begin{aligned} G_I^R &= \tfrac{g1 G_{IC}}{g1+g2+g3} - G_I^* \\ G_{II1}^R &= \tfrac{g2 G_{II1C}}{g1+g2+g3} - G_{II1}^* \\ G_{II2}^R &= \tfrac{g3 G_{II2C}}{g1+g2+g3} - G_{II2}^* \end{aligned} \tag{2.18}$$

The methodology can be easily adapted for any mixed-mode final failure criteria and for non-linear traction separation laws. Power law final failure criterion and linear traction separation law are chosen here for simplicity and demonstration purpose.

2.3.2 Single Element Test Problem

Consider a composite single element test case as shown in figure 2.11. Bottom face of the element is constrained in all directions and prescribed displacements are applied on the nodes at the top face. Ratio of the prescribed 1, 2 and 3 displacements at the top surface are 1:2:3

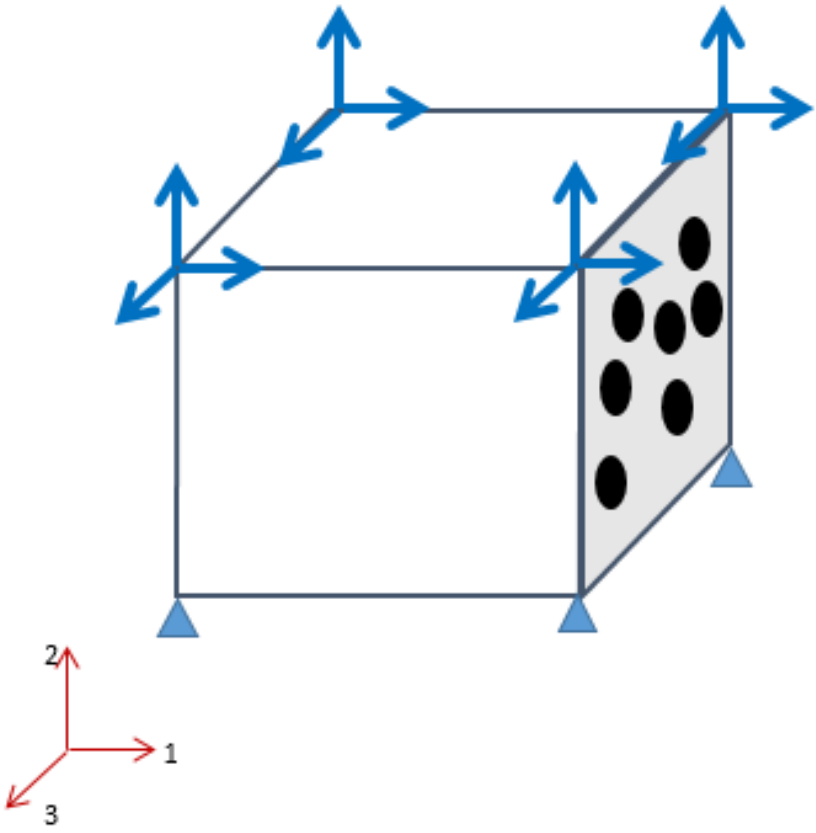

Figure 2.11: 3D element mixed mode loading on 1-3 plane

The resultant stress-strain responses of the relevant components are shown in figure 2.12. It can be seen from the results that the incremental mixed mode evolution law assures that the tractions vanish simultaneously when the final failure criteria (power law) is satisfied. Simulation results without the mixed mode evolution law retains non-zero stress values when

the final failure criteria is satisfied.

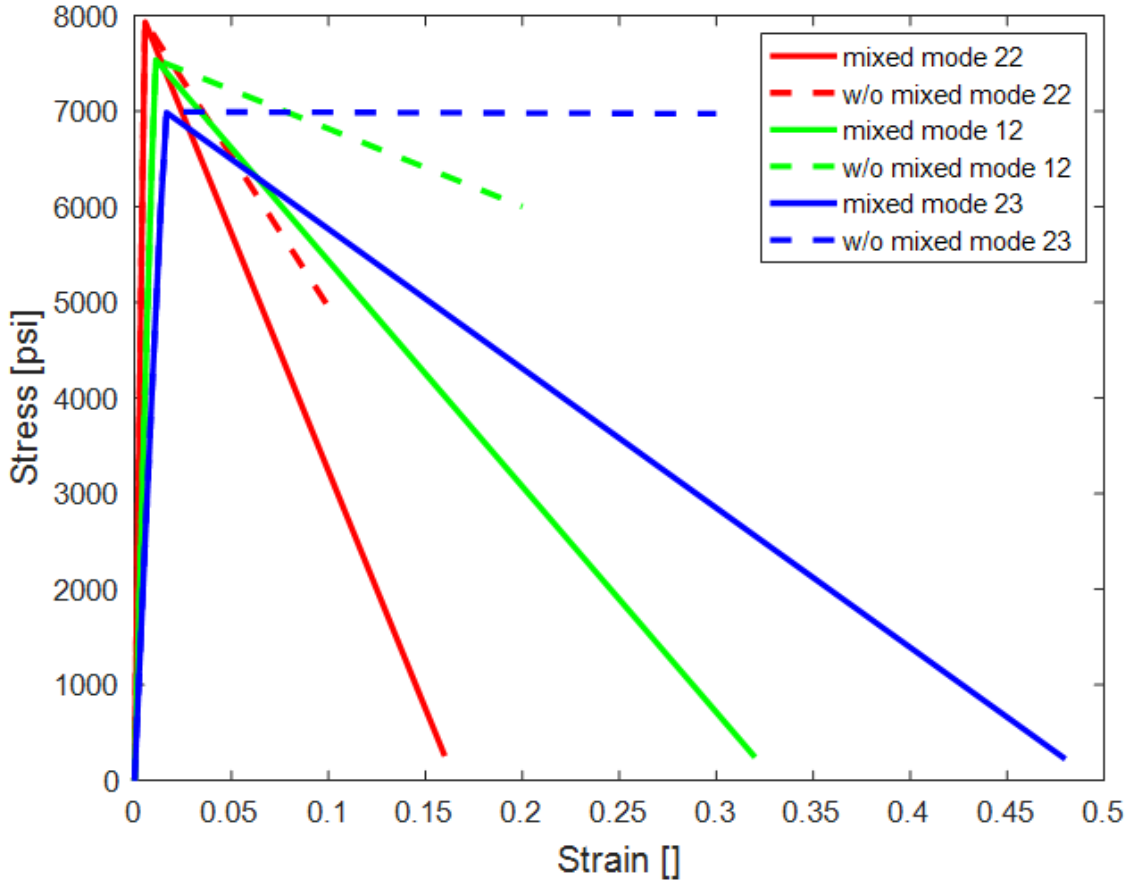

Figure 2.12: Stress-strain response with and without the mixed mode evolution law

2.4 Modeling of Bearing Failure

Fiber kinking is an instability facilitated by the non-linear shear response of the matrix. Since fiber kinking/compressive failure is one of the key mechanisms in the failure analysis of bolted joints, modifications have been made to implementation of this failure mode to account for the effect of bolt pretension and other spatial constraints. Fiber kinking instability is influenced by the 3D state of stress and significant compressive stresses in transverse and out of plane directions can potentially stabilize the shear non-linear response and increase the

effective fiber compressive strength. While this is an area which requires a more experimental and numerical study, a simplified approach is taken in this analysis to capture the effects of spatial constraints.

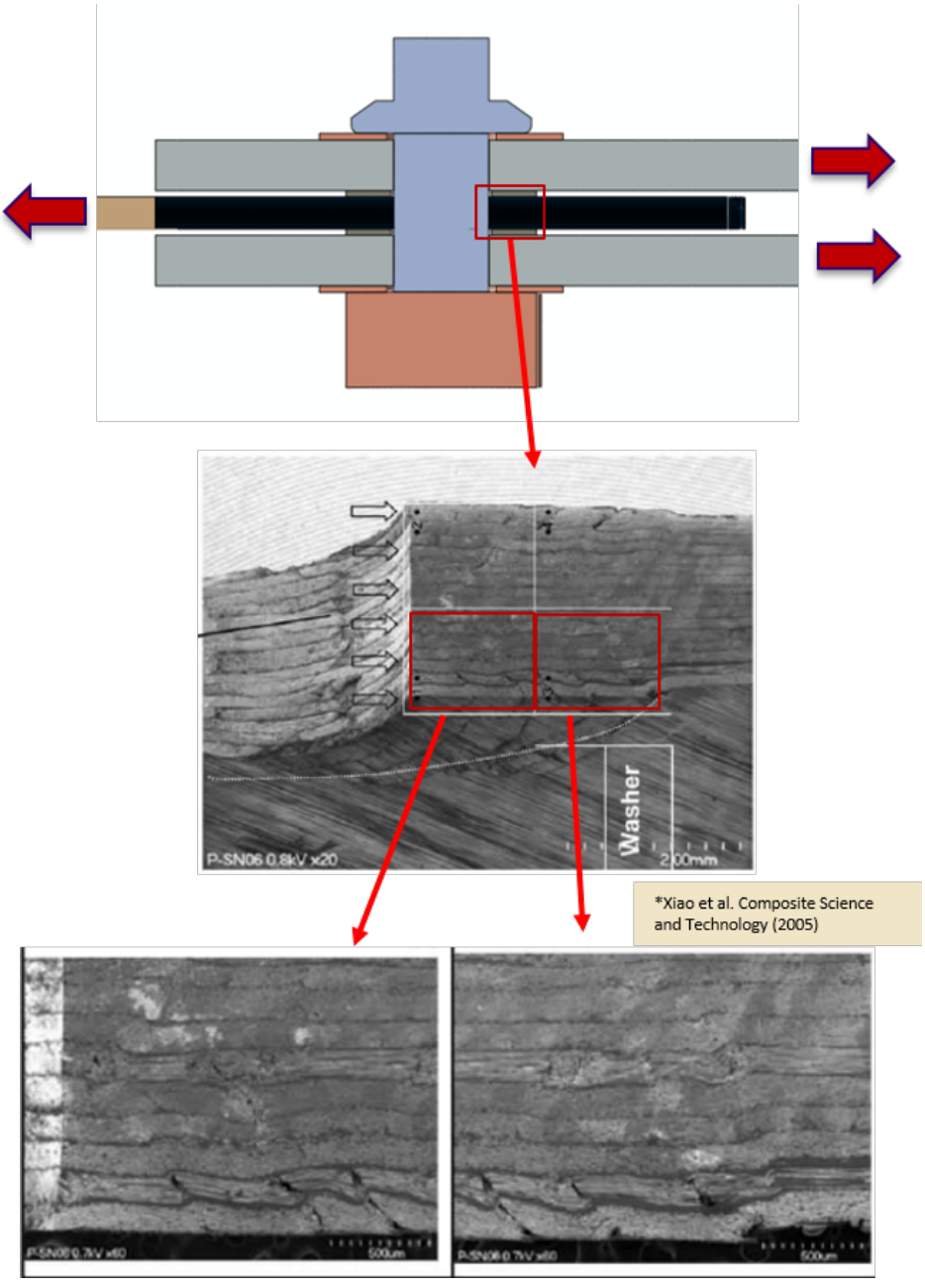

Figure 2.13: Multiple kink band formation in bearing failure

Residual stress approach is used for modeling the bearing failure mechanisms in bolted joint problems. When the fiber compressive failure occurs in a confined space, the debris resulting from it does not 'escape' and acts a medium for transferring stresses to the parts of laminate which have not failed. Figure 2.13 shows the multiple kink band mechanism observed in bolted joint experiments. This behavior is effectively modeled using the residual stress approach. The deletion of elements, based on current, deformed volume, is also used in the model to capture progressive bearing and tear out failure mechanism correctly. Without this, the simulation would abort due to excessive element distortion errors as the material gets compressed. New interior contact surfaces are created with deletion of elements and the ability of the scheme to retain the load with the element deletion scheme is also verified.

2.5 Global Crack Spacing and Failure Interaction

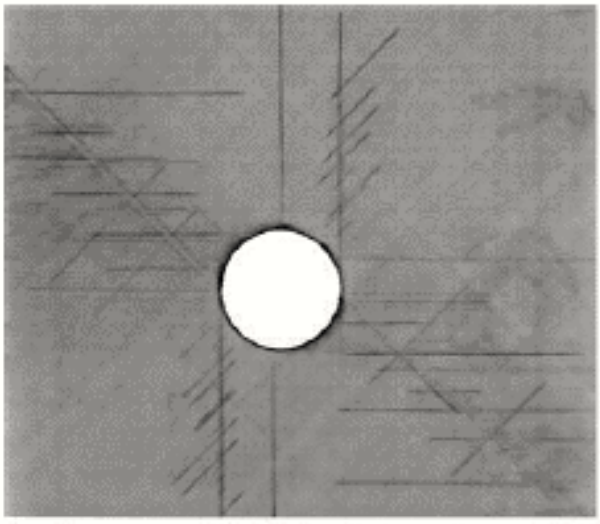

Figure 2.14: Quasi-isotropic OHT coupon at 95% peak load [15]

Based on the experimental observations in literature (figure 2.14) , splitting crack is a significant failure mechanism especially in 0 layer dominated layups. Splitting cracks in the 0 layer occur due to shear stress concentrations tangent to the hole and grow parallel to the

fiber direction. Growth of splitting crack is a mechanism which helps in reducing the fiber direction stress concentration near the hole. This reduction depends on the length of the splitting crack as well as on the delamination at the adjacent layer interfaces. This causes the stresses to be redistributed around the hole and thus controls the progressive failure events. This complex mechanism makes it a hard problem to capture with a standard progressive failure analysis tool unless special care is taken. Yan et. al. [38] who studied the difference between open hole tensile and filled hole tensile strengths for different layups also concluded that difference in the splitting crack growth is also the cause of the difference in strength between those cases. They reported filled hole tensile strengths to be lower than the corresponding open hole tensile strengths. Based on these observations, it was identified that the progressive failure analysis tool has to be enhanced with additional features to help capture the splitting crack better.

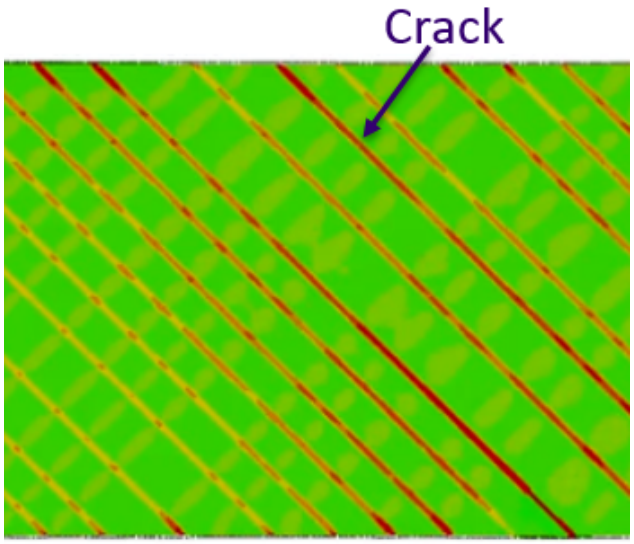

Figure 2.15: Crack tracking in a -45 ply

A crack spacing scheme has been added to I2CBM failure analysis tool to keep a global record of the cracks formed in each layer. Crack paths in the layers maintain a certain sep-

aration between each other based on experimental observations. Intra-interlaminar failure interaction is enabled along the crack paths which caused the initiation of delamination along with cracks in the adjacent plies. This feature overcomes the difficulties in a homogenized lamina finite element to effectively model the failure mode interactions and helps to localize the crack growth effectively. Similar approaches are used in the literature by explicitly inserting cohesive elements along the crack paths observed in experiment [15, 25]. Such methods require additional work at the model building stage. However, current implementation of the crack tracking algorithm in I2CBM is predictive in that crack paths based are based on computed stress fields along with a suitable criterion for onset. Thus, there is no need to insert a crack path at the model building stage. Figure 2.15 shows the development of matrix cracks in a -45 layer with the global crack tracking algorithm implemented in I2CBM.

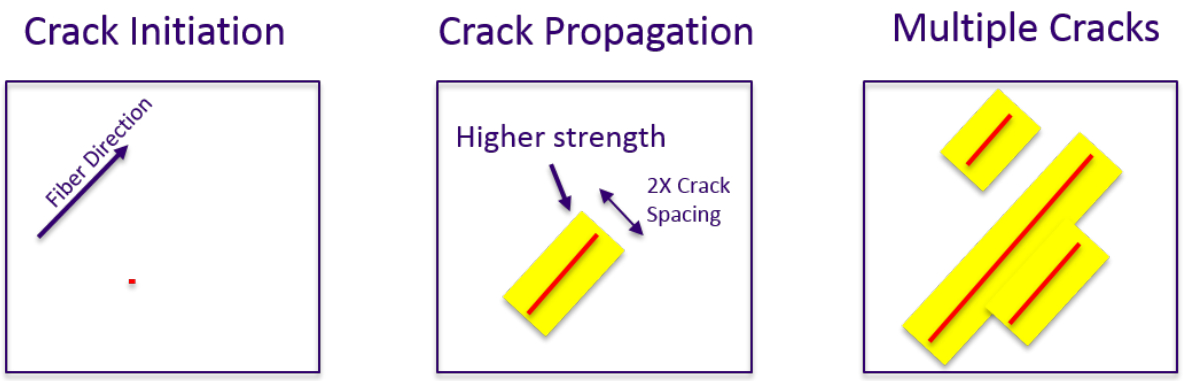

Figure 2.16: Crack tracking scheme

Figure 2.16 demonstrates the scheme used for keeping a record of the matrix cracks existing in the model. Characteristics of different stages in crack tracking algorithm are explained below.

1. Crack initiation : Crack path initiation point is decided by the stress distribution for the given problem and the failure initiation criteria chosen. Crack path insertion at the preprocessing stage is not required. 2. Crack propagation : Crack spacing parameter as

indicated in the figure shows decides the region where the strength is set higher in order to facilitate the localization of the crack path. Crack spacing parameter can be calculated using analytical methods, micro-mechanical modeling or based on experimental observations. 3. Multiple cracks : Different crack paths can form an evolve independently. The scheme is implemented as a non-local method where information about each crack path is stored and updated at every increment. It is also made sure that a minimum spacing (crack spacing) is always maintained between crack paths.

Crack tracking is automatically disabled when the matrix compression stress is significant. Therefore it is disabled in the regions where bearing or compression failure mechanism is critical.

Nairn [22] used variational approach to analyze the development of discrete transverse cracks occurring in a cross-play specimen under tensile loading. He presented a relationship between the fracture toughness G_m and crack spacing l_n as shown in equation 2.19.

$$G_m = \sigma_c^2 \frac{E_{22}^2}{E_C^2} t_{90} C_{22} [2\chi(\rho/2) - \chi(\rho)] \tag{2.19}$$

where,

$$
\begin{aligned}
&\chi(\rho) = 2\alpha\beta(\alpha^2 + \beta^2 \tfrac{cosh(2\alpha\rho) - cos(2\beta\rho)}{\alpha sin(2\beta\rho) + \beta sinh(2\alpha\rho)}) \\
&\rho = \tfrac{l_n}{t_{90}} \\
&\alpha = q^{1/4} cos(\tfrac{\theta}{2}) \\
&\beta = q^{1/4} sin(\tfrac{\theta}{2}) \\
&q = \tfrac{C_{00}}{C_{22}} \\
&p = \tfrac{C_{02} - C_{11}}{C_{22}} \\
&\theta = tan^{-1}(\sqrt{\tfrac{4q}{p^2} - 1}) \\
&C_{00} = \tfrac{1}{E_{22}} + \tfrac{1}{\lambda E_{11}} \\
&C_{11} = \tfrac{1}{3}(\tfrac{1}{G_{12}} + \tfrac{1}{\lambda G_{21}}) \\
&C_{02} = \tfrac{\nu_{12}}{E_{22}}(\lambda + \tfrac{2}{3}) - \lambda \tfrac{nu_{21}}{3E_{11}} \\
&C_{22} = (\lambda + 1)(3\lambda^2 + 12\lambda + 8) \\
&\lambda = \tfrac{t_{90}}{t_0}
\end{aligned}
\tag{2.20}
$$

Fracture toughness calculated using the above equation is plotted as function of crack spacing in figure 2.17. As shown in the figure, fracture toughness value is constant for crack spacing values below 0.2". For the purpose of this study a crack spacing value of 0.04" is used. However equations 2.19 and 2.20 are applicable only for the mode I cracking in a cross-ply configuration. For mixed-mode discrete cracks appearing in a generic layup, crack spacing parameters will have to calculated using other methods such as micromechanics FE modeling and this is left as future work.

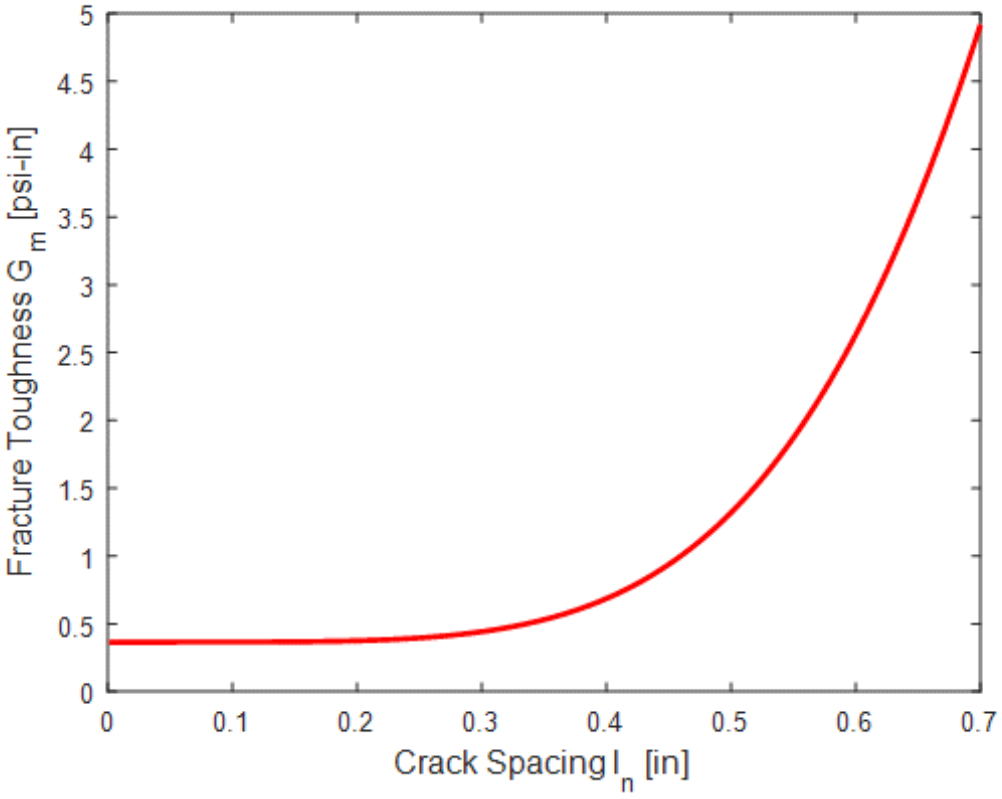

Figure 2.17: Transverse mode I fracture toughness as a function of crack spacing

2.5.1 Intra-inter Failure Interactions

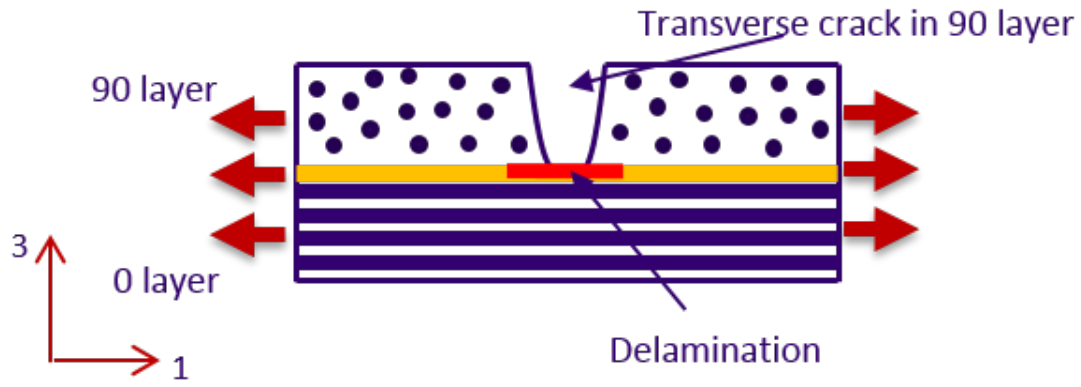

Figure 2.18: Interaction between in-plane failure and delamination

The requirement for enabling active interaction between in-plane matrix failure and delamination can be explained with a cross ply ($[0/90]_s$) laminate under tension as shown in figure 2.18. Matrix rich interface layer between 0 and 90 layers are shown in yellow. Under tensile loading, matrix transverse cracks form in the 90 layer and this causes higher shear stresses to develop at the ply interface right below the transverse crack (region shown in red). Micro-mechanics modeling of the entire laminate can capture these effects accurately, but a homogenized modeling approach of the plies will have limitations in getting the interface stresses accurately and can be very sensitive to the mesh refinement in that region. This would mean that interface layer strength properties will have to be calibrated. In order to overcome this limitation, an in-plane failure triggered delamination initiation feature is added to the model. Intra-inter communication is triggered only along the crack paths and not along the higher strength region.

2.6 Other Relevant Modifications

2.6.1 Fiber Direction Fracture Toughness Correction

Progressive failure in the fiber direction is influenced by the presence of transverse normal stresses. In the case of tensile failure, compressive stresses in the through thickness direction can assist the failure process due to poisons effects and due to the compressive failure in the matrix. This leads to an effective fiber direction tensile toughness when the through thickness stress is compressive. On the other hand under compressive through thickness stress, fiber direction compressive failure becomes more stable due to the fundamental nature of fiber kinking mechanism. These effects are incorporated into the model as corrections for fiber direction toughness with other normal stresses as presented in equations 2.21 and 2.22 for fiber tensile and compressive failure respectively. These effects are considered only for compressive through thickness stresses in this study. The coefficients T and C are determined by calibrating against experimental data. In this case filled hole tension/compression data (Chapter 3) is used for the calibration. A micromechanics model study can provide more insights into the toughness corrections with stress triaxiality and is planned as a future study.

$$G_{Ic}^{fT} = G_{Ic}^{fT0}(1 - \mu^T(\frac{-\sigma_{22}}{\sigma_{22c}} + \frac{-\sigma_{33}}{\sigma_{33c}})) \tag{2.21}$$

$$G_{Ic}^{fC} = G_{Ic}^{fC0}(1 + \mu^T(\frac{-\sigma_{22}}{\sigma_{22c}} + \frac{-\sigma_{33}}{\sigma_{33c}})) \tag{2.22}$$

2.6.2 Correct Element Characteristic Length Calculation

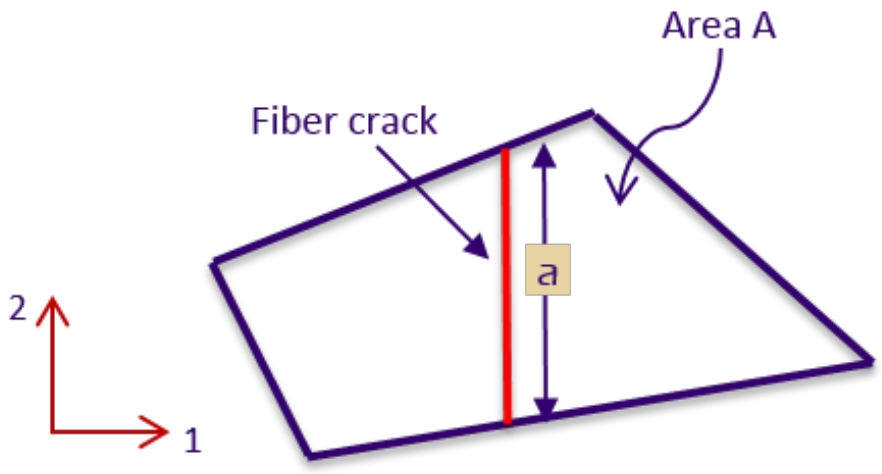

Figure 2.19: Fiber crack in an element

In a crack band model, element characteristic length is an important parameter needed to ensure that correct amount of energy is dissipated by an element when cracked. Figure 2.19 shows the fiber crack modeled using a 2D element. Length of the crack passing through the centroid (integration point in a reduced integration element) is given by a. Correct value for the element characteristic length should be the ratio between the element area A and crack length a. However the value provided as element characteristic length by commercial FE solvers such as Abaqus is usually the square root of the area. This value is inaccurate especially when the element aspect ratio is large. Also value of he characteristic lengths in different modes of failure can be different. It is ensured in I2CBM that characteristic lengths for different modes are calculated for correct energy dissipation.

2.6.3 Spatial Variation of Strength

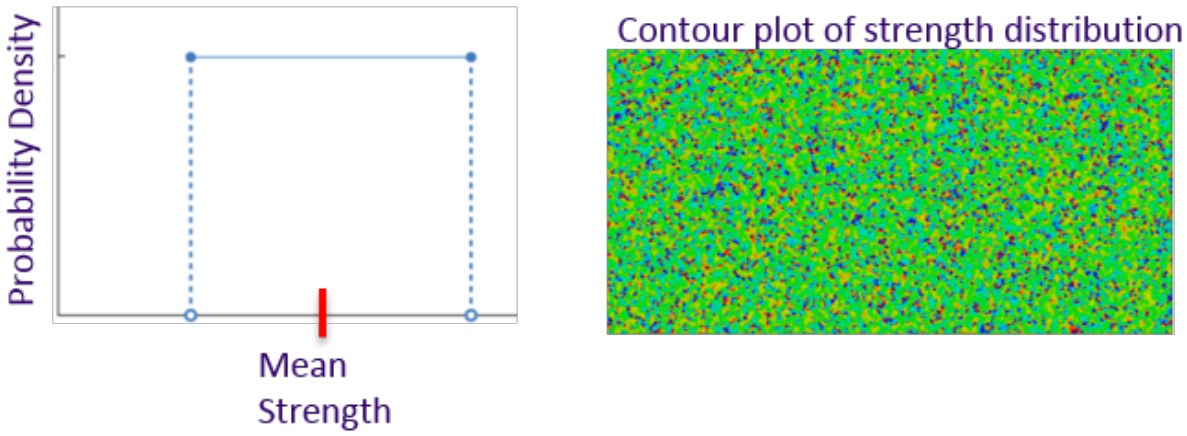

Figure 2.20: Spatial Variation of Strength

Spatial variation of strength properties are non-uniform in actual composite materials and hence it is required to account for this in the modeling. Mean and variance of strength values measured using standard coupon level tests are treated as inputs in this model and a uniform distribution of the strength properties si created as shown in figure 2.20. This helps in effectively localizing the cracks when under a uniform stress state. Other distributions such as Weibull distributions will be considered in the future study.

2.6.4 Crack Band Implementation

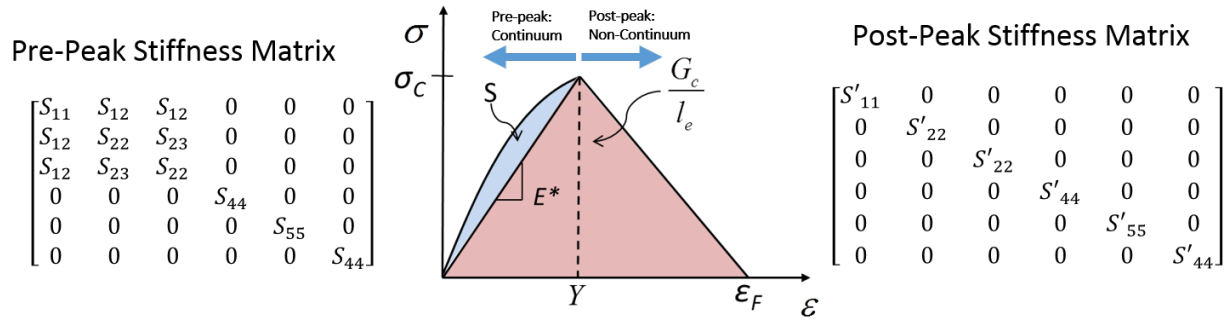

Figure 2.21: Stiffness matrix in crack band implementation

Multiple crack planes can coexist in an I2CBM element. Before the failure initiation (pre-peak), a fully populated stiffness matrix exists and the definition of poisson's effects are meaningful in this region as the material is still in a continuum state. However the definition of possion's effect terms (off-diagonal terms in the stiffness matrix) can be highly ambiguous as the material is essentially in a non-continuum state. Therefore, post failure initiation stiffness matrix for the element is treated as a diagonal matrix as shown in figure 2.21. This allows to treat each mode separately without mutual interactions in the post-peak region. Cracks in transverse and delamination planes are caused due to matrix failure mechanisms and hence failure in one plane is assumed to trigger the failure in other plane.

Chapter 3

OPEN HOLE AND FILLED HOLE SIMULATIONS

Single shear bolted joints are widely used as a method for joining composite parts in aircraft. Countersunk holes are used in joints for creating non-protruding smooth surfaces. As a first step towards a detailed progressive failure analysis of such bolted joint configurations, it is critical to assess the analysis method using simpler problems like open hole tension/compression and filled hole tension/compression cases. Unlike fixed diameter holes, countersunk holes can have significant 3D stress states near the countersunk transition region and can have local out of plane deformation modes, suggesting that a 3D analysis tool is required for accurate predictions. With the introduction of a bolt with a preload, 3D stress state become quite significant and a simplified 2D model becomes no longer useful. These factors combined with complex progressive failure mechanisms of composite laminates makes it a challenging problem to solve using progressive failure analysis tools.

3.1 Open Hole Tension

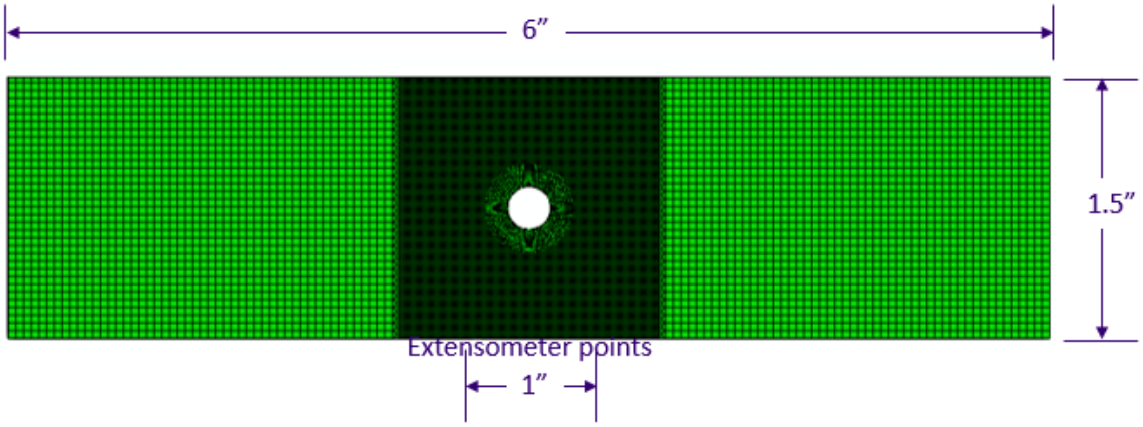

Figure 3.1: Open Hole Tension FE Model

Finite element model used for the open hole tension simulation has the dimensions as indicated in figure 3.1. Countersink hole at the center has diameter varying from 0.25 to 0.50 over the thickness corresponding to 20 plies. Each ply has a thickness of 0.053 and is modeled independently using fiber aligned mesh as shown in the close up view in figure 3.2. A combination of 6 and 8 noded reduced integration solid elements (C3D6 and C3D8R in Abaqus) are used for capturing the geometry. The use of 6 noded wedge elements are limited only to the regions where it is unavoidable due to the geometry features. Two layups [45/0/-45/0/90/0/-45/0/45]3 (C1) and [45/0/-45/0/90/0/-45/0/45]4 (C2) are considered for this study. Matrix rich layers are modeled in every ply interface to capture delamination. The ratio of thicknesses of the ply and interface layers are kept as 10:1. Fine mesh of in-plane characteristic length 0.01 is used in the middle region and coarse mesh is used in the outside region as seen in figure 3.1. Mesh size chosen near the hole ensures that the crack band characteristic length criteria are met for all the failure modes of interest.

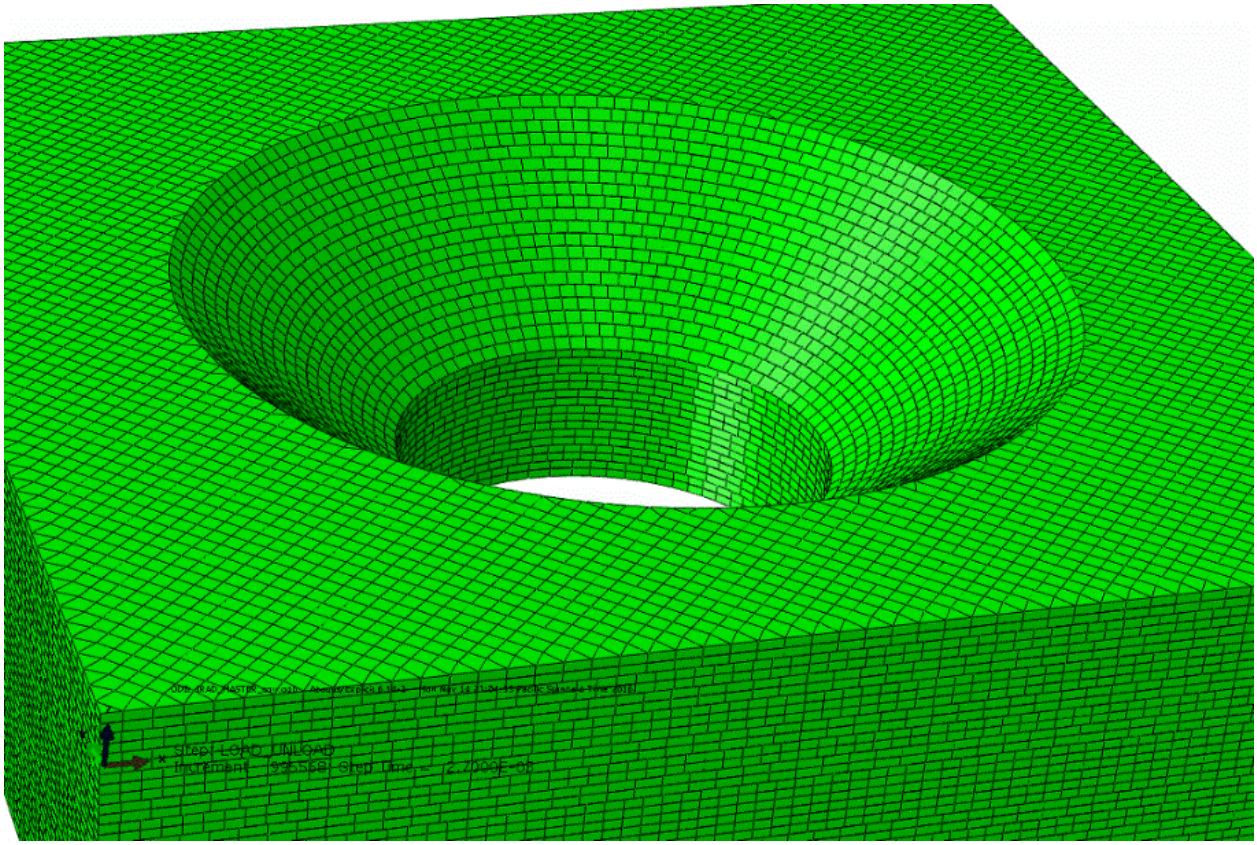

Figure 3.2: Fiber Aligned Mesh

3.1.1 Results and discussion

Open hole tensile load-displacement response and lamina failure pattern at 96% of the peak load are shown in figure 3.3 for the C1 laminate. With the global crack tracking algorithm, the model is able to capture the steady splitting crack growth in the 0 layer. Figure 3.4 shows the development of splitting crack growth along the points in the load-displacement response. Cracks developed in the 90/45/-45 layers are also seen to be clearly influenced by splitting crack path in the 0 layer. This failure pattern is in agreement with the CT scan image of the quasi-isotropic laminate in figure 2.14. With 44% of 0 layers in the C1 laminate, it is to be expected that splitting crack is one of the main driving failure mechanism as it reduces the stress concentration near the hole, thus influencing the progression of failure in

other layers as well. Similar failure patterns were also observed in the C2 laminate case. Load displacement response of the C2 laminate is given in figure 3.5.

For both the cases, simulation results match well with the experiments. In the case of C1 laminate, test data shows a slight stiffening effect which is a characteristic feature of such 0 layer dominated laminates. However there is no stiffening effect in the simulation (caused by fiber modulus increasing with tension) and hence the mismatch in stiffness close to the peak is due to this aspect. It is also known that the slippage of the extensometer points has caused the non-linear region in the C2 response.

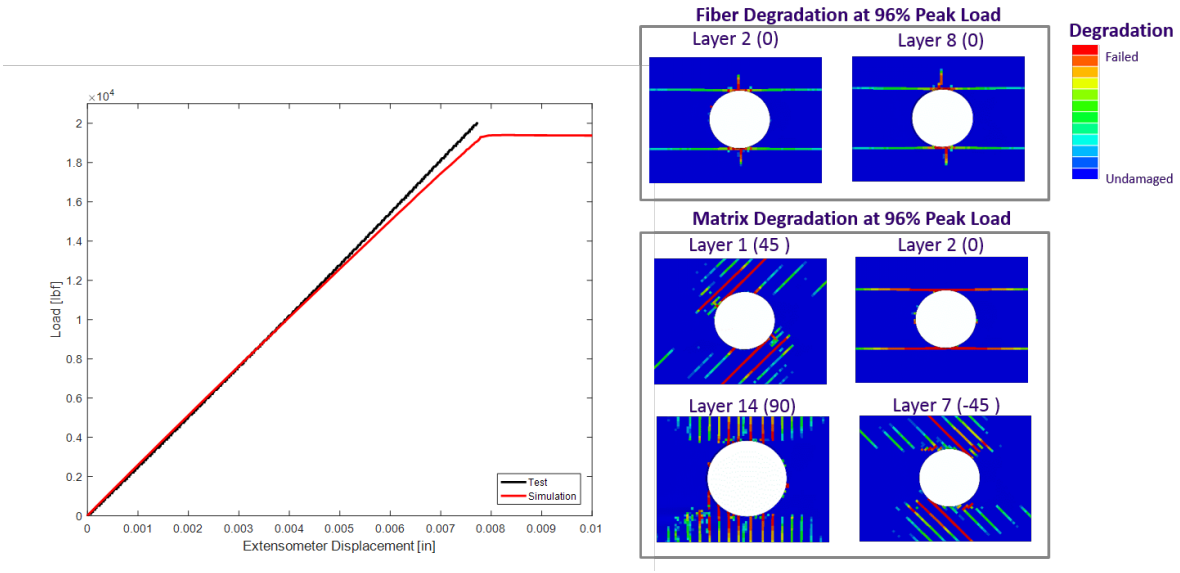

Figure 3.3: Open hole tension simulation of C1 laminate

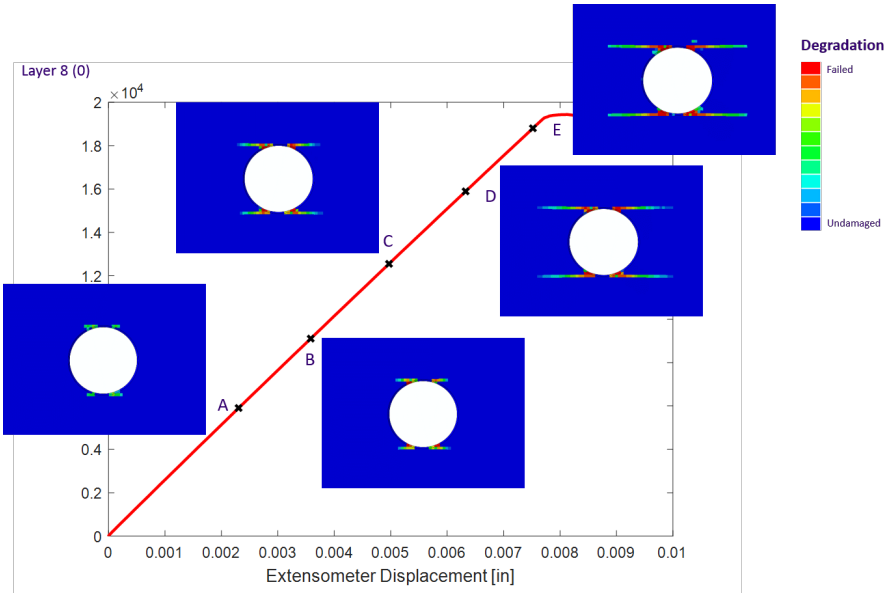

Figure 3.4: Splitting crack growth

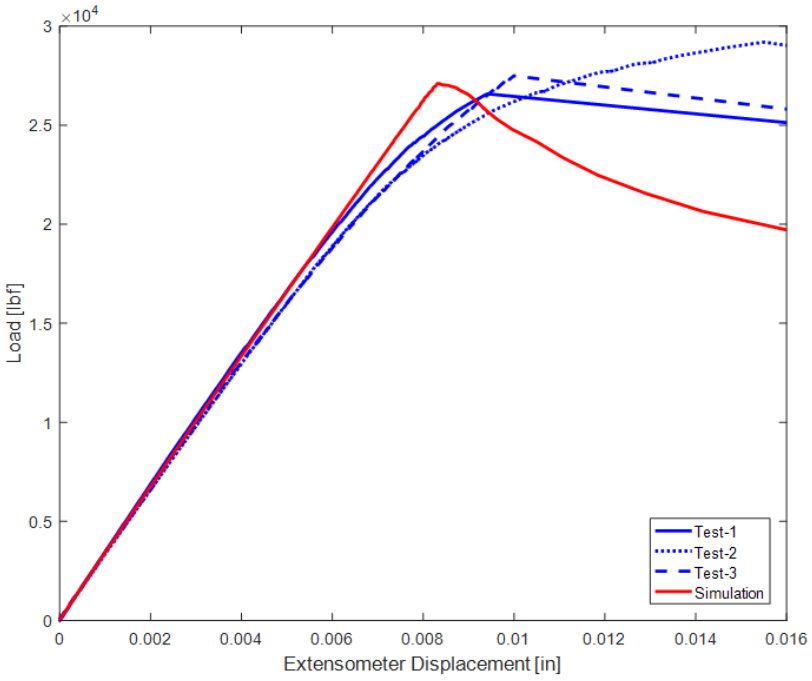

Figure 3.5: Open hole tension simulation of C2 laminate

3.2 Filled Hole Tension

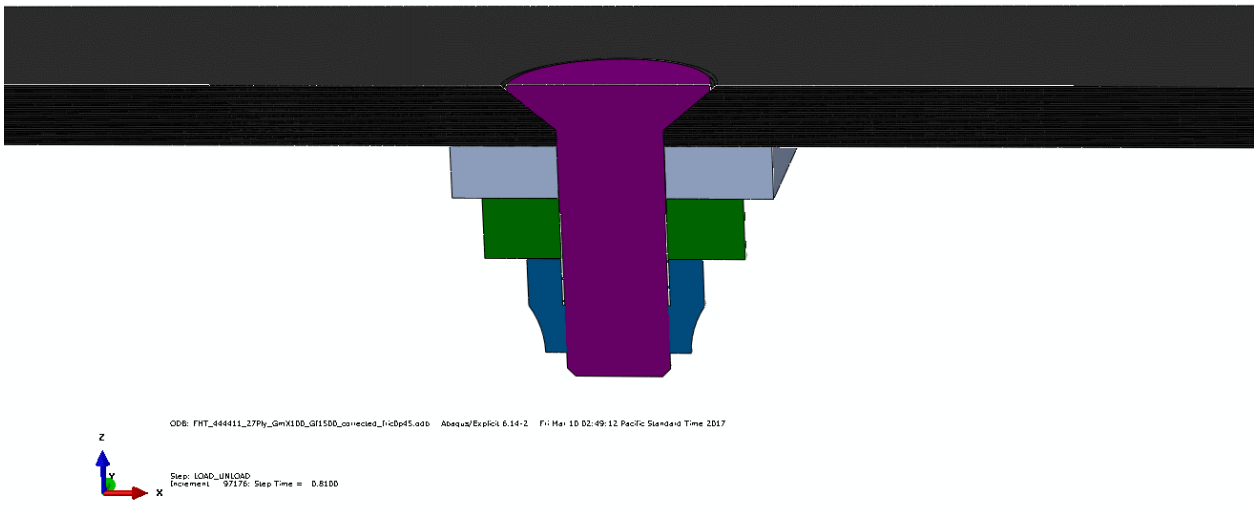

Figure 3.6: Filled Hole Tension FE Model

A section view of the filled hole tension model is shown in figure 3.6. Composite coupon in the model has the same mesh as the open hole tension model. The analysis was carried out as a two step process with the first step corresponding to application of pretension of the bolt and the second step corresponding to the static loading till failure.

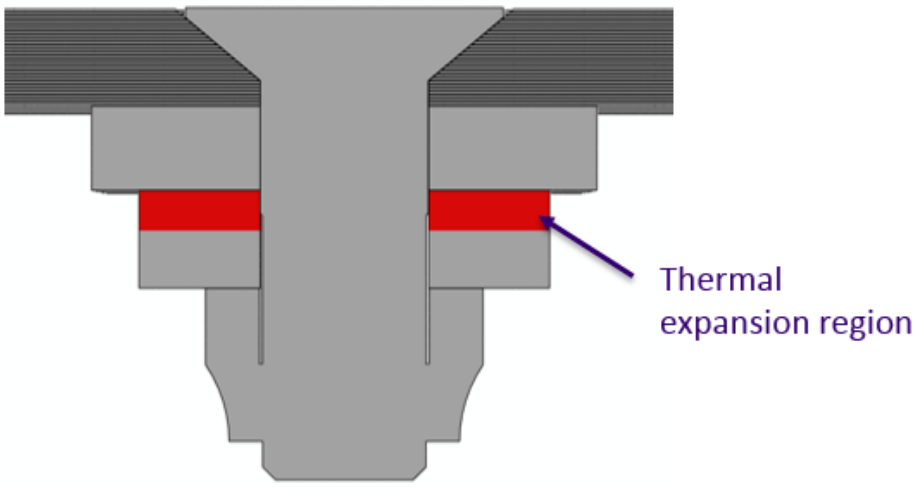

Figure 3.7: Bolt pretension with thermal analysis

Pretension is introduced in the bolt shank with the thermal expansion of the washer as highlighted in figure 3.7. This is similar to the approach used by Egan et al. [14] and ensures the stress accuracy in the countersunk region.

3.2.1 Results and discussion

Filled hole tension analysis of C1 laminate was used for calibrating the toughness correction factors under through thickness compressive stresses. Response of the C1 laminate and the failure patterns at 91% of the peak load are shown in figure 3.8. In comparison to the open hole tension case, the length of the splitting cracks in the 0 layers are smaller, which agrees well with the experimental observation presented by Yan et al. [38]. As a consequence of this stress concentration near the hole, the 0 layer does not get sufficient stress redistribution leading to an early fiber failure initiation. The bolt pretension also causes additional matrix failure in the countersunk region which does not occur in the open hole case. Due to the through thickness constraints, fiber failure process zone develops rather slowly and that causes the global response to have a non-linear behavior. The I2CBM model is able to capture this non-linear region fairly well as seen in the tests. Explicit solver with mass

scaling does cause some additional oscillations in the simulation, but overall the trend is captured very well by the model and agrees well with the experiments. It is noted that the horizontal axes corresponds to extensometer data and not the overall laminate elongation in far-field.

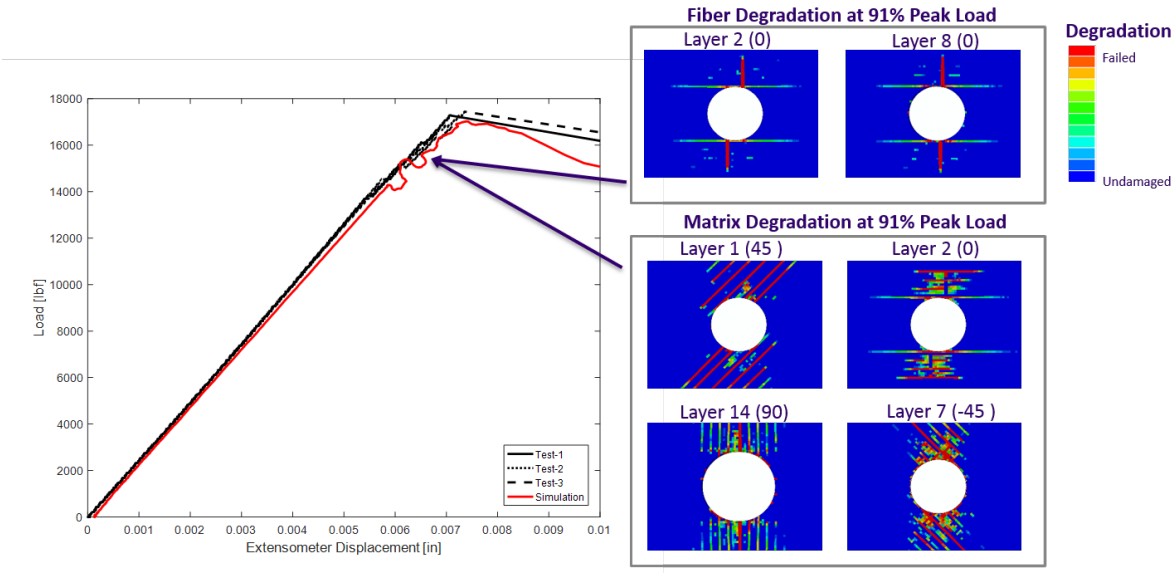

Figure 3.8: Filled hole tension simulation of C1 laminate

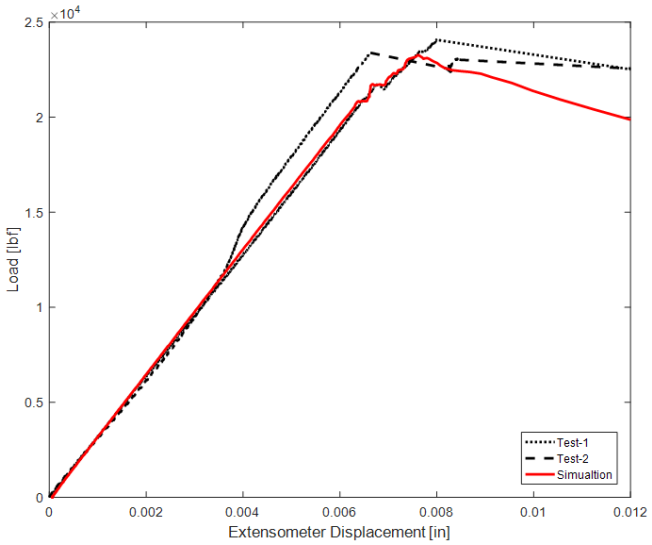

Figure 3.9: Filled hole tension simulation of C2 laminate

C2 laminate also shows similar non-linear region prior to catastrophic failure as shown in figure 3.9. Analysis of this case was run with the calibrated parameters from C1 and the results agree very well with the experiments demonstrating the predictive capability of the method. Failure patterns are similar to that of the C1 case. The extent of the non-linear region in C2 is relatively smaller compared to C1. This is because the percentage of 0 layers in the countersunk region is smaller in the C2 laminate.

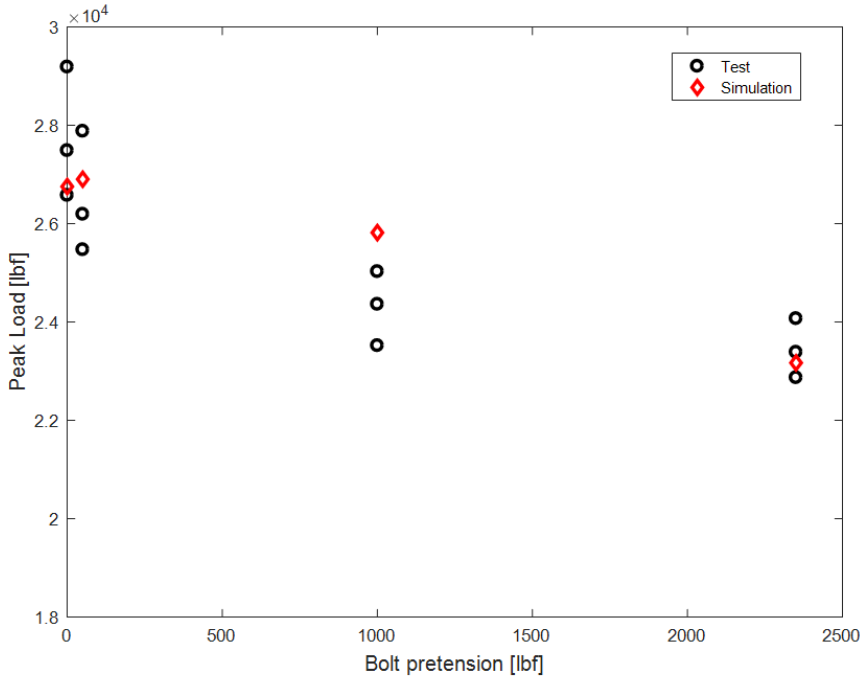

Figure 3.10: Filled hole tension strength vs. bolt preload

Fiber direction toughness corrections presented in equation 2.21, enables the model to capture the effect of bolt pretension on the filled hole tensile strength as shown in figure 3.10. For the case with very low bolt preload (50lbf), both the experiment and the simulation show the response close to the open hole tension case thus adding more confidence to the predictive capability of the I2CBM model.

3.3 Open Hole Compression and Filled Hole Compression

The same FE model shown in figure 3.1 is used for open hole and filled hole compression simulations. The coarse mesh region shown in the figure is prevented from moving in the out of plane direction to ensure that global buckling does not occur.

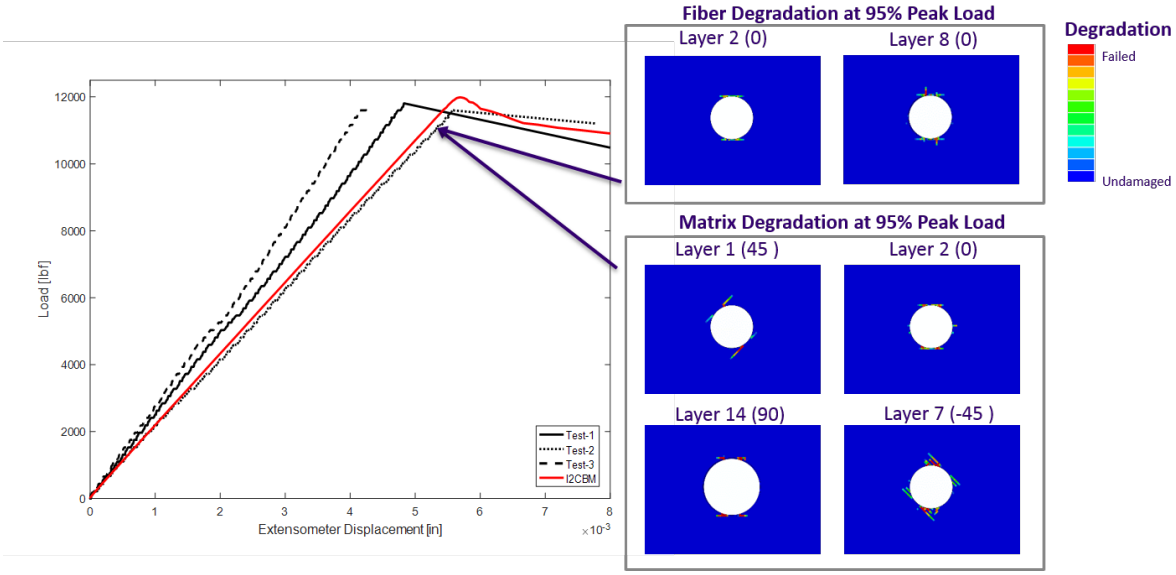

Figure 3.11: Open hole compression simulation of C1 laminate

Figure 3.11 shows the load-displacement comparison between the experiment and the simulations. Ply failure patterns shown by the simulation close to the peak load is also shown in the figure. Unlike the open hole tension case, ply matrix failure patterns are prior to reaching the peak load is not significant. Fracture of the laminate is mostly characterized by the fiber compressive failure which is modeled using crack band. As shown by the experiments and simulations filled hole compression strength is larger than the open hole compression strength. This has to be expected as the fiber compressive failure is characterized by kink band formation or the local buckling of carbon fibers. Bolts and washer in the filled hole coupon can provide a stabilizing effect as it offers spatial constraints with respect to the out of plane movement. Increased bolt pretension further increases this effect increasing the failure load of the specimen. Comparison between the filled hole compression tests and simulation is shown in figure 3.12. Sensitivity study with respect to the bolt pretension value is also shown in figure 3.13. Strength values predicted by I2CBM agrees very well with the experiments and it validates that the fracture toughness correction approach presented in equation 2.22.

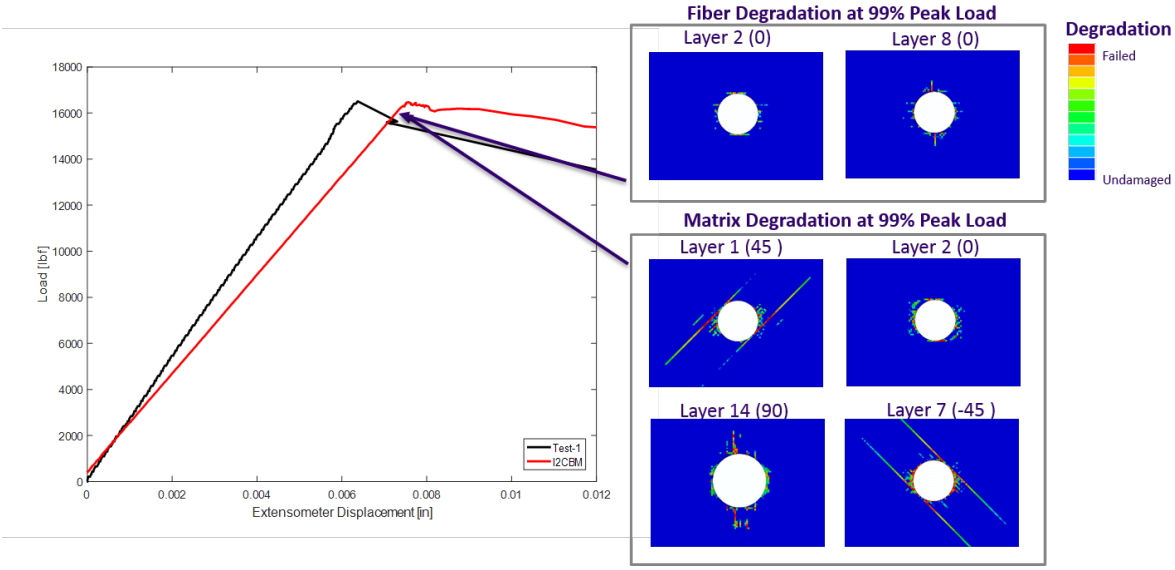

Figure 3.12: Filled hole compression simulation of C1 laminate

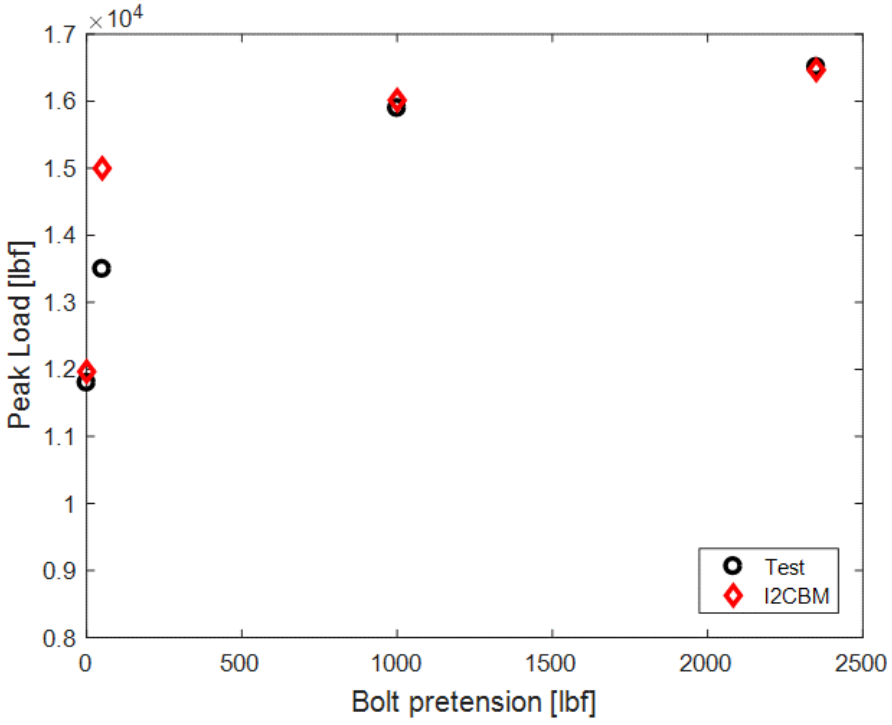

Figure 3.13: Filled hole compression strength vs. bolt preload

3.4 Conclusions

The I2CBM progressive damage and failure analysis tool is able to capture the complex failure mechanisms involved in the open hole tension and filled hole tension cases are demonstrated using a countersunk hole configuration. Non-local crack tracking methods and failure interaction features in the method facilitates the gradual splitting crack growth in 0 layers as observed in experiments. Effect of the through thickness constraints are modeled using toughness changes caused by lateral constraint stresses. The calibration step was performed for the C1 laminate and predictive results obtained for the C2 laminate with the same set of input parameters. Filled hole bolt pretension sensitivity study demonstrate the predictive capability of the analysis tool. Similar to the experiments, the model predictions capture the non-linear region in the filled hole tension load-displacement plot prior to two piece failure.

Chapter 4

BOLTED JOINT SIMULATIONS

Even though composites material are finding increasing use in aviation and automotive sectors, the primary joining mechanism in most applications remain bolted joints. Unlike bonding, bolted joints provide ease in maintainability and less prone to failure due to manufacturing induced failure. However, wherever there is a joint, bolted or bonded, it will still be a likely site of damage and failure initiation in a structure. This is due to the fact that bolts require holes (or cut-outs) which act as a stress riser within a structure. Hence, the need to properly size the bolted joint becomes of utmost concern in a structural design.

Bolted joint analysis, using a computational framework, and that which is applicable for modern aerospace structures, is a significant challenge owing to the complex nature of loading, and subsequent damage and response of the damaged material. There are two parts to a bolt load, first the contact load on the hole inside surface, which is largely compressive. Second, the overall tensile load experienced by the bearing by-pass ligament. Hence, if one were to isolate the failure regions, it would be the compressive/shear damage and failure due to the bolt contact load and the tensile/shear damage and failure in the bypass ligament. There is however, significant interaction between the two regions, which can cause net section failure, shear-out failure, bearing failure or any combination of the above [13].

Considerable literature is available which have identified the influencing parameters on failure of bolted joints. As with general application of laminated composites, bolt bearing strength is influenced by stack-up, hole size, ratio of hole diameter to width, ratio of hole diameter to free edge in loading direction [9, 1]. In addition, bearing strength of bolted joints are significantly influenced by clamp up load [10, 30, 8]. Higher clamp up loads tend to increase bearing strength, however it also can change the mode of failure. Clamp up

loads introduce both through thickness confinement of the composite, as well as friction. The process of bearing failure due to through thickness confinement is well explained via experimental and microCT imaging by Xiao et al [35] and Wang et al [34]. Their results show that bearing strength is influenced by the compressive strength of the 0° ply. Ultimate strength, on the other hand, is due to much more complicated set of failure sequence. As the loading progresses, the 0° plies split, leading to failure in other off axis plies, which cause shear failure. Further loading induces bending of the undamaged ligament causing extensive delamination and 90° matrix failure. The complete two piece failure of a bolted joint has almost all possible failure modes associated with a composite material, making prediction using numerical methods challenging.

Finite Element Analysis of bolted joint bearing strength prediction has been conducted in the past for pin loaded [3, 18] and bolted [7, 36, 20] composite lap joints. Both continuum damage and failure models [7] and Discrete failure models like XFEM [1] have been employed. Much of the past work has been concentrated on the prediction of bearing failure, however, as demonstrated by Crews [10], bearing failure and ultimate failure can differ quite significantly in magnitude especially under high bolt clamp up loads. Simulating progressive failure upto ultimate load in a finite element framework, will require a model which captures in plane and out of plane failure modes and the interaction of the two.

In this study a new 3D Inter-Intra Crack Band Model (I2CBM) is proposed which takes into account through thickness clamp load induced change in compressive behavior and the interaction between inter and intra laminar failures. In next sections a detailed explanation of I2CBM model is provided, followed by numerical analysis conducted and compared against two bolted joint configurations, a Double Lap Shear Bolted Joint (DLBJ) and a Single Lap Shear Bolted Joint (SLBJ).

DLBJ and SLBJ tests were conducted for a generic 36 ply composite laminate with hole diameter (D) of 0.25". Both specimens have a specimen width to diameter (W/D) ratio of 6 and edge distance of 1.5*D. Composite laminate were modeled using a layer-by-layer approach where each layer of the composite ply and matrix layer is modeled explicitly.

Laminate was design for a 44% - 0°, 44% - ± 45° and 12% - 90° plies.

To reduce the model size, a refined fiber aligned mesh region was generated around the bolt (figure 4.1,4.2). The mesh size in this region follows Bazant's criteria [4] which provides an upper limit to the mesh size for a given energy release rate. The fine region is smoothly transitioned to the coarse region.

The complete bolted joint analysis is conducted using ABAQUS explicit. It is a two step analysis where the first step is to simulate bolt pre-tension load and the second, the progressive failure. Bolt pre-tension load is introduced by conducting a thermal analysis of the bolt. With initial temperature of the bolt shank kept at zero degrees K, a negative temperature boundary condition was applied on the bolt shank. Material thermal properties were modified such that the bolt shank contracts only in the axial direction, hence inducing bolt pre-tension.

General contact algorithm is used for all interface regions. An erosion set is defined for the fine mesh region where the bolt is expected to elongate and erode the mesh. By defining an erosion set and defining internal surfaces, the code is able to re-generate the contact surfaces as the elements are eroded. Thus, ensuring force transfer as the elements get deleted.

In DLBJ, composite specimen is bolted between two steel reaction skins. FEM model for DLBJ is shown in figure 4.1, Here, relative displacement measurements are made with an extrensometer attached to the steel plates and composite test specimen, while the loading is applied in a load-controlled setting. SLBJ has a countersunk hole and bolted to a steel plate. The specimen was loaded and then unloaded under displacement control. The dimensions, mesh and boundary conditions are shown in figure 4.2.

Experimental results found in the literature show the absence of delamination in the region where the effect of bolt pretension is transferred to the specimen[35]. Hence intra-inter communication is disabled in the region under the washer and the delamination strength values are set high to prevent it's occurrence. It was observed in the simulation that the premature delamination failure near the hole reduces the effectiveness of modeling bearing failure using residual stress state. Correct delamination strength values and intra-inter com-

munication are used in all the other regions for effectively capturing the final two-piece failure mechanism.

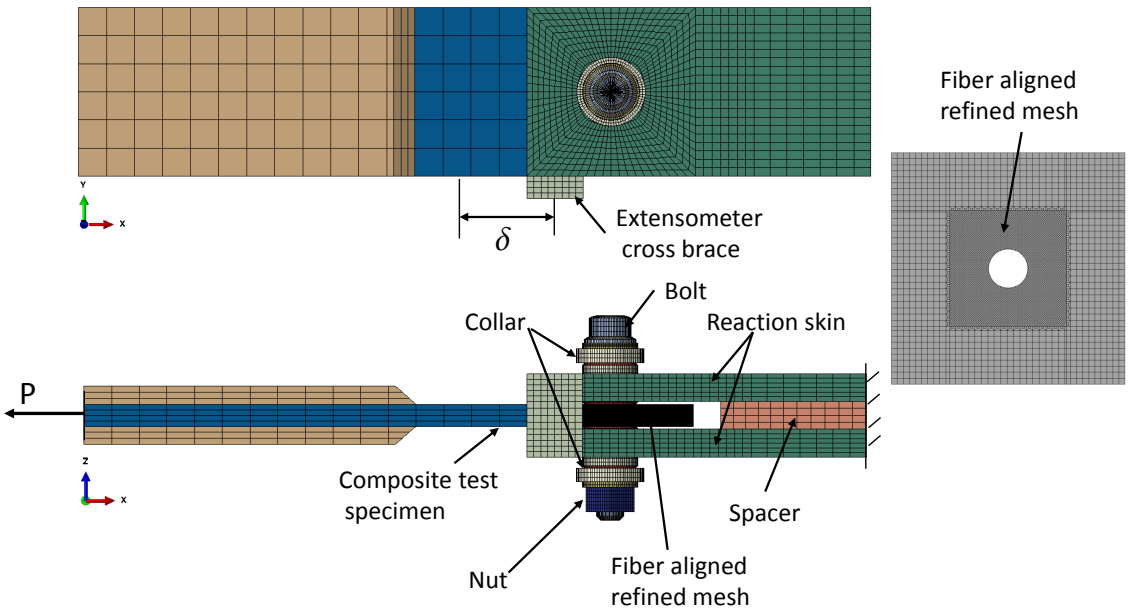

Figure 4.1: Double Lap Shear Bolted Joint model

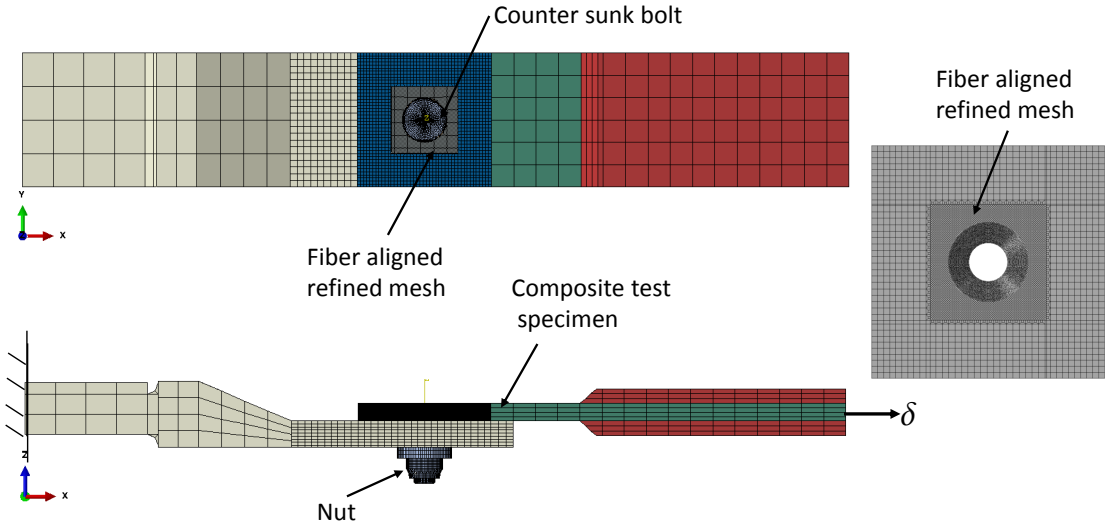

Figure 4.2: Single Lap Shear Bolted Joint model

4.1 Double Lap Shear Bolted Joint

Load-displacement response of the DLBJ is compared against experimental data in figure 4.3. The initial non-linearity in the response indicated as point A, is caused by the bearing failure and the section view of the failure pattern at that point is also shown in figure 4.3. Peak load is captured well in the simulation because of the model's ability to capture the bearing failure mechanism accurately. The reason for the error in the initial stiffness in the simulation is unknown and it is possibly caused by uncertainty in experimental measurements and/or uncertainty in *in-situ* lamina elastic properties. Similar to the experiment, simulation was carried out using load controlled boundary conditions. The trend in the post peak behavior of the simulation agrees well with the experiment and the failure events in the post peak region are catastrophic and dynamic in nature due to the load controlled boundary condition. However the model is able to capture the post peak failure mechanisms fairly well. The failure pattern in various layers at the bearing load is shown in figure 4.4. Splitting cracks in the 0 layer and shear cracks tangent to the hole in the 45 layer are dominant. Also, the fiber

failure regions are localized in each ply according to fiber orientation.

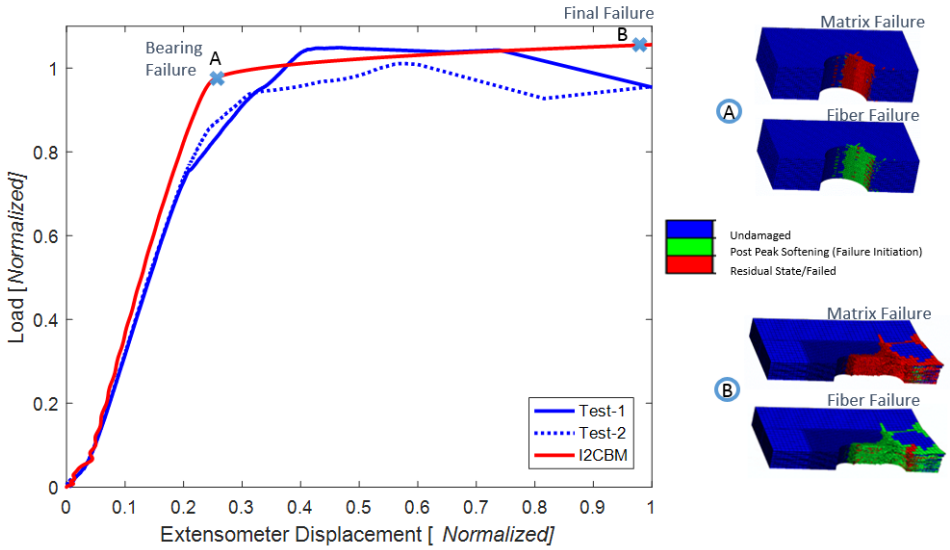

Figure 4.3: Load-displacement repsonse of double lap shear bolted joint

Figure 4.5 compares the final failure pattern in the simulation with the failed specimen. Failed specimens show predominantly bearing and tear out failure mechanism. Capability of the model to behave in a very stable manner throughout the catastrophic failure events is remarkable. Element size change in the model was kept intentionally to test the ability of the model to capture the two piece failure as observed in the experiment. Stress concentrations created by the change in mesh size act as the point at which final two piece failure occurs. The deletion scheme used in the simulation removes the elements undergoing excessive distortion and hence is not shown in the images. The model could not capture some of the delamination and 90 layer transverse crack failure mechanisms shown in the figure and it can be attributed to the dynamic nature of the failure events. Also, from a design point of view, the post peak failure mechanisms are not very important. The model showed negligible yielding in the bolt and the same was observed in the experiments.

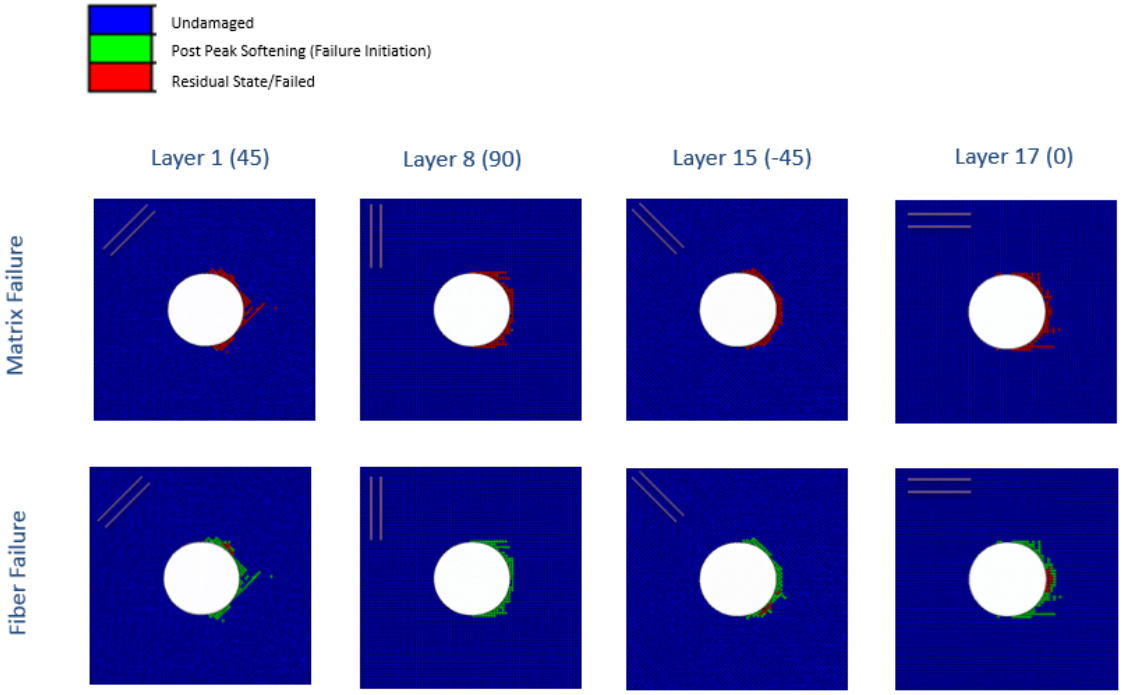

Figure 4.4: Failure pattern in double lap shear bolted joint at bearing load

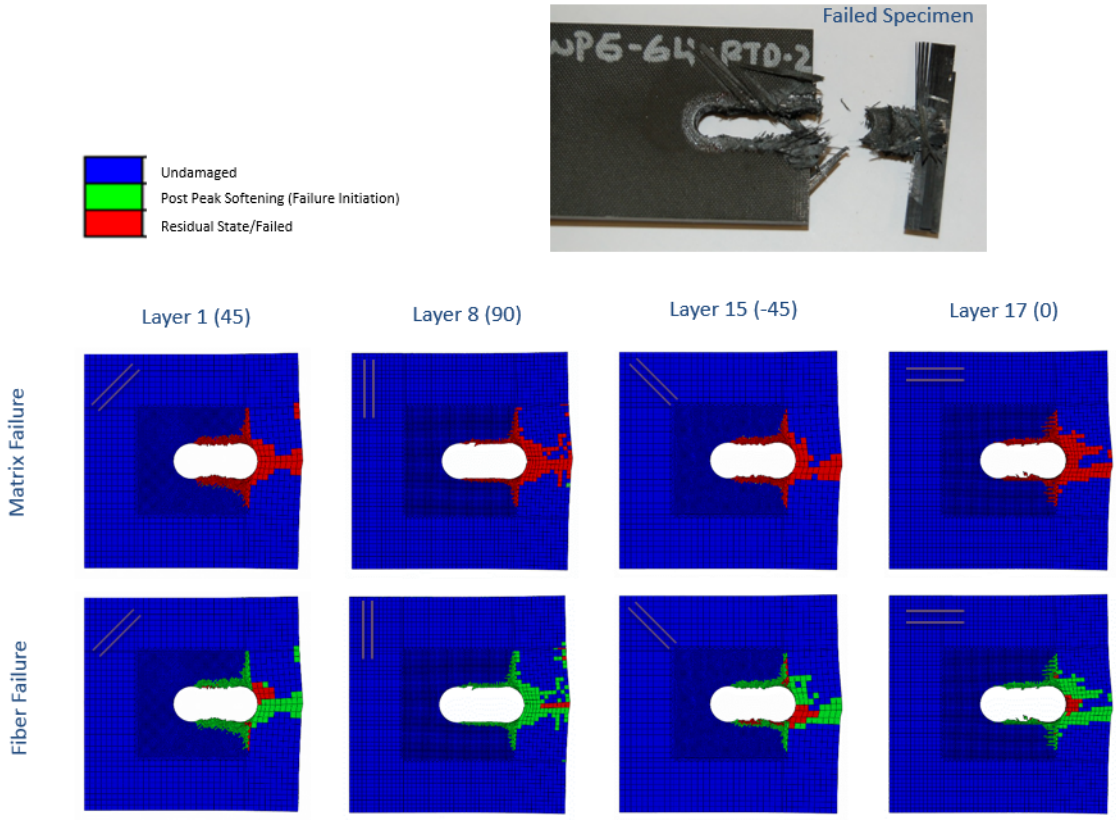

Figure 4.5: Final failure pattern in double lap shear bolted joint

4.2 Single lap Shear Bolted Joint

The SLBJ specimen was tested and simulated using displacement controlled loading. Griping end of the specimen was loaded to a particular displacement value and then unloaded back to zero displacement. The load-displacement response shows excellent agreement with the experiment (figure 4.6). Similar to the DLBJ results, there is disagreement in the initial stiffness value of the response. The initial non-linear part of the loading curve is caused by the bearing failure in the composite as indicated at point A. This initial non-linear also agrees fairly well with the experiment. Subsequent non-linear region is a combination of laminate bearing failure and bolt yielding. At point B in the curve, bolt yielding becomes a significant event and . Failure pattern in the specimen is compared against the test specimen in figure

4.7. Both the failed region in the specimen and yielding in the bolt agree very well with the experimental data. Accuracy of the unloading curve is highly dependent on the laminate damage and bolt yielding during the loading step. The yielded bolt causes a contact with the other side of the counter sunk hole during an early stage of the unloading part and eventually leads to a negative load when unloaded fully. The analysis shows remarkable agreement with experiments in the unloading path, suggesting that the model is able to capture the bearing failure mechanism very well. Discrepancy in the final load state at the end of unloading is caused by the error in contact calculations when the edge of the bolt head comes in contact with the countersunk hole region.

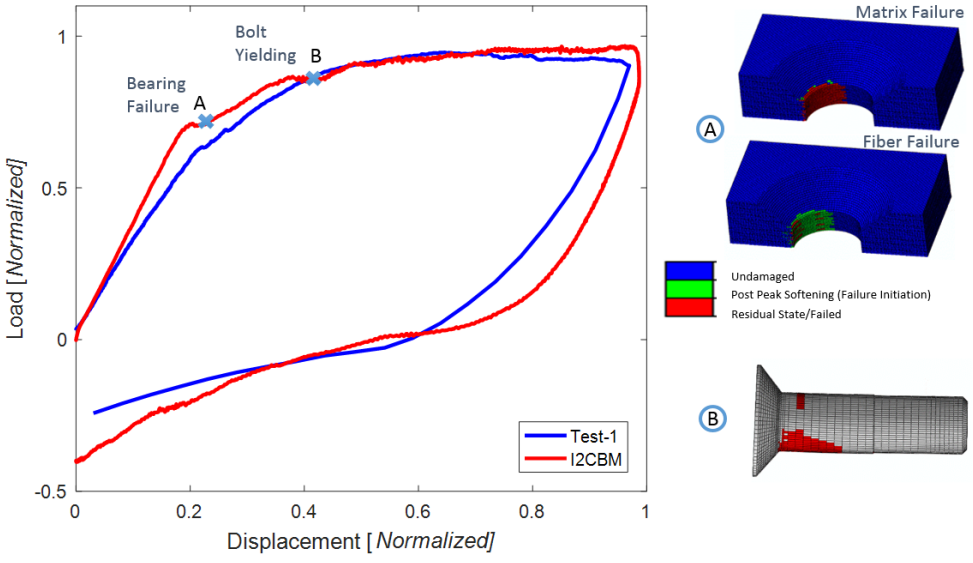

Figure 4.6: Load-displacement repsonse of single lap shear bolted joint

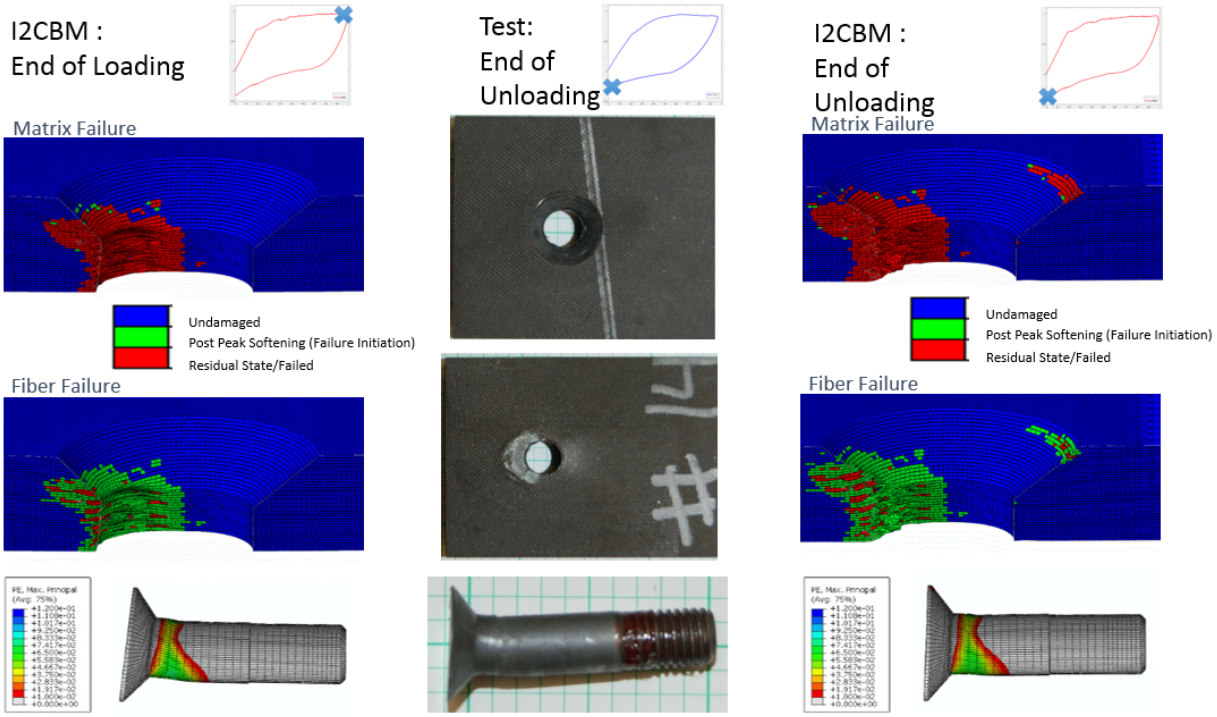

Figure 4.7: Final failure pattern in single lap shear bolted joint

All the simulations were carried out using 80 processors with Abaqus 6.14 explicit solver. The loading step took 15 hrs to complete for a model of 500,000 elements.

4.2.1 Effect of Laminate Thickness and Bolt Pretension

Effect of the laminate thickness on the single lap shear joint response is studied using three layups layups [45/0/-45/0/90/0/-45/0/45]3 (C1), [45/0/-45/0/90/0/-45/0/45]4 (C2) and [45/0/-45/0/90/0/-45/0/45]5 (C3). Comparison between experiments and simulations for these three cases are presented in figures 4.8, 4.9 and 4.10 respectively. Simulation of the C1 laminate showed a bit higher load than the experiment while the other layups showed great agreement with the experiment. Failure patterns in these cases are similar to the patterns shown in figure 4.7.

Load vs. displacement response for the C2 laminate for different preload values (2350lbs,

1000lbs and 100lbs) are presented in figures 4.9, 4.11 and 4.12. Experimental and simulation results does not show any significant sensitivity to the bolt preload value. Similar results were obtained for the other laminates as well and hence is not shown here.

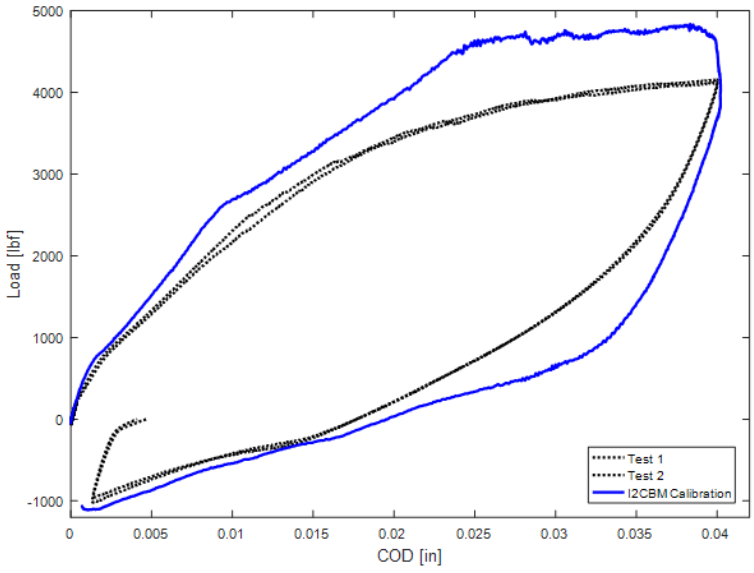

Figure 4.8: Load-displacement repsonse of C1 laminate

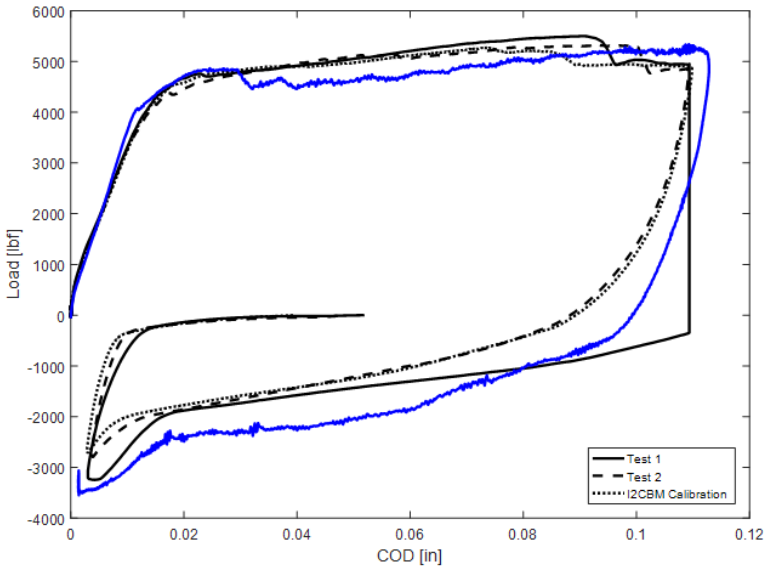

Figure 4.9: Load-displacement repsonse of C2 laminate

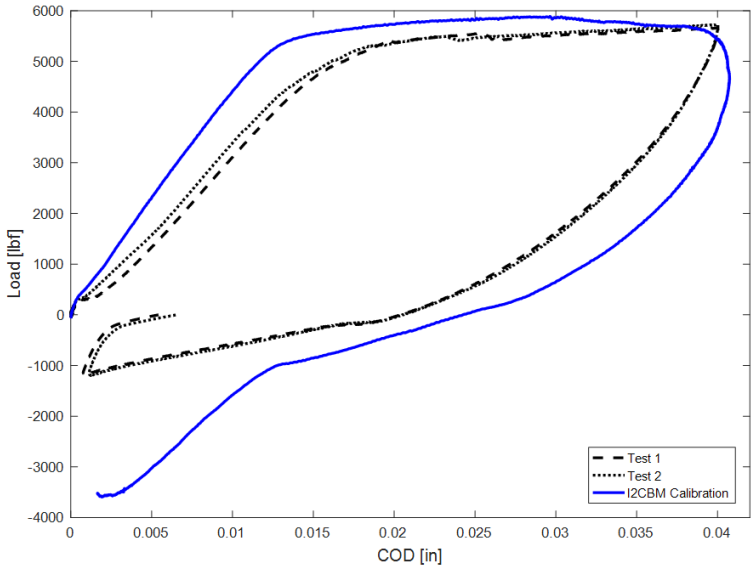

Figure 4.10: Load-displacement repsonse of C3 laminate

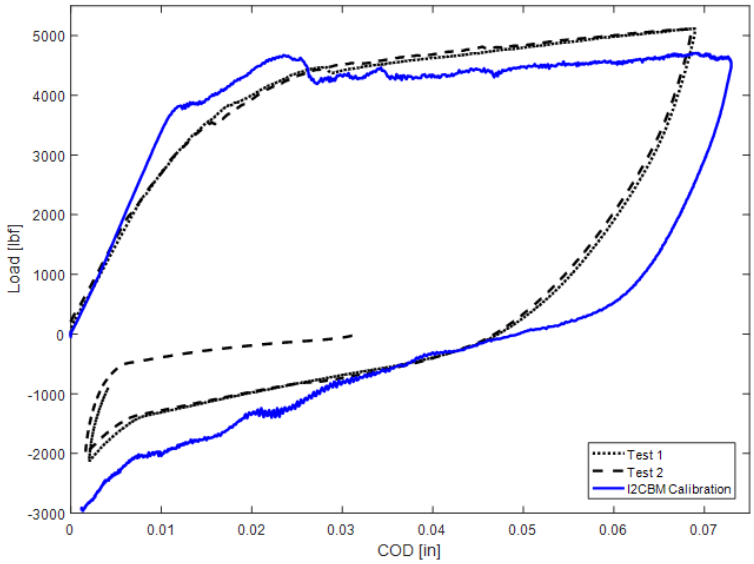

Figure 4.11: Load-displacement repsonse of C2 laminate : 1000lbs bolt pretension

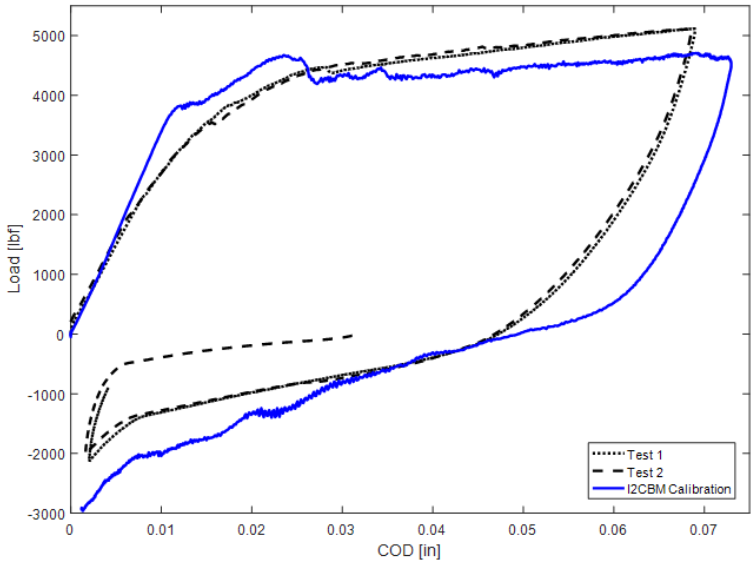

Figure 4.12: Load-displacement repsonse of C2 laminate : 100lbs bolt pretension

4.3 Conclusions

The I2CBM model for progressive failure analysis of composites is introduced and used to model single lap shear and double lap shear bolted joints. The residual stress state modeling is able to accurately characterize the bearing failure mechanism observed in bolted joints. The model displayed exceptionally stable behavior even during catastrophic failure events due to the robust failure and element deletion schemes used. The model is also able to capture th effect of the laminate thickness well for the layups considered.

Chapter 5

CONCLUSIONS AND FUTURE WORK

5.1 Original Contributions

1. A 3D progressive failure analysis model which combines Schapery theory with crack band failure model was developed for application to static strength analysis problems. Existing 2D Schapery formulation was extended to 3D state of stress as part of this work. Crack band model is based on three generalized crack planes and their mutual interactions can potentially capture all the failure modes observed in composites with the limitations of a homogenized modeling approach. The model can do predictive simulations with a standard set of coupon level test data as the input.

2. A novel incremental mixed mode evolution law based on physically meaningful assumptions has been developed and implemented. The method is much simpler and intuitive compared to all the other mixed mode evolution laws existing in the literature. The method is ensures that all the tractions at the crack plane vanish simultaneously and is generic enough to adapt to desired failure and energy criteria.

3. A smart global crack spacing scheme was developed as part of this thesis. It can keep a record of all the matrix cracks present in various layers in the laminates irrespective of the number of processors used in the finite element analysis. This approach can use the crack spacing as a material/geometry parameters and can produce failure patterns as observed in experiments. Similar approaches existing in the literature requires the insertion of cohesive elements in predefined crack paths. But this approach picks the crack paths based on the local stress state in a continuum failure analysis frame work.

4. A scheme for interaction between in-plane failure and associated delamination is implemented. This helps in overcoming some of the difficulties associated with homogenized

modeling of composites and can trigger the delamination based on adjacent ply in-plane failure initiation.

5. Predictive capability of the I2CBM simulation tool is demonstrated using various open hole and filled hole simulations. Simulations agree well with experiments both in terms of the global load-displacement response and failure patterns. A model for the fiber toughness correction as a function of the triaxial stress state is introduced and demonstrated through the pretension sensitivity study in filled hole tension/compression simulations.

6. Modeling of the bearing failure through residual stress approach is demonstrated and validated through various bolted joint simulations. The model is able to accurately capture the behavior of the single and double shear lap joint configurations for various layups and laminate thickness values.

5.2 Future Work

1. Sensitivity of the model with respect to crack spacing parameters has to be further studied and understood better. The method has demonstrated the capability to capture critical failure mechanism such as a splitting crack growth in open hole/filled hole simulations. The determination of crack spacing parameters has to be come from analytical/micro-mechanics FE/experimental studies, which were beyond the scope of this thesis and hence not studied. With accurate determination of parameters, the method can be be used for capturing the complex failure mechanisms observed in coupon level tests of layups such as $[90/0]_s$ and $[45/-45]_s$.

2. Comparison between micro-mechanics model and intra-inter interaction enabled homogenized model can provide additional insights into importance of failure mode interactions. This can push the homogenized modeling approach to it's maximum accuracy and efficiency.

3. I2CBM accounts for three pre-defined crack planes with the crack band model. This method of modeling can potentially capture failure in any plane as long as the mutual interactions between the predefined failure planes (especially all the modes which are associated with matrix failure) are well understood. Micro-mechanics based study can help this process

and can tune the I2CBM model to produce the exact response observed in a micro-mechanics simulation.

4. Various simulation cases presented in this thesis shows that the tool can be used as a predictive tool. In order to be used a virtual testing tool, it has to undergo rigorous tests with different layup and material configurations. This can be carried out using the test data available in the literature as well as with the experimental data presented in the Appendix A.

5. Extension of the model to fatigue loading applications is in progress. Inputs needed for the model and sensitivity of the simulations with respect to modeling parameters are to be understood.

6. The model has to be tested for simulating dynamic loading scenarios such as face on and edge on impact problems.

7. Environmental factors such temperature and moisture can influence the load bearing capacity of composite structural parts. The cost associated with tests under different environmental conditions are quite high and hence is a problem of great interest to airframers. These effects have to be incorporated into the current failure analysis tool.

8. Modeling of fiber compressive failure under transverse compressive stresses is achieved using residual stress approach and fiber fracture toughness correction with transverse stresses. For the layups and loading cases considered here, this approach works good but it has to be tested against different layups and material systems to understand if the parameters change as a function of the layup. Establishing standard coupon level tests to calibrate these parameters can also be beneficial.

9. The approach presented in this thesis randomly distributes the strength values at all the points on a test coupon. This means hat there is no correlation between strength values at any two points. However in reality spatial correlation can exist and the future work can focus on incorporating this into the analysis and study if it can effectively capture localized cracks.

BIBLIOGRAPHY

[1] Hilton Ahmad, AD Crocombe, and PA Smith. Strength prediction in cfrp woven laminate bolted double-lap joints under quasi-static loading using xfem. *Composites Part A: Applied Science and Manufacturing*, 56:192–202, 2014.

[2] J. H. Ahn and A. M. Waas. Prediction of compressive failure in laminated composites at room and elevated temperature. *AIAA Journal*, 40(2):346–358, 2002.

[3] Alaattin Aktaş, Hüseyin İmrek, and Yusuf Cunedioğlu. Experimental and numerical failure analysis of pinned-joints in composite materials. *Composite structures*, 89(3):459–466, 2009.

[4] Z. P. Bazant and B. H. Oh. Crack band theory for fracture of concrete. *Materiaux et constructions*, 16(93):155–177, 1993.

[5] S. Boyd, W. Ji, A. P. K. Joseph, and A. M. Waas. Single edge notch tension test on cross-ply laminated composites for intralaminar fracture properties. In *55th AIAA/ASME/ASCE/AHS/SC Structures, Structural Dynamics, and Materials Conference*, National Harbor, Maryland, 2014.

[6] P. P. Camanho and G. Catalanotti. On the relation between the mode i fracture toughness of a compoiste laminate and that of a 0 py; analytical model and experimental validation. *Engineering Fracture Mechanics*, 78:2535–2546, 2011.

[7] PP Camanho and FL Matthews. A progressive damage model for mechanically fastened joints in composite laminates. *Journal of Composite Materials*, 33(24):2248–2280, 1999.

[8] TN Chakherlou, B Abazadeh, and Jeffrey Vogwell. The effect of bolt clamping force on the fracture strength and the stress intensity factor of a plate containing a fastener hole with edge cracks. *Engineering Failure Analysis*, 16(1):242–253, 2009.

[9] TA Collings. The strength of bolted joints in multi-directional cfrp laminates. *Composites*, 8(1):43–55, 1977.

[10] John H Crews. Bolt-bearing fatigue of a graphite/epoxy laminate. In *Joining of composite materials*. ASTM International, 1981.

[11] P. Davidson, E. J. Pineda, C. Heinrich, and A. M. Waas. A unified model for predicting the open hole tensile and compressive strengths of composite laminates for aerospace applications. In *AIAA/ASME/ASCE/AHS/ASC 54th Structures, Structural Dynamics, and Materials Conference*, Boston, MA, 2013.

[12] Anthoy M. Waas Dianyun Zhang and Chian-Fong Yen. Progressive damage and failure response of hybrid 3d textile composites subjected to flexural loading, part ii: mechanics based multiscale computational modeling of progressive damage and failure. *International Journal of Solid and Structures*, 75-76:321–335, 2015.

[13] D Duthinh. Connections of fiber-reinforced polymer (frp) structures. a review of the state of the art. *NIST Report*, NISTIR 652, 2000.

[14] B. Egan, C.T. McCarthy, M.A. McCarthy, P.J. Gray, and R.M. Frizzell. Modelling a single-bolt countersunk composite joint using implicit and explicit finite element analysis. *Computational Materials Science*, 64:203–208, 2012.

[15] S.R. Hallett, B.G. Green, W.G. Jiang, and M.R. Wisnom. An experimental and numerical investigation into the damage mechanisms in notched composites. *Composites*, 40:613–624, 2009.

[16] A. P. K. Joseph, A. M. Waas, W. Ji, and E. J. Pineda. The est model for predicting progressive damage and failure of open hole bending specimens. In *AIAA/ASME/ASCE/AHS/ASC 57th Structures, Structural Dynamics, and Materials Conference*, San Diego, CA, 2016.

[17] A. P. K. Joseph, A. M. Waas, W. Ji, E. J. Pineda, S. L. Liguore, and S. P. Wanthal. Progressive damage and failure prediction of open hole tension and open hole compression specimens. In *AIAA/ASME/ASCE/AHS/ASC 56th Structures, Structural Dynamics, and Materials Conference*, Kissimmee, FL, 2015.

[18] Larry B Lessard and Mahmood M Shokrieh. Two-dimensional modeling of composite pinned-joint failure. *Journal of composite materials*, 29(5):671–697, 1995.

[19] K. Marlette. Hexcel 8552 im7 unidirectional prepreg 190 gsm & 35%rc qualification material poperty data report. Ncamp test report cam-rp-2009-015 rev a, NIAR, Wichita State university, 2011.

[20] MA McCarthy, CT McCarthy, VP Lawlor, and WF Stanley. Three-dimensional finite element analysis of single-bolt, single-lap composite bolted joints: part imodel development and validation. *Composite structures*, 71(2):140–158, 2005.

[21] Nicolas Mos, John Dolbow, and Ted Belytschko. A finite element method for crack growth without remeshing". international journal for numerical methods in engineering. *International Journal for Numerical Methods in Engineering*, 46(1):131–150, 1999.

[22] J. A. Nairn. The strain-energy release rate of composite microcracking - a variational approach. *Journal of Composite Materials*, 23:1106–1129, 1989.

[23] W. H. Ng, A. G. Salvi, and A. M. Waas. Characterization of the in-situ non-linear shear response of laminated fiber-reinforced composites. *Composites Science and Technology*, 70:1126–1134, 2010.

[24] Nhung Nguyen and Anthoy M. Waas. A novel mixed-mode cohesive formulation for crack growth analysis. *Composite Structures*, 156:253–262, 2016.

[25] O.J. Nixon-Pearon, S.R. Hallett, P.W. Harper, and L.R Kawashita. Damge development in open-hole composite specimens in fatigure. part 2: numerical modeling. *Composite Structures*, 106:890–898, 2013.

[26] E. J. Pineda and A. M. Waas. Numerical implementation of a multiple-isv thermodynamically-based work potential theory for modeling progressive damage and failure in fiber-reinforced laminates. *International Journal of Fracture*, 182(1):93–122, 2013.

[27] W. Ramberg and W. R. Osgood. Description of stressstrain curves by three parameters. *Technical Note No. 902*, 1943.

[28] S. Rudraraju, A. Salvi, K. Garikipati, and A. M. Waas. Predictions of crack propagation using a variational multiscale approach and its application to fracture in laminated fiber reinforced composites. *Composite Structures*, 94(11):3336–3346, 2012.

[29] R. A. Schapery. A theory of mechanical behavior of elastic media with growing damage and other changes in structure. *Journal of Mechanics and Physics of Solids*, 38(2):215–153, 1990.

[30] Kunigal N Shivakumar and John H Crews. Bolt clampup relaxation in a graphite/epoxy laminate. In *Long-term behavior of composites*. ASTM International, 1983.

[31] D. L. Sicking. *Mechanical characterization of nonlinear laminated composites with transverse crack growth*. PhD thesis, Texas A&M University, College Station, Texas, 1992.

[32] DSC Simulia. *Abaqus User Manual - V6.12*. DSC Simulia, 2012.

[33] M. P. F. Sutcliffe, S. L. Lemanski, and A. E. Scott. Measurement of fiber waviness in industrial composite components. *Composites Science and Technology*, 72:2016–2023, 2012.

[34] Hong-Sheng Wang, Chang-Li Hung, and Fu-Kuo Chang. Bearing failure of bolted composite joints. part i: experimental characterization. *Journal of Composite Materials*, 30(12):1284–1313, 1996.

[35] Yi Xiao and Takashi Ishikawa. Bearing strength and failure behavior of bolted composite joints (part i: Experimental investigation). *Composites Science and Technology*, 65(7):1022–1031, 2005.

[36] Yi Xiao and Takashi Ishikawa. Bearing strength and failure behavior of bolted composite joints (part ii: modeling and simulation). *Composites science and technology*, 65(7):1032–1043, 2005.

[37] W. Xu and A. M. Waas. On the crack band model and its practical implementation in commercial finite element codes. *Engineering Fracture Mechanics (to be published)*, 2014.

[38] Y. Yan, W.D. Wen, F.K. Chang, and P. Shyprykevich. Experimental study on clamping effects on the tensile strength of composite plates with a bolt-filled hole. *Composites*, 30:1215–1229, 1999.

Appendix A

PROGRESSIVE DAMAGE AND FAILURE PREDICTION OF OPEN HOLE TENSION AND OPEN HOLE COMPRESSION SPECIMENS

This work was presented at the AIAA/ASME/ASCE/AHS/ASC 56th Structures, Structural Dynamics, and Materials Conference and the paper is available in the open literature [17]

A.1 Abstract

Progressive damage and failure in open hole composite laminate coupons under tensile and compressive loading conditions is modeled using Enhanced Schapery Theory (EST). The input parameters required for EST are obtained using standard coupon level test data and are interpreted in conjunction with finite element (FE) based simulations. The capability of EST to perform the open hole strength prediction accurately is demonstrated using three different layups of IM7/8552 carbon fiber composite. A homogenized approach uses a single composite shell element to represent the entire laminate in the thickness direction and this requires the fiber direction fracture toughness to be modeled as a laminate property. The results obtained using the EST method agree quite well with experimental results.

A.2 Introduction

The deformation response of laminated fiber reinforced composite panels with open holes can be used to assess modeling tools used in structural integrity and damage tolerance (SIDT) studies. Davidson et al [11] presented a unified model for the open hole tension (OHT) and open hole compression (OHC) strength predictions using Enhanced Schapery Theory[26]

(EST). The EST model is used in the present study to determine the damage and failure evolution in open hole compression and tension specimens made of IM7/8552 material.

EST is proven to be an effective way of modeling the in-plane micro damage and failure evolution in composite laminates. Ability of this model to predict the strength of coupons with holes and notches under remote uniaxial loading conditions has been reported in the literature[26, 11]. In EST, the pre-peak non-linearity caused by micro damage in plies is modeled using polynomial functions which represent how the shear and transverse lamina moduli get affected by the development of micro damage in the polymer matrix. Upon reaching a critical limit in micro damage accumulation, the subsequent failure which is represented as a negative tangent to the slope of the stress-strain response (post peak region) is modeled using crack band theory[4]. Details of the EST formulation can be found in Pineda and Waas, 2013[26].

In this study, the composite laminate is modeled using shell elements and this ensures computational efficiency of the model. Previous studies with EST have considered fiber direction fracture toughness as a material property even when all the layers are modeled using a single shell element. In the present approach this property is calculated as a function of the composite layup according to an approach suggested by Camanho and Catalanotti [6]. EST predictions are compared against open hole tension and open hole compression test data as well as with the test results published in NIAR test report[19] for three different layups of IM7/8552 material.

A.3 Finite Element Modeling

Standard dimensions as per ASTM-D5766 is used for the finite element modeling of the open hole specimens. Dimensions and boundary conditions used for modeling are shown in figure A.1. Out of plane degrees of freedom of all the nodes are restricted and the boundary conditions are applied on the left and right edges of the model. Nodes on the left edge are prevented from in-plane rotation and movement in x-direction, while prescribed displacement values in the x-direction and fixed in-plane rotation conditions are applied to the nodes on

the right edge. EST is implemented as a user material subroutine (VUMAT) within the Abaqus/explicit solver and the in-plane failure of the laminate is modeled using 4-noded reduced integration shell elements (S4R). The same model is used for the open hole compression simulation with the remote loading direction being reversed. The failure/fracture properties used are dependent on the local stress state (tension vs. compression) and this aspect is incorporated in EST. Mesh sizes were determined based on a convergence study of the stress field near the hole and also by considering the element size restrictions imposed by the crack band model.

Three different layups are considered for this study and the layups are listed in table A.1. Differences in the layer interfaces and the directional stiffness of the layups allows to test the applicability of the EST model and also understand it's limitations. The exact same mesh and modeling approach is used for all three layups and it was also found in the study that depending on the layup mesh refinement requirements could be different. The mesh chosen here gives a converged gradient stress field near the hole for all three layups.

A.3.1 Input Parameters

All input parameters required for EST are obtained using coupon level tests and in some cases, using inverse calculations using FE models of the coupon tests. Schapery microdamage functions are crucial for accurate modeling of pre-peak matrix non-linearity and these functions control the change in transverse and shear moduli as function of the micro cracks in the matrix[29, 31]. ± 45 tension tests are used to characterize the elastic damage response of the matrix according to the procedure give in Ng et al [23]. While shear microdamage function is determined directly from the test data, tranverse microdamage function is calculated using a virtual test of the RUC with the matrix equivalent stress strain response backed out from the ± 45 test data as an input[23]. Microdamage functions are expressed as fifth order polynomials and tableA.2 shows the coefficients of the polynomials calculated using the above mentioned method. Micro damage functions in compression are assumed to be same as that in tension for the analyses presented here.

TableA.3 summarizes the lamina strength and fracture input parameters used in the model. Virtual testing is used for calculating fiber direction compressive strength (due to kinking). Fiber misalignment angle of 1.2, which is the typical value found in industrial composites [33], is used in the compressive strength calculation done using micromechanics. Details of such a calculation are outlined in Davidson et al[11]. Different longitudinal stuffness (E_{11}) values are used in tension and compression as observed in the experiments and also reported in the literature [19].

One of the critical factors in modeling the progressive failure using a crack band approach is estimating the correct fracture toughness values as they control the post peak softening behavior and hence the failure evolution. Fiber direction fracture toughness of the 0 layer can be obtained using a single edge notch tension (SENT) test/simulation, of the [90/0]s specimen as reported in Boyd et al.[5]. This value is then scaled for different layups as discussed in the following section, using the approach suggested by [6]. For compressive loading, fiber direction overstress fracture toughness is not known and it is assumed to be about 25% of the value in tension. This assumption is further validated by comparing with the test results. Intralaminar mode I and mode II fracture toughness values are assumed to be the same as the corresponding interlaminar properties obtained from DCB and ENF tests. Matrix mode I fracture toughness in compression is assumed to be same as in tension.

A.3.2 Fracture Toughness Corrections

Composite shell elements ensure same in-plane strains for all the layers in the laminate and this in turn establishes the relative stresses in the layers as a function of the layup. Strain compatibility conditions between the layers add constraints to the model and this will lead to all the layers dissipating energy in the event of failure. But in reality this might not happen as delamination modes can dissipate energy and relax some layers. Hence using the fiber fracture toughness of the 0 layer for all the layers could be incorrect and will lead more energy dissipation than what is required depending on the laminate stacking. Camanho and Catalatonni [6] developed a model to determine the fracture toughness of the laminate as a

function of lamina fracture toughness. Fracture toughness of the i-th layer is calculated as a function of the material properties and 0 layer fracture toughness using Classical Lamination Theory and Linear Elastic Fracture Mechanics as given in the equation below.

$$G_c^i = \frac{E_{eq}^0}{E_{eq}^i} \frac{\chi^{i^2}}{\chi^{0^2}} \Omega^{i^2} G_c^0 \tag{A.1}$$

Assuming self-similar crack growth in all layers, effective laminate fracture toughness is calculated as the weighted average of the toughness of the individual layers.

$$G_c^L = \frac{\sum_i G_c^i t^i}{t^L} \tag{A.2}$$

Laminate fracture toughness values calculated using equation A.2 is given in table A.3. These values scale with the fraction of 0 layers present in the laminate. Thus, when the entire laminate is modeled as a single entity, the fracture toughness to be used will be different for different laminate stacking.

The second correction used in the fracture toughness values is with respect to the logarithmic strain used by Abaqus in Explicit simulations when the non-linear geometry option is turned on. This has been studied by Xu and Waas, [37], and a schematic shown in figure A.2 depicts the error which can arise due to this. A linear separation to crack strain conversion assumption used in the implementation of traction-separation law is only valid when the finite element computation uses engineering strain for the calculations. In order to overcome this, fracture energy is corrected by a factor as shown in equation A.3, which is taken from Wu and Waas[37]

$$G_{corrected} = \frac{\sigma_c l_e}{2} \ln\left(1 + \frac{2G_c}{\sigma_c l_e}\right) \tag{A.3}$$

This ensures the correct correlation between the final crack separation in the traction-separation law with the VUMAT implementation in Abaqus. Errors arising due to this issue are problem dependent and if the final crack strain for the problem is considerably large or not [37].

A.3.3 Enahnced Schapery Theory and Implementation

EST formulation combines Schapery theory with crack band approach to have the capability to model both the damage (pre-peak) and failure (post-peak) in composites. In EST, damage is defined as microcracks developing in the matrix under shear and transverse loading and at the lamina level this is seen as pre-peak non-linearity. While damage influences the transverse and shear moduli, longitudinal stiffness is not affected by it. Failure accounts for all the macroscopic cracks occurring in the lamina. These macroscopic cracks results in the post peak softening at the lamina level response and it is modeled using the crack band model of Bazant and Oh [4]. Figure A.3 shows the fundamental idea behind EST where total strain is the sum of elastic and crack strains (equation B.1).

$$\varepsilon = \varepsilon_e + \varepsilon_{cr} \tag{A.4}$$

The area indicated by S in the figure accounts for the energy dissipated due to micro-damage evolution. G_c/l_e term shows the energy dissipated in the case of failure, where G_c is the fracture toughness of the material and l_e is the element characteristic length used in the finite element implementation. The EST formulation developed by Pineda and Waas [26] is used here and this accounts for three major failure mechanisms: matrix mode I cracking, matrix mode II cracking and axial fiber failure (mode I). Therefore the total work potential of the model can be expressed as a sum of the elastic strain energy, microdamage potential S and the failure potentials denoted by S_I^m, S_{II}^m and S_I^f. Using CLT this total work potential can be written as,

$$W = \frac{1}{2}(E_{11}\varepsilon_{11}^2 + E_{22}(S)\varepsilon_{22}^2 + G_{12}(S)\gamma_{12}^2) + Q_{12}\varepsilon_{11}\varepsilon_{22} + S_I^m + S_{II}^m + S_I^f \tag{A.5}$$

According to the assumption of Schapery theory, E_{22} and G_{12}, are functions of Schapery microdamge potential, S. Their evolution is shown in the equation A.6, where e_s and g_s are the functions measured using the approach discussed earlier, in the input parameters section.

$$\begin{aligned} E_{22} &= E_{220} e_s(S) \\ G_{12} &= G_{120} g_s(S) \end{aligned} \tag{A.6}$$

Total energy of the system should be constant with respect to the damage/failure potentials. This principle is used for obtaining the microdamage evolution equation in terms of S_r=$S^(1/3)$ as shown in equation A.7.

$$\varepsilon_{22}^2 E_{220} \frac{de_s}{dS_r} + \gamma_{12}^2 G_{120} \frac{dg_s}{dS_r} = -6S_r^2 \tag{A.7}$$

EST assumes that the damage mechanism won't be active until a transition from damage to failure is effected. The Hashin-Rotem failure criteria are used for determining the failure initiation point. Fiber failure criteria is considered to be independent of the matrix failure criteria and it is give by equation A.8, while the matrix mode I and mode II failure are connected and the mixed mode failure criteria for the matrix is given by, A.9.

$$\begin{aligned} \left(\frac{\varepsilon_{11}}{X_T}\right)^2 &= 1, \;\; \varepsilon_{11} \geq 0 \\ \left(\frac{\varepsilon_{11}}{X_C}\right)^2 &= 1, \;\; \varepsilon_{11} < 0 \end{aligned} \tag{A.8}$$

$$\begin{aligned} \left(\frac{\varepsilon_{22}}{Y_T}\right)^2 + \left(\frac{\gamma_{12}}{Z}\right)^2 &= 1, \;\; \varepsilon_{22} \geq 0 \\ \left(\frac{\varepsilon_{22}}{Y_C}\right)^2 + \left(\frac{\gamma_{12}}{Z}\right)^2 &= 1, \;\; \varepsilon_{22} < 0 \end{aligned} \tag{A.9}$$

When a failure criterion is met, degraded secant stiffness can be computed according to equation A.10. These equations can be derived with the help of figure A.3. Mesh objectivity of the model is obtained by smearing the crack energy over the element dimension l_e, perpendicular to the crack direction.

$$
\begin{aligned}
E_{11} &= E_{110}\frac{X_T(\varepsilon_{11F}-\varepsilon_{11})}{\varepsilon_{11}(\varepsilon_{11F}-X_T)}, \quad \varepsilon_{11F} = \frac{2G_{IC}^{f}}{E_{110}X_T} \\
E_{22} &= E_{22}^{*}\frac{Y_T(\varepsilon_{22F}-\varepsilon_{22})}{\varepsilon_{11}(\varepsilon_{22F}-Y_T)}, \quad \varepsilon_{11F} = \frac{2G_{IC}^{m}}{E_{22}^{*}Y_T} \\
G_{12} &= G_{12}^{*}\frac{Z(\gamma_{12F}-\gamma_{12})}{\gamma_{12}(\gamma_{12F}-Z)}, \quad \gamma_{12F} = \frac{2G_{IIC}^{m}}{G_{12}^{*}Z}
\end{aligned}
\tag{A.10}
$$

Larger element characteristic length l_e can cause the area under the stress strain curve to decrease and can cause a vertical stress drop at a critical value. An element of length larger than this critical value will lead to physically incorrect snap-back behavior. The critical element length to prevent this condition is given by,

$$
l_e < \min\left\{\frac{2G_{IC}^{f}}{E_{110}X_T^2}, \frac{2G_{IC}^{m}}{E_{22}^{*}Y_T^2}, \frac{2G_{IIC}^{m}}{G_{12}^{*}Z^2}\right\} \tag{A.11}
$$

Mesh size should be carefully chosen when working with crack band model so that the issues related to negative post-peak slope can be avoided. In this study mesh size was chosen such that it is one order of magnitude less than the crack band element characteristic length given in equation B.2.

A.4 Results and Discussion

All the open hole tension and compression tests were carried out as per ASTM standards D5766 and D6484 respectively. Extensometer of 2" gage length was used for measuring the displacements at points located 1" away from the hole on each side in the loading direction. Displacements are measured from the finite element models at the locations corresponding to extensometer heads to compare the load-displacement response with the test data for all the cases. Progression of failure events are also listed along with the load-displacement plots. Sequence of failure initiations are the same between the layups, but the extensometer displacements corresponding to these events are different between laminates as it depends on the stress distribution near the hole. As we go from stiffer to softer laminates, 0 layer fiber failure initiation occurs at higher displacement value. This has to be expected since

the softer laminate will have a smaller stress concentration near the hole. For an open hole coupon under tensile loading, transverse failure initiation in 90 layer is the first failure event in all the laminates and this degrades the transverse stiffness in that layer which in turn increases the stresses in the 45 and 0 layers. Increased stress in the 45 layer forces it to have a transverse/shear failure initiation and this leads to a fiber failure initiation in the 0 layer. This sequence of events lead to the final complete failure of the 0 layer in fiber direction and two-piece failure ensues.

Load-displacement comparison for the stiff 50/40/10 laminate is shown in figure A.4. Strength predicted by EST is within the error bounds of the experiment, however there is a mismatch in the slope of the curve. Experimental data shows a small stiffening behavior while EST shows some non-linear softening behavior due to the matrix microdamage evolution and also due to the progressive failure in 90 and 45 layers. The stiffening effect seen in the experiment can be attributed to the elastic stiffening of the carbon fibers reported in the literature [31], while the EST model does not account for this behavior of the fibers. However this effect is not very significant and is not observed in open hole testing of the other layups. Final failure patterns in all the layers of the laminate are compared with the actual failed specimen in figure A.5. Within the limitation of a shell theory, EST is able to capture the failure patterns quite accurately.

The peak load predicted by EST for the medium stiff 25/50/25 laminate is about 11% higher than the test results (figureA.6). Compared to the other 2 layups, this layup has the most number of 45/90 interfaces and hence this is more prone to delamination because of the earlier in-plane failure initiation in 90 and 45 layers. Hence allowing delamination mode of failure is critical in getting an accurate prediction for this layup. In order for the EST simulation to match with the test result, fiber direction fracture toughness can be further reduced which is an indirect way of accounting for the energy loss due to delamination. Final failure pattern for this layup is also compared with the test specimen in figure A.7.

For the soft 10/80/10 laminate, EST under-predicts the peak load as shown in figure A.8. +45/-45 interfaces present in this particular layup differentiates it from the other layups.

+45/-45 interface offers more resistance towards delamination than all the other interfaces present. In order to account for this extra resistance, fiber direction fracture toughness can be increased so that EST prediction matches with the test data. Increasing the fiber direction fracture toughness from 8.6N/mm to 12.0N/mm makes the prediction close to the test result. Final failure pattern shown in figure A.9 agrees very well with the failure of the actual test specimen.

The sequence of failure events are seen to change when the remote loading changes from tension to compression. Since the transverse failure strain in compression is fairly large, fiber failure initiation becomes the first failure event which is shortly followed by the transverse/shear failure initiation in the 45 layer. Final catastrophic failure occurs due to the complete fiber failure in the 0 layer under compression. Past studies have shown the micromechanics of open hole failure in compression, captured through a global-local approach, sometimes referred to in the literature as an embedded element method. Fiber kink banding is dominant and this is accurately captured in the open hole models by Ahn and Waas[2] and also by Davidson et al. [11].

In the present studies, the kink banding toughness is modeled as the overstress fiber direction toughness in compression. The open hole compression strength prediction for the 50/40/10 laminate agrees well with the test results as shown in figure A.11. The trend for compressive strength predictions are similar to the tensile cases. Compressive strength of the 25/50/25 is over-predicted (figure A.12) similar to it's tensile counterpart. For the softer 10/80/10 laminate, EST under-predicts the strength as shown in figure A.14. Final pattern comparisons for the 50/40/10, 25/50/25 and 10/80/10 laminates are shown in figures A.11, A.13 and A.15, respectively. Load-displacement curves for all the open hole compression cases show a significant non-linear behavior, while the EST model shows mild nonlinearity. This difference can be due to the difference in matrix non-linearity between tensile and compressive loading cases. In this study matrix non-linear behavior is assumed be the same in both tension and compression. Figures A.16 and A.17, and table A.4 summarizes results of the open hole strength predictions for all the laminates.

A.5 Conclusion

Enahnced Schapery Theory (EST) is a computationally efficient effective model for capturing the in-plane failure in a composite laminate with stress concentrations due to holes/notches. All the layers in a composite laminate can be modeled using a single shell element in this approach which reduces the computational time by a large margin. Capability of the EST model to predict the open hole strength from coupon level test data is demonstrated for the three different layups of IM7/8552 material. Another advantage of EST is the unified modeling approach for both tension and compression. Within the limitations of a shell model, agreement of the predictions with the test results is excellent. The difficulties and limitation of using a shell model for failure analysis are also addressed here. When delamination becomes a key failure mechanism, error in the predictions can be high. In those instances, this can be overcome to a certain extent by scaling the fiber direction fracture toughness as a laminate property as demonstrated here. A more physically reasonable approach would be introducing cohesive elements between the EST shell layers at the critical interfaces to account for the delamination. This approach will be computationally more expensive than the single shell EST approach, but still much faster than modeling with 3D elements. This modeling strategy is currently being investigated.

A.6 Acknowledgments

The authors are grateful for sponsorship from the Boeing company. Useful discussions with Steve Precup, Mostafa Rassaian and Gerry Mabson are gratefully acknowledged.

Laminate (% 0 plies /% ±45 plies /% 90 plies)	Lay-up
50/40/10	[0/45/0/90/0/-45/0/45/0/-45]s
25/50/25	[45/0/-45/90]2s
10/80/10	[45/-45/0/45/-45/90/45/-45/45/-45]s

Table A.1: List of laminates studied

Schapery Curves ($Pa^{-1/3}$)		Remark
es0	1.0	Transverse damage coefficients in tension/compression. Calculated from virtual transverse test of RUC using ±45° tension test results
es1	-1.32E-3	
es2	-5.7E-5	
es3	-3.29E-7	
es4	-6.94E-10	
es5	0.0	
gs0	1.0	Shear damage coefficients. Calculated from ±45° tension test
gs1	-7.36E-3	
gs2	2.7E-5	
gs3	4.76E-7	
gs4	1.28E-9	
gs5	3.56E-11	

Table A.2: Schapery microdamage functions

Property	**Value (Units- SI)**	**Remark**
Lamina Properties		
E_{11}	154.46E+09 (140.9E+09)	$[90°/0°]_s$ Tension Test (NIAR Report - 0° Compression Test)
E_{22}	7.20E+09	90° Tension Test
ν_{12}	0.34	0° Tension Test
G_{12}	4.87E+09	±45° Tension Test
Failure Properties		
X_T	0.0147	0° Tension Test
X_C	0.0131	Predicted for 1.2° fiber misalignment
Y_T	0.0080	90° Tension Test
Y_C	0.0462	90° Compression Test
Z	0.0227	±45° Tension Test
Fracture Toughness		
G_{IT}^{f}	40.5E+3, 21.0E+3, 8.6E+3	For 50/40/10, 25/50/25 and 10/80/10 laminates respectively
G_{IC}^{f}	10.1E+3, 5.3E+3, 2.2E+3	For 50/40/10, 25/50/25 and 10/80/10 laminates respectively
G_{IT}^{m}	0.384E+3	DCB Test
G_{IC}^{m}	0.384E+3	Assumed same as tension
G_{II}^{m}	2.184E+3	ENF Test

Table A.3: Material properties for EST

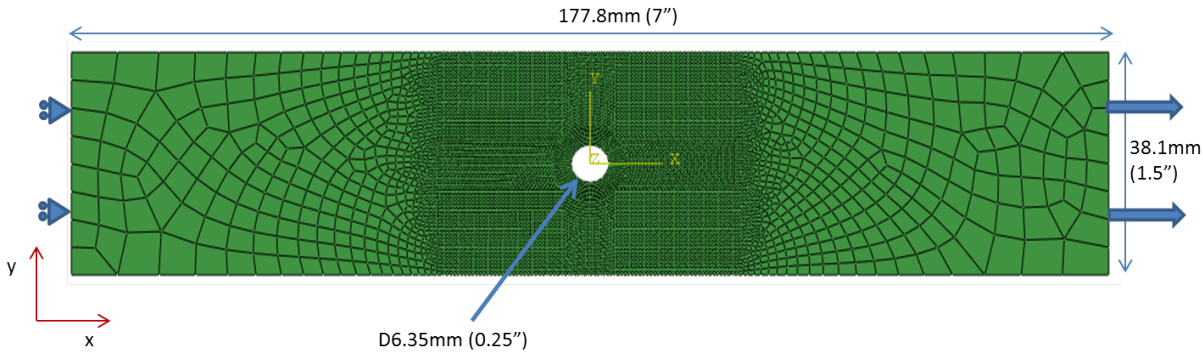

Figure A.1: Finite element model

Case	Peak Stress [MPa]			Modulus [GPa]	
	EST Prediction	Test Data	NIAR Report	EST Prediction	Test Data
OHT 50/40/10	652.2	628.1±21.4	597.0±34.1	82.9	90.3±4.3
OHT 25/50/25	480.0	432.8±12.4	406.8±11.3	54.6	57.2±6.6
OHT 10/80/10	284.8	315.9±3.9	301.0±12.3	35.1	37.2±2.8
OHC 50/40/10	457.1	455.8±24.1	436.9±18.7	76.3	83.4±9.0
OHC 25/50/25	394.4	346.1±7.6	337.1±10.0	50.9	51.7±5.6
OHC 10/80/10	277.1	289.7±5.2	264.8±9.0	33.2	33.8±4.7

Table A.4: Open hole tension/compression results summary

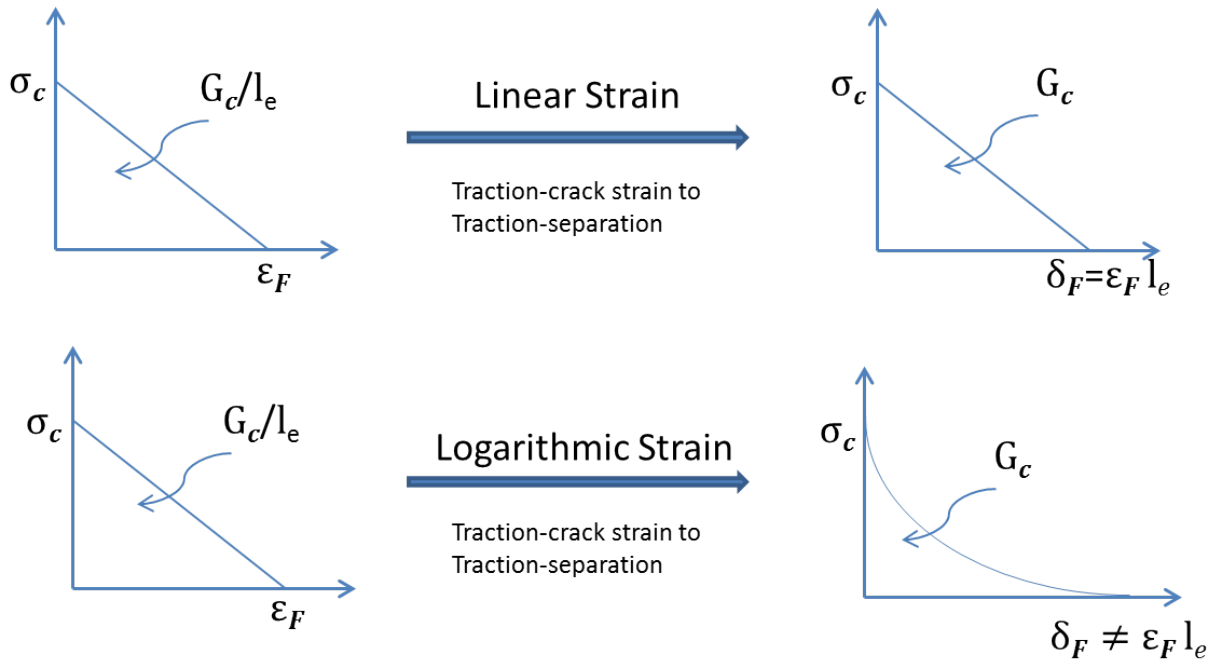

Figure A.2: Fracture toughness correction for logarithmic strain

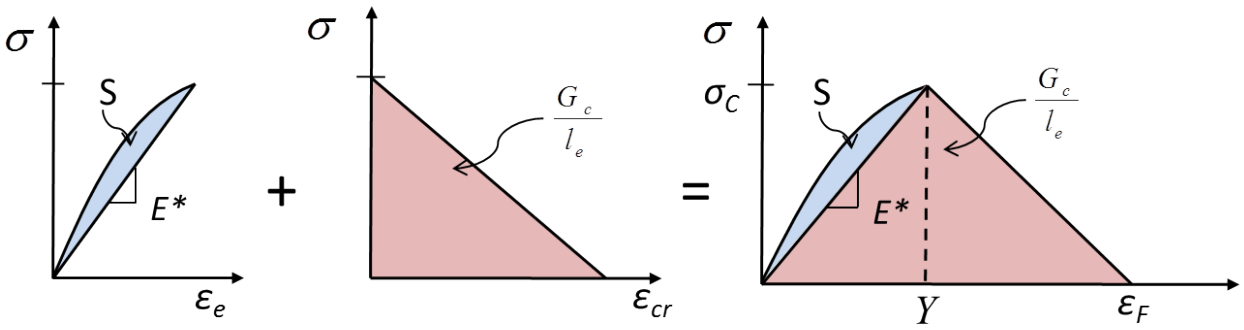

Figure A.3: Stress-strain response of EST element

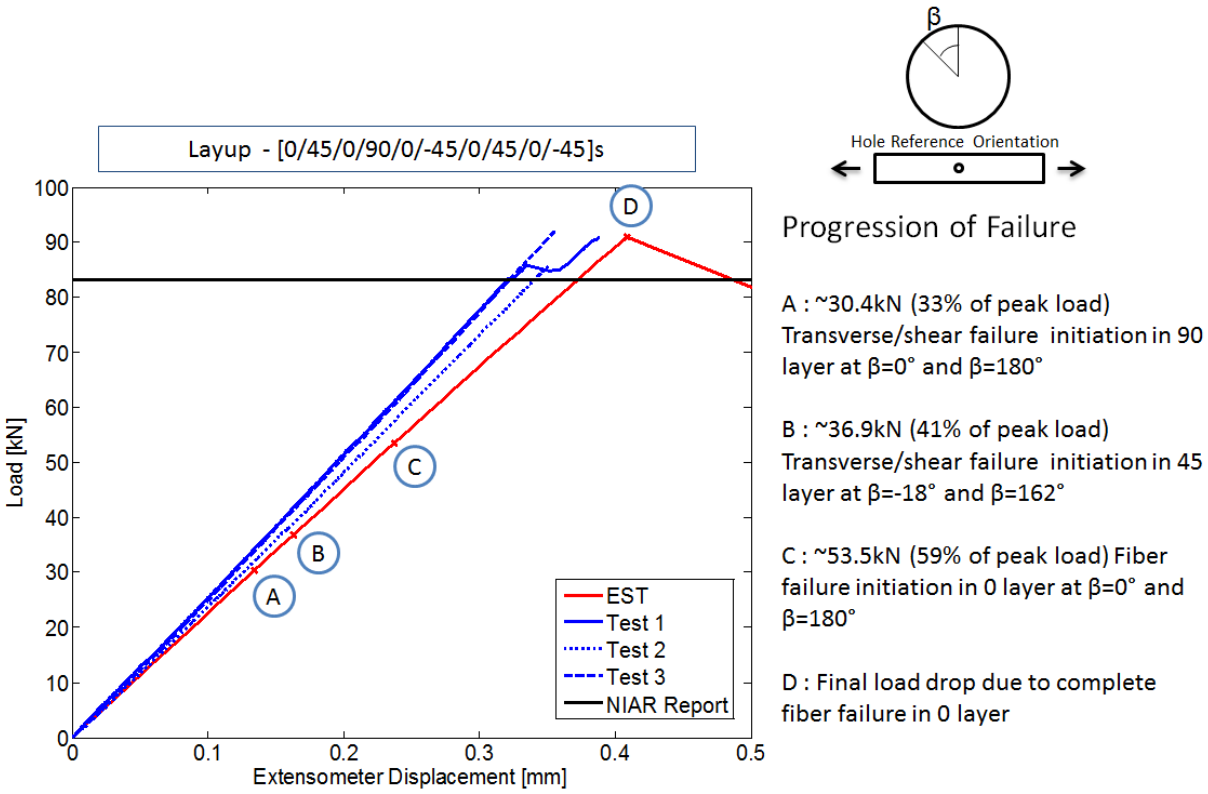

Figure A.4: Load-displacement plot for open hole tension of 50/40/10 laminate coupon

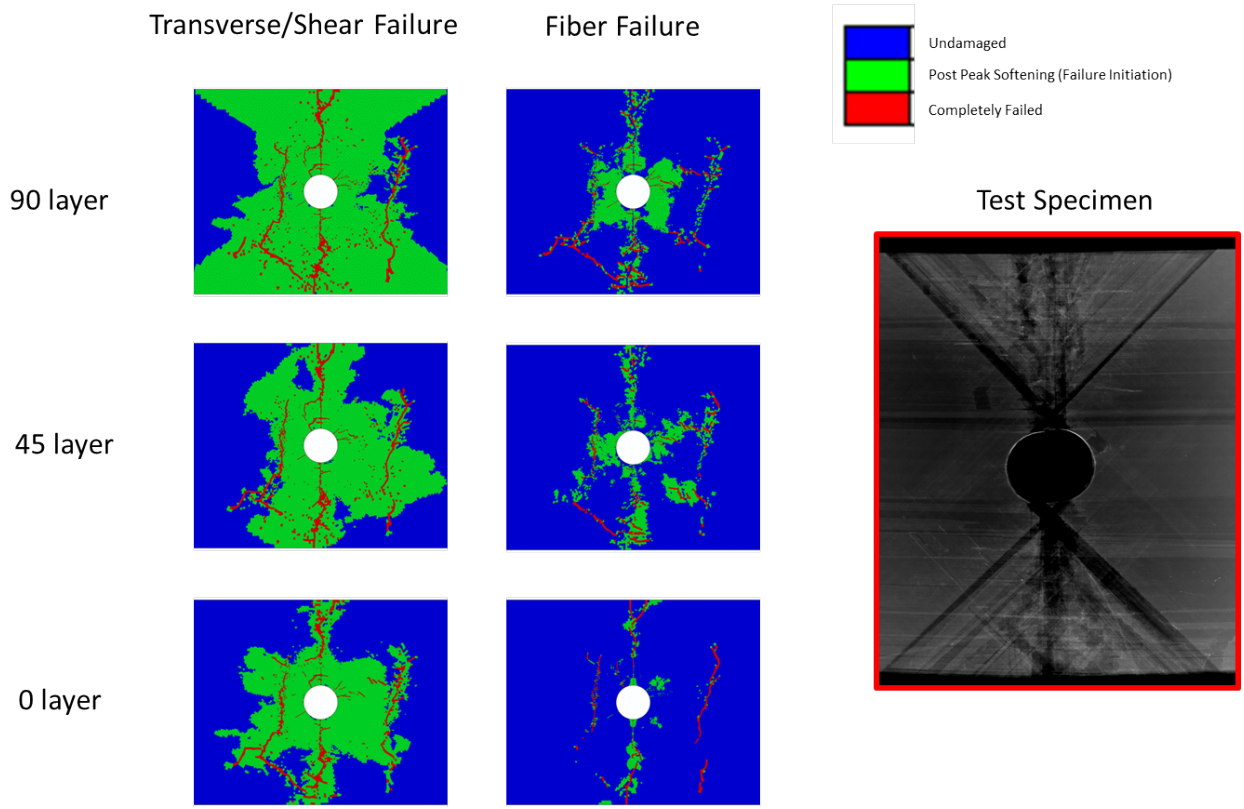

Figure A.5: Failure of 50/40/10 laminate coupon under tension

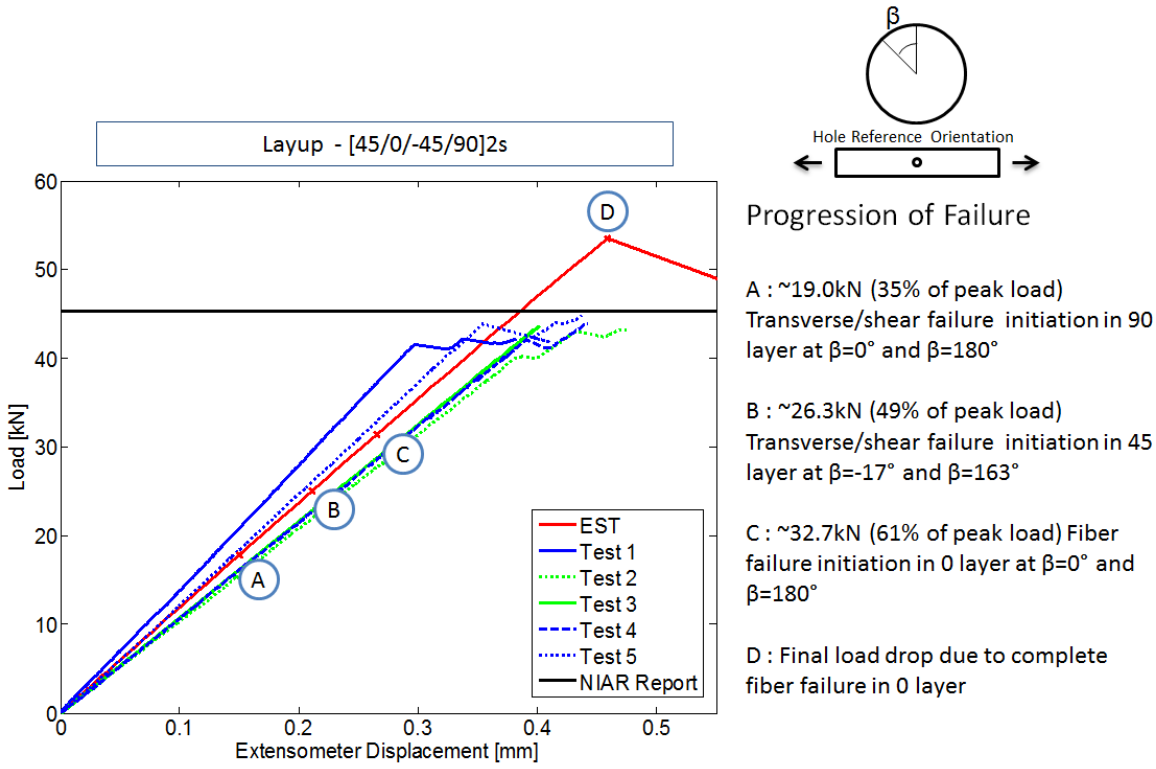

Figure A.6: Load-displacement plot for open hole tension of 25/50/25 laminate coupon

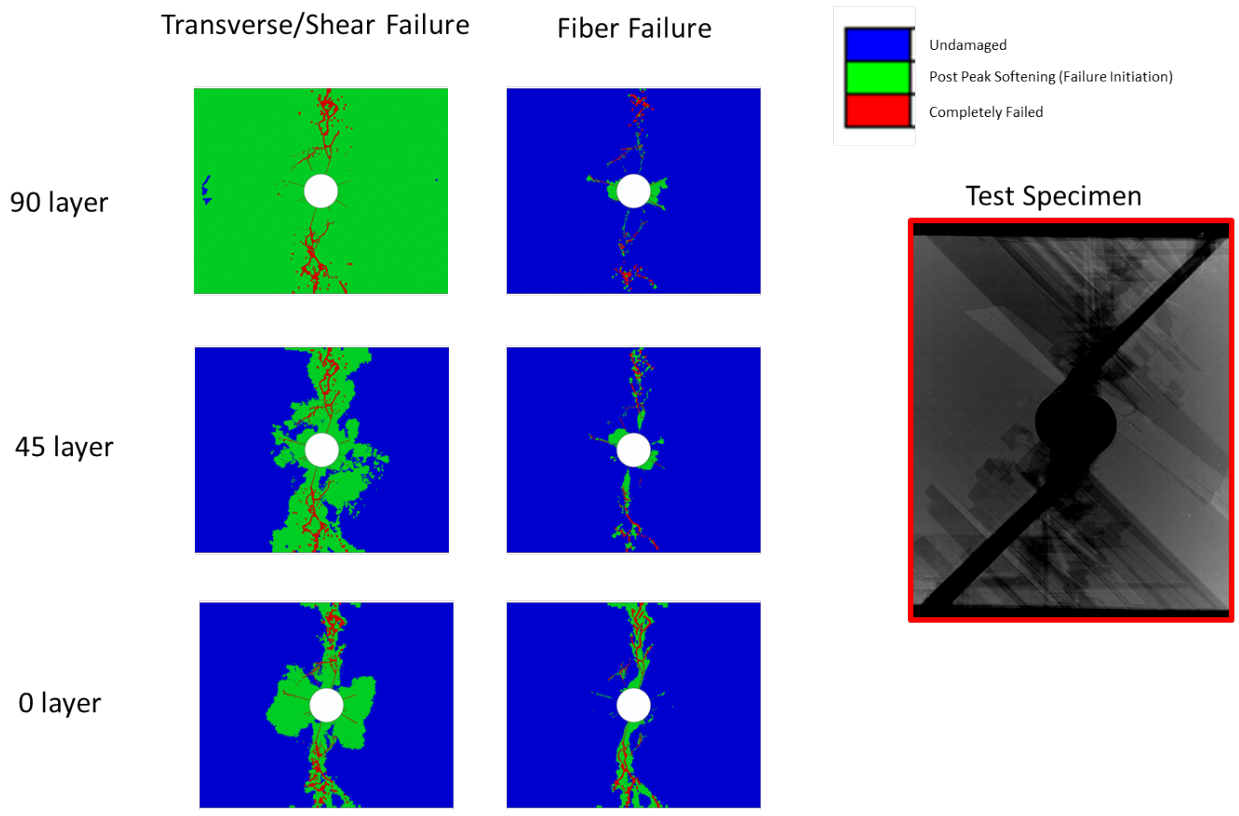

Figure A.7: Failure of 25/50/25 laminate coupon under tension

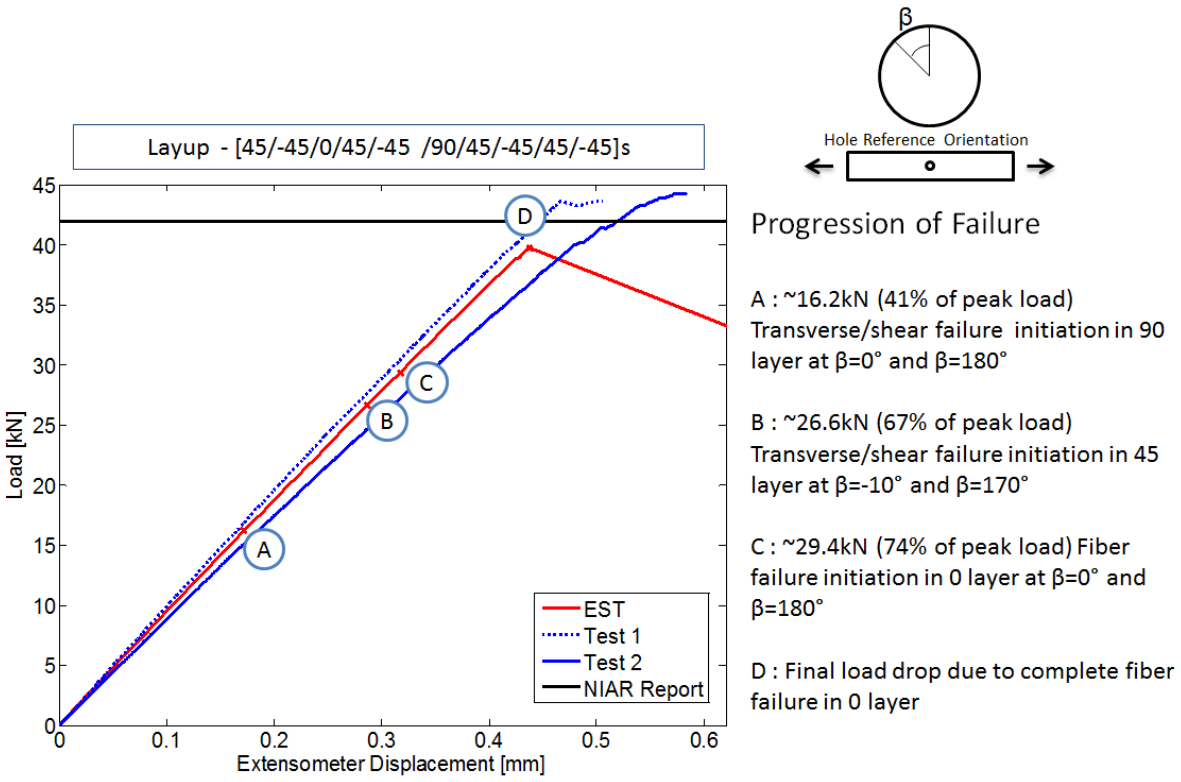

Figure A.8: Load-displacement plot for open hole tension of 10/80/10 laminate coupon

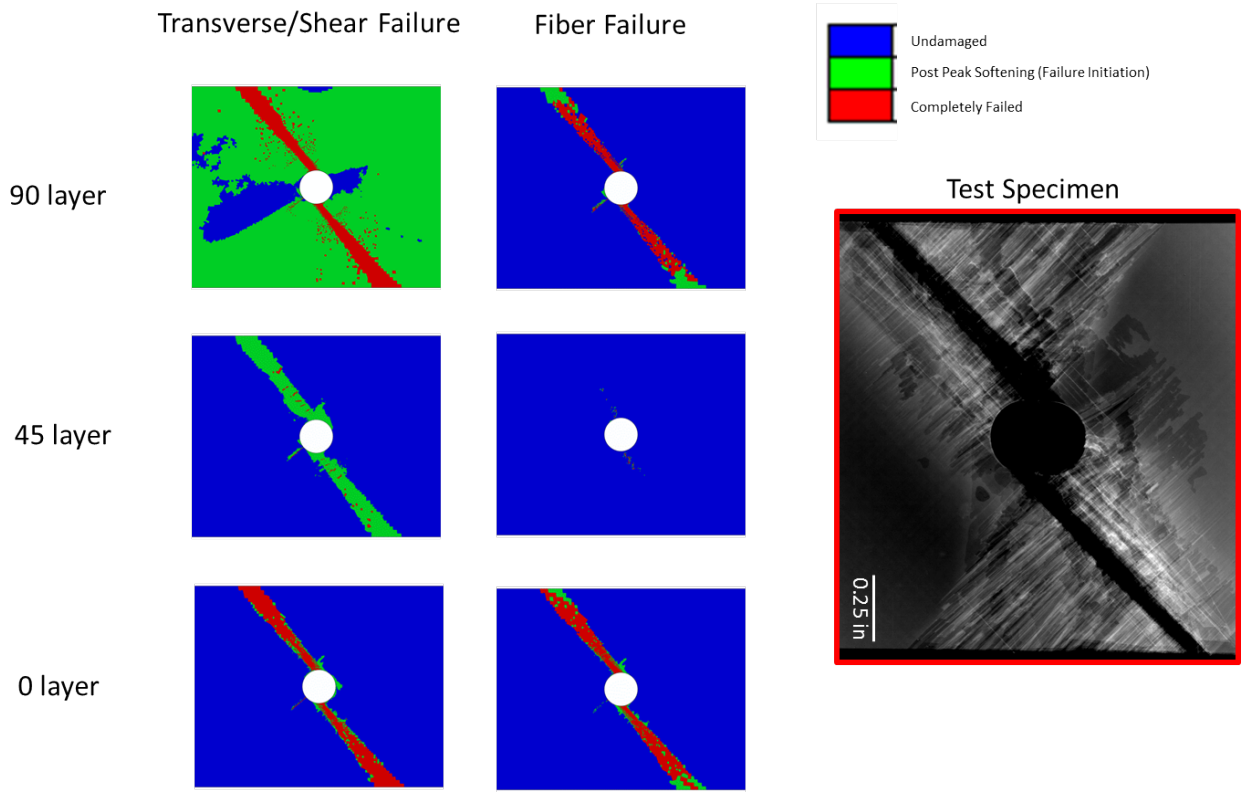

Figure A.9: Failure of 10/80/10 laminate coupon under tension

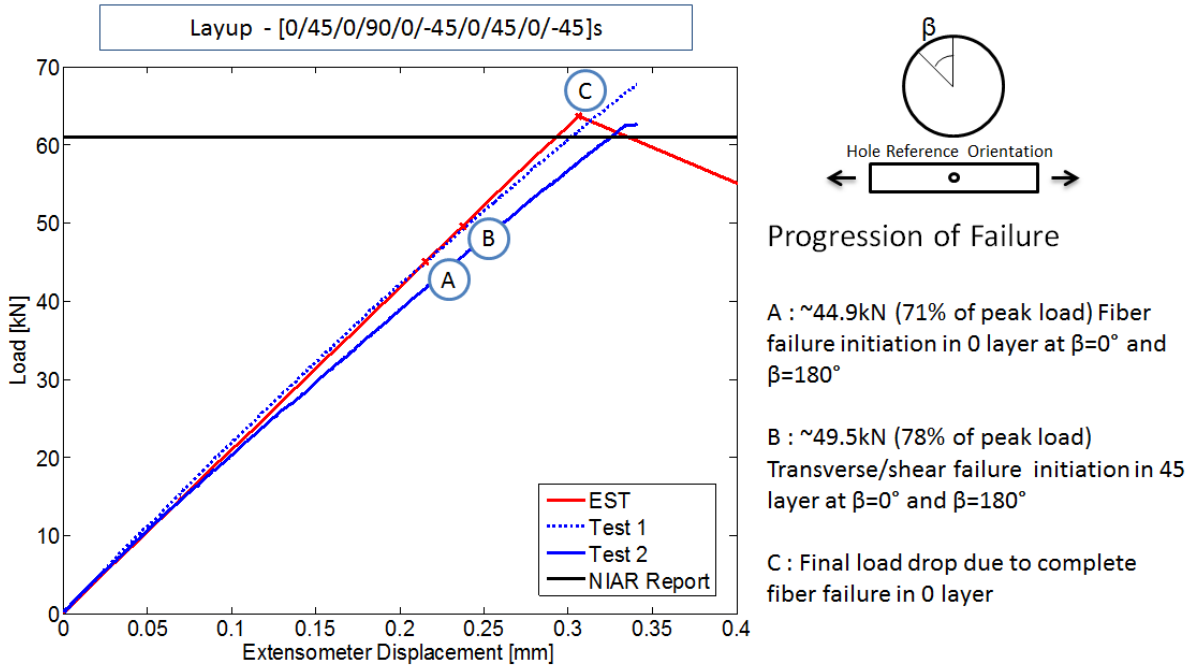

Figure A.10: Load-displacement plot for open hole compression of 50/40/10 laminate coupon

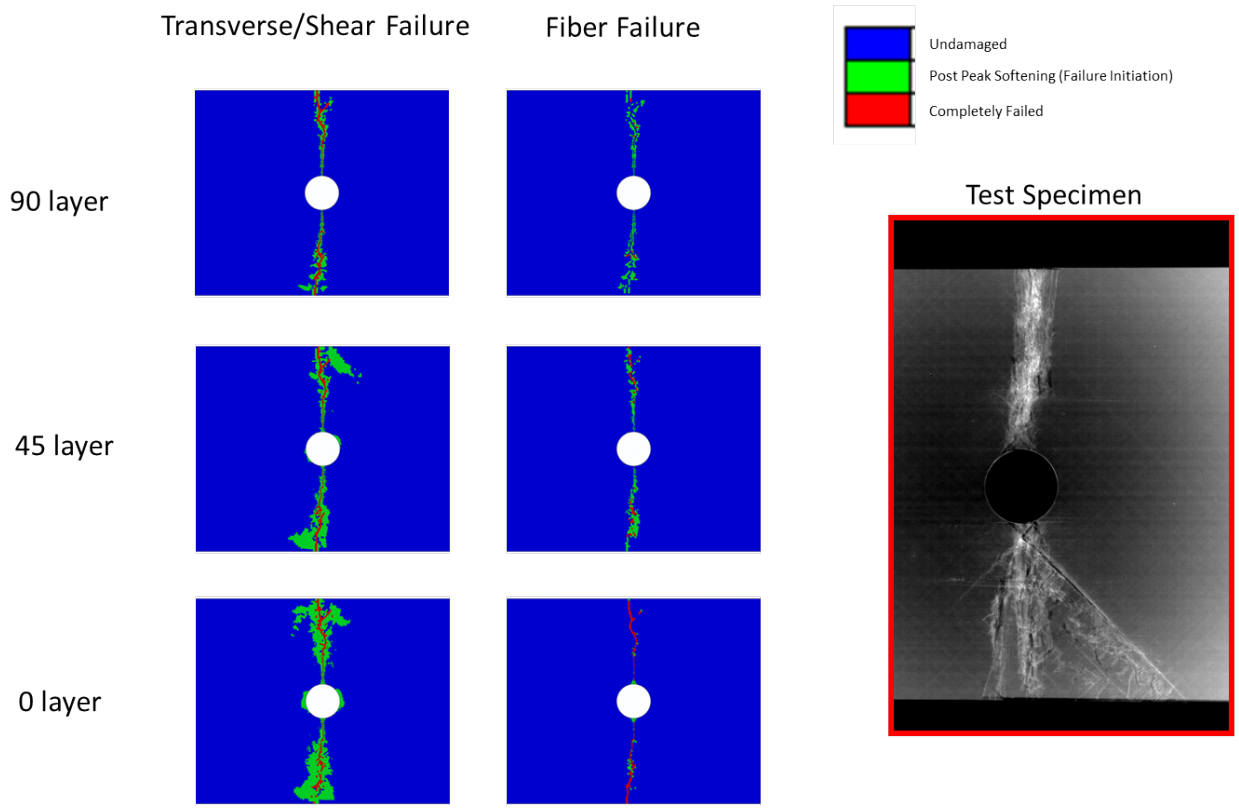

Figure A.11: Failure of 50/40/10 laminate coupon under compression

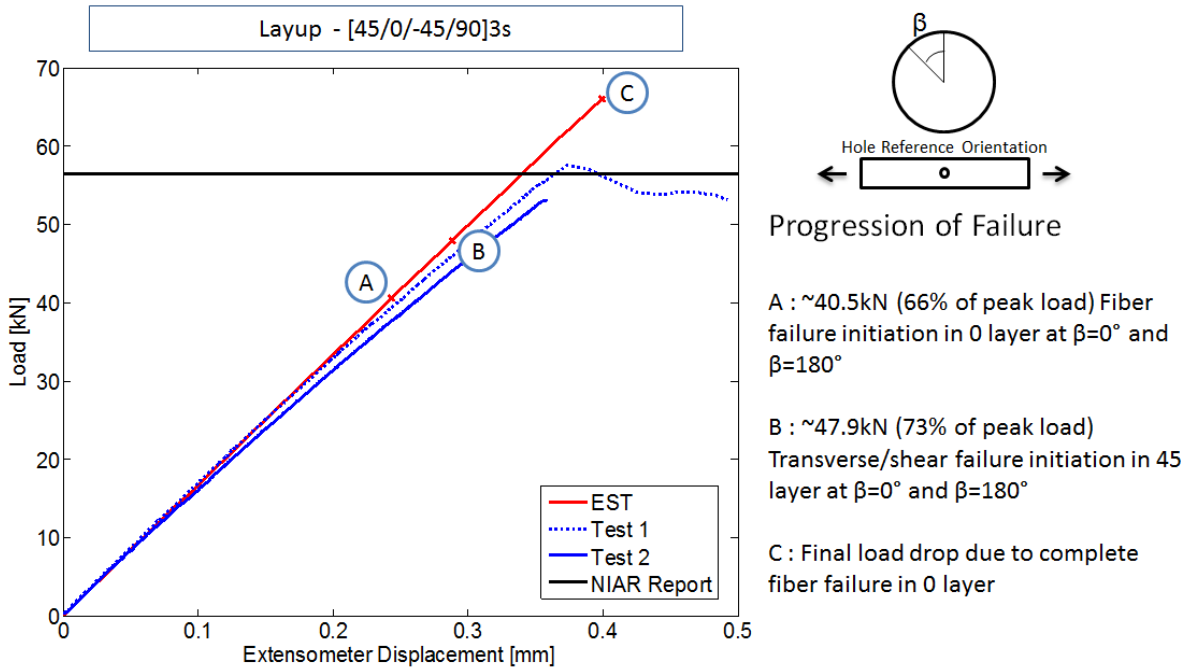

Figure A.12: Load-displacement plot for open hole compression of 25/50/25 laminate coupon

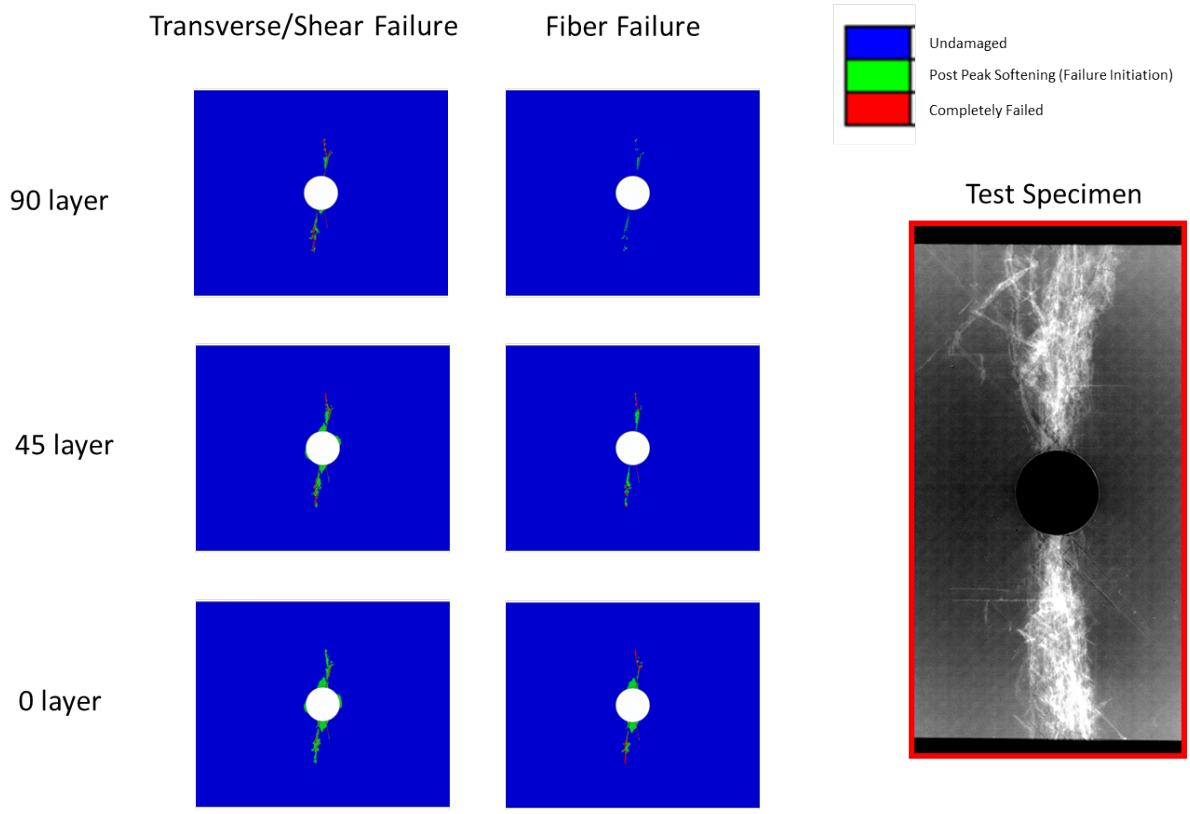

Figure A.13: Failure of 25/50/25 laminate coupon under compression

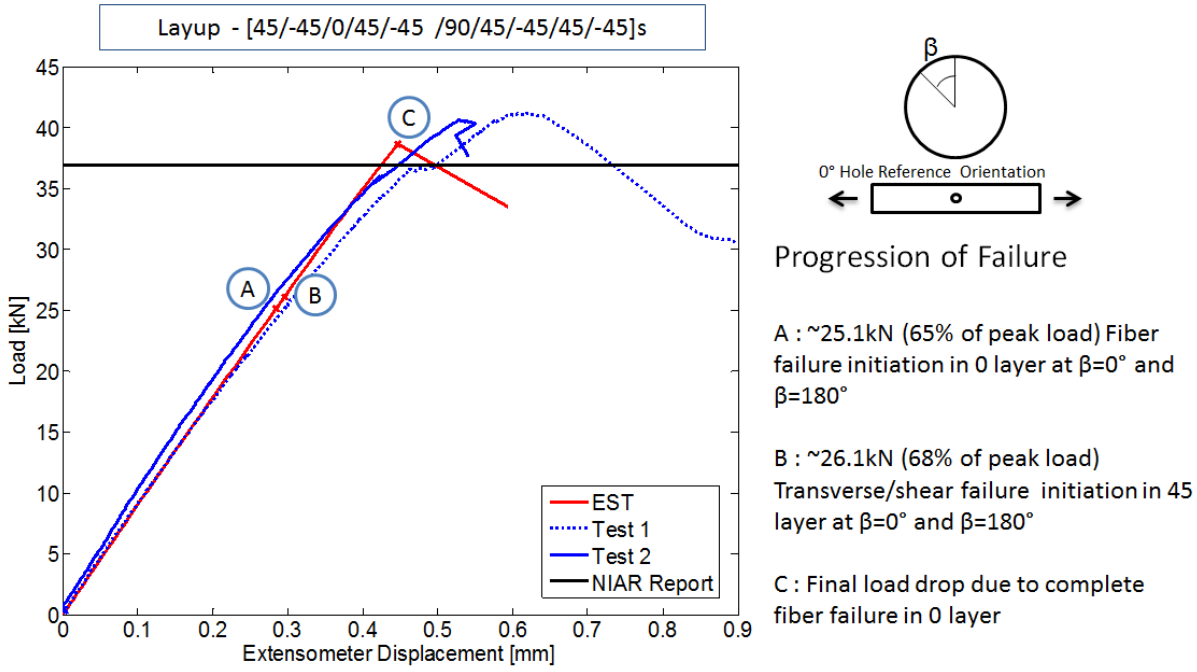

Figure A.14: Load-displacement plot for open hole compression of 10/80/10 laminate coupon

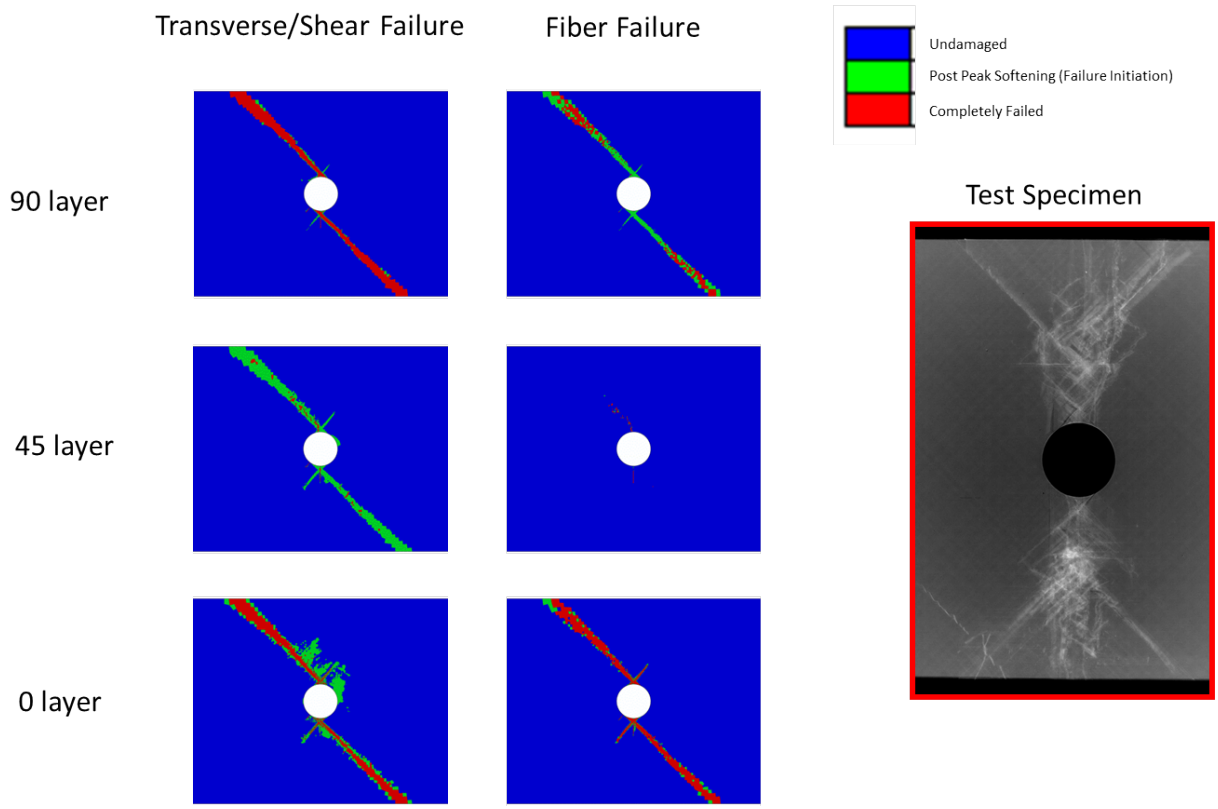

Figure A.15: Failure of 10/80/10 laminate coupon under compression

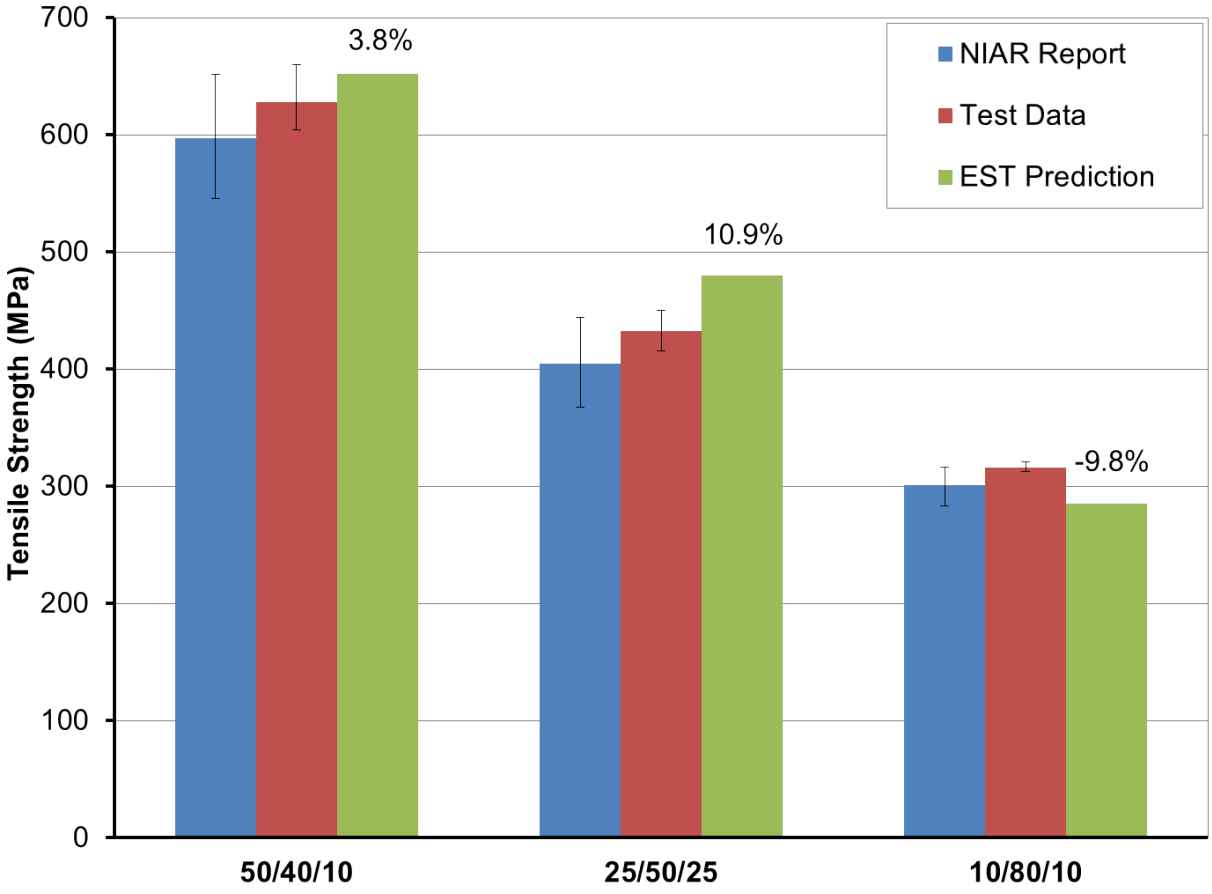

Figure A.16: Open hole tension predictions compared with experiments

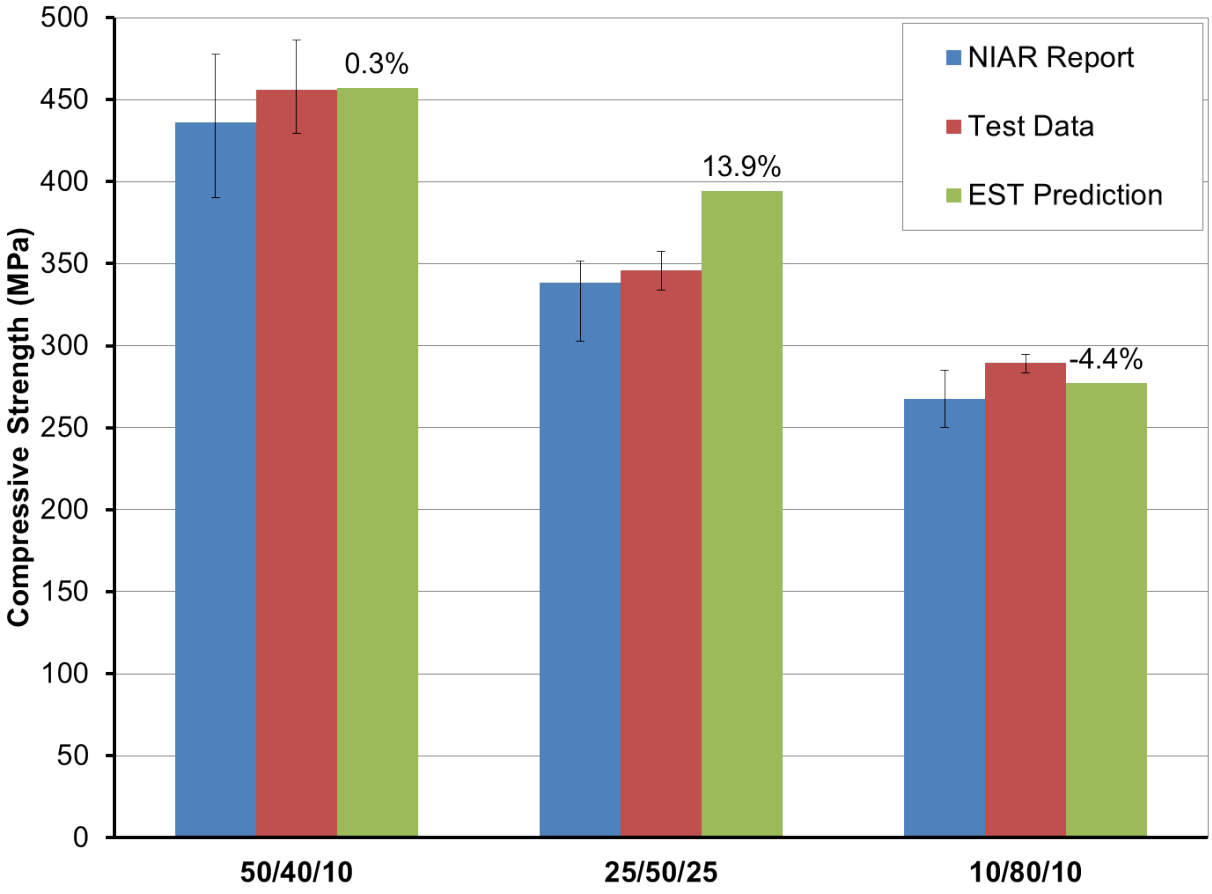

Figure A.17: Open hole compression predictions compared with experiments

Appendix B

THE EST MODEL FOR PREDICTING PROGRESSIVE DAMAGE AND FAILURE OF OPEN HOLE BENDING SPECIMENS

This work was presented at the AIAA/ASME/ASCE/AHS/ASC 57th Structures, Structural Dynamics, and Materials Conference and the paper is available in the open literature [16]

B.1 abstract

Progressive damage and failure in open hole composite laminate coupons subjected to flexural loading is modeled using Enhanced Schapery Theory (EST). Previous studies have demonstrated that EST can accurately predict the strength of open hole coupons under remote tensile and compressive loading states. This homogenized modeling approach uses single composite shell elements to represent the entire laminate in the thickness direction and significantly reduces computational cost. Therefore, when delaminations are not of concern or are active in the pre-peak regime, the version of EST presented here is a good engineering tool for predicting deformation response. Standard coupon level tests provides all the input data needed for the model and they are interpreted in conjunction with finite element (FE) based simulations. Open hole bending test results of three different IM7/8552 carbon fiber composite layups agree well with EST predictions. The model is able to accurately capture the curvature change and deformation localization in the specimen at and during the post catastrophic load drop event.

B.2 Introduction

Failure analysis of laminated fiber reinforced composite panels with open holes is a challenging problem because of the various failure modes involved and their mutual interactions. This complex problem presents the challenge of developing progressive failure analysis tools which can carry out the analysis in a cost effective and mesh-objective manner. Enhanced Schapery Theory (EST)[26, 17] achieves this task by accounting for the pre and post peak non-linearities using the Schapery theory[29, 31] and crack band[4] models respectively. EST is a lamina level deformation, damage and failure prediction approach. Consequently, the inputs to EST that reflect the effects of damage and failure at scales below this scale (those that can be modeled using micromechanics, for example the kink band angle in fiber compression) must also be obtained in a manner that preserves the length scale of interest. Previous studies carried out by Davidson et al.[11] and Joseph et al.[17] presented a unified model for the open hole tension (OHT) and open hole compression (OHC) strength predictions using Enhanced Schapery Theory (EST). The EST model is extended in the present study to address the failure events when the open hole coupon is subjected to flexural loading. The complexity of the failure events due to the stress concentrations near the hole is escalated to the next level with the presence of a bending moment in the specimen that subjects some plies to tensile loading and others to compressive loading. Therefore, and unlike the in-plane tension or compression problem, a specimen subjected to bending has varying in-plane strains in the through-the-thickness direction and hence is a very good problem to validate any progressive failure model.

This paper compares EST predictions for three different IM7/8552 carbon fiber composite laminates under bending loading conditions with experiments. The results demonstrate ESTs capability for making excellent prediction while keeping computational costs to a minimum. Computational efficiency is achieved by using a single composite shell element for modeling all the layers in the thickness direction. The disadvantage of this approach is it's inability to capture delamination failure modes and therefore it is suitable for layup families where

delamination events prior to the peak load point are negligible. This family, fortunately, is quite large.

B.3 Finite Element Modeling

Progressive failure of the open hole bending (OHB) specimens under 4-point bend loading conditions as shown in figure B.1, is analyzed using EST. The model has a load span of 76.2mm and a support span of 152.4mm. Abaqus general contact algorithm is used for modeling the contact between the plate and the load/support pins. Pins are modeled using Abaqus analytical rigid elements and the diameters of the support and load pins are 9.525mm and 6.35mm respectively. All the degrees of freedom of the support pins are fixed and displacements in the z-direction are applied on the loading pins. Finite element mesh (figure B.2) used in the study satisfies the stress convergence requirements and the crack band requirements for element size. Geometric non-linearity is used in the model as the rotations are significant under flexural loading.

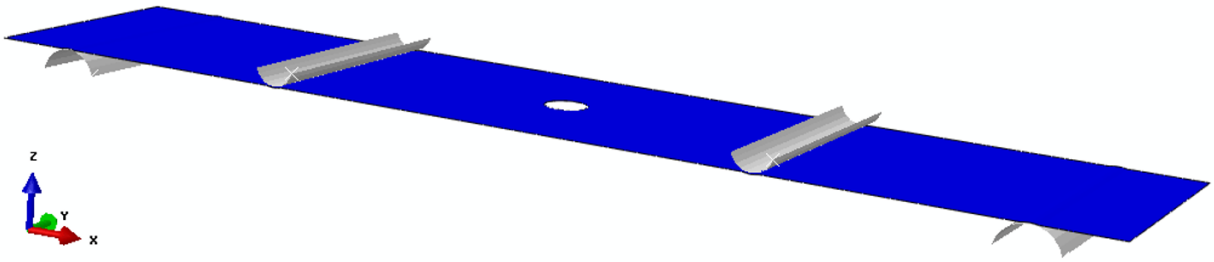

Figure B.1: Open hole bending model

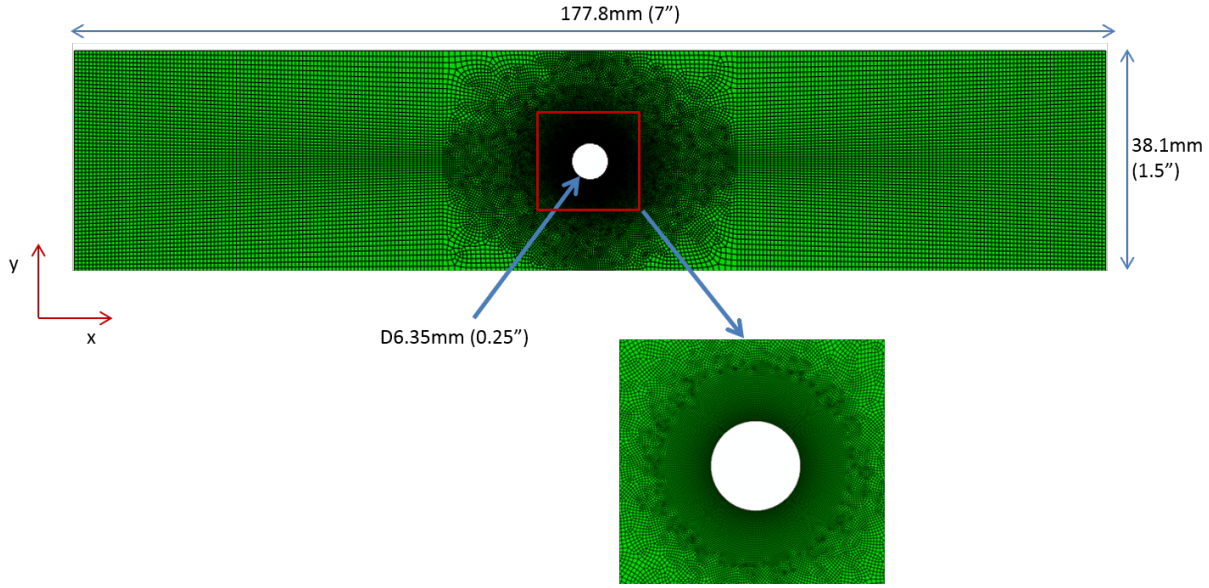

Figure B.2: Finite element model mesh

EST is implemented as a user material subroutine (VUMAT) within the Abaqus/explicit solver (Abaqus is the name of a widely use commercial finite element software package) and the in-plane failure of the laminate is modeled using 4-node shell elements. Since EST cannot account for delamination mode of failure, the results obtained using EST are expected to give an upper bound for the strength of the laminate. Table B.1 shows the three different layups used for the OHB analyses. The same mesh and modeling approach is used for all three layups and it was also found in the study that depending on the layup, mesh refinement requirements could be different. The mesh chosen here gives a converged gradient stress field near the hole for all three different layups.

Laminate (% 0 plies /% ±45 plies /% 90 plies)	Lay-up
50/40/10	[0/45/0/90/0/-45/0/45/0/-45]s
25/50/25	[45/0/-45/90]2s
10/80/10	[45/-45/0/45/-45/90/45/-45/45/-45]s

Table B.1: List of laminates studied

B.3.1 The EST Model and Input Parameters

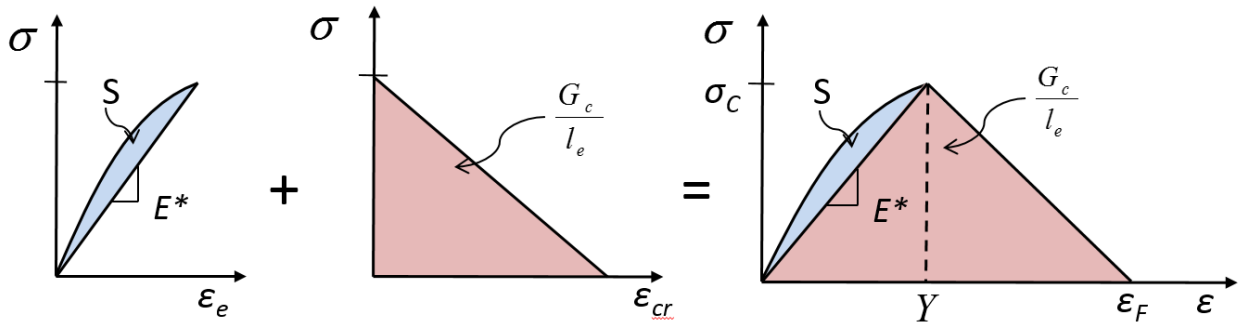

Figure B.3: Stress-strain response of EST element

A typical stress-strain response of an EST element is shown in figure B.3. The model assumes that the pre-peak non-linearity is caused by the development of matrix micro-cracks, predominantly due to local states of shear (and also transverse strains). In EST micro-crack development is referred to as damage, while the coalescence of these microcracks which forms macroscopic crack is referred to as failure. In essence, if a suitable measure of stress and corresponding conjugate strain response shows a positive tangent stiffness (but one that changes), and if the instantaneous and decreasing tangent stiffness is positive, then damage is accruing at the microscale (which is how the body is dissipating energy), while the state at which this tangent stiffness for the first time becomes negative is identified as the onset of failure. Matrix micro-cracking affects only the transverse and shear stiffness properties

and the axial stiffness value is unaffected by it[29, 31]. This assumption is valid as the axial stiffness is dominated by the fiber material properties. Schapery theory uses polynomial functions for representing the non-linear behavior in transverse and shear responses. Schapery microdamage functions used in this study are given in table B.2 for IM7/8552. Shear microdamage functions are directly calculated from ±45 tension tests and the transverse microdamage response is obtained from the virtual testing of a representative unit cell (RUC) according to the procedure give in Ng et al [23]. It is also assumed that transverse microdamge function is the same in both tension and compression, even though different responses are permitted within the theory.

Schapery Curves ($Pa^{-1/3}$)		**Remark**
es0	1.0	Transverse damage coefficients in tension/compression. Calculated from virtual transverse test of RUC using ±45° tension test results
es1	-1.32E-3	
es2	-5.7E-5	
es3	-3.29E-7	
es4	-6.94E-10	
es5	0.0	
gs0	1.0	Shear damage coefficients. Calculated from ±45° tension test
gs1	-7.36E-3	
gs2	-2.7E-5	
gs3	4.76E-7	
gs4	1.28E-9	
gs5	3.56E-11	

Table B.2: Schapery microdamage functions

Microcracks that develop in the matrix coalesce to form macroscopic cracks, and at the

onset of failure Schapery damage evolution is disabled in the model. In the absence of shear, transverse failure can occur without the development of micro-cracks or damage. Three main in-plane failure mechanisms are addressed in EST and these are matrix mode I cracking, matrix mode II cracking and axial fiber failure (mode I). While axial failure is independent of the matrix failure modes, matrix mode I and mode II failure are related to each other and their interaction is defined by a mixed-mode failure initiation and propagation laws[26, 17]. All three failure mechanisms are modeled using crack band theory. The fundamental principle behind the crack band theory is expressed by the equation below (equation B.1).

$$\varepsilon = \varepsilon_e + \varepsilon_{cr} \tag{B.1}$$

Crack band theory is an effective, element level approach to model the onset and propagation of macroscopic cracks in a mesh objective manner. The theory is a two parameter failure model which requires the strength and fracture toughness parameters as input,[4]. Strain-based initiation criteria define various failure mode initiations in EST. Upon the initiation of failure, the crack band model acts like entities in series with one representing the elastic part and the other representing the cracking mechanism. The total strain in the element is a sum of the elastic strain and the crack strain as shown in equation B.1. This idea is effectively summarised in the figure B.3. The area indicated by S in the figure accounts for the energy dissipated due to microdamage evolution. G_c/l_e term shows the energy dissipated in the case of failure, where G_c is the fracture toughness of the material and l_e is the element characteristic length perpendicular to the crack direction.

Property	Value (Units- SI)	Remark
Lamina Properties		
E_{11}	154.46E+09	$[90°/0°]_s$ Tension Test
E_{22}	7.20E+09	90° Tension Test
ν_{12}	0.34	0° Tension Test
G_{12}	4.87E+09	±45° Tension Test
Failure Properties		
X_T	0.0147	0° Tension Test
X_C	0.0131	Predicted for 1.2° fiber misalignment
Y_T	0.0080	90° Tension Test
Y_C	0.0462	90° Compression Test
Z	0.0227	±45° Tension Test
Fracture Toughness		
G_{IT}^{f}	40.5E+3, 21.0E+3, 8.6E+3	For 50/40/10, 25/50/25 and 10/80/10 laminates respectively
G_{IC}^{f}	10.1E+3, 5.3E+3, 2.2E+3	For 50/40/10, 25/50/25 and 10/80/10 laminates respectively
G_{IT}^{m}	0.384E+3	DCB Test
G_{IC}^{m}	0.384E+3	Assumed same as tension
G_{II}^{m}	2.184E+3	ENF Test

Table B.3: Material properties for EST

All the elastic and failure properties required for the EST model are shown in table B.3. The axial and transverse stiffness properties are assumed to be the same in both tension and compression. But the failure properties are assumed to be different in tension and compression. One of the critical parameters which affects the peak load is the fiber direction fracture toughness. Since EST uses a single composite shell element, it is required to scale the fracture toughness with the layup according to the approach suggested by Camanho and Catalatonni [6]. More discussions on the failure parameters can be found in Joseph et al. [17]. All the input parameter used in this open hole bending study are the same as the

input parameters used in the previous open hole tension/compression study[17]. The reader is advised to refer to Pineda and Waas [26] and Joseph et al. [17] for more details on the EST model. A discussion on the mesh-objectivity of the EST model can be found in Pineda and Waas [26].

A limitation of the crack band model is the maximum element size which can be used for producing mesh objective results. This correspond to the element size for which the stress-strain response in figure A.3 shows a vertical stress drop after the peak stress. Element sizes larger than this lead to physically incorrect snap-back behavior. The critical element length to prevent this behavior is given by,

$$l_e < \min\left\{\frac{2G^f_{IC}E_{110}}{X^2_T}, \frac{2G^m_{IC}E^*_{22}}{Y^2_T}, \frac{2G^m_{IIC}G^*_{12}}{Z^2}\right\} \tag{B.2}$$

B.4 Results and Discussion

Failure events in the bending case are much more complex than in-plane loading cases such as open hole tension and open hole compression. When subjected to bending, the top layers of the specimen undergo compressive loading and the bottom layers undergo tensile loading. Figures B.4, B.6 and B.8 show the load displacement plot form the EST simulations compared against the test results for the laminates 50/40/10, 25/50/25 and 10/80/10 respectively. Load in the plots correspond to the total reaction force in the z-direction on the load pins and the displacement is the movement of the loading pin in the z-direction. For each layup EST simulations are compared against two test results. Table B.4 shows the summary of the comparison.

Laminate	Peak Stress [kN]		Modulus [kN/mm]	
	EST Prediction	Test Data	EST Prediction	Test Data
50/40/10	3.89	3.65	0.43	0.41
25/50/25	4.83	3.53	0.47	0.44
10/80/10	2.18	2.09	0.21	0.20

Table B.4: Open hole tension/compression results summary

For the 50/40/10 laminate, EST prediction agrees very well with the experiments as shown in figure B.4. This layup has a large percentage of 0 layers and hence the strength is mainly driven by the fiber failure mechanisms. The approach of fiber direction fracture toughness scaling is also more appropriate in this layup due to the 0 layer dominance. Every +45 or -45 or 90 layer in this layup is sandwiched between 0 layers and this can significantly suppress the matrix failure mechanisms in them. This might not hold true if the +45,-45 or 90 layers were thicker as matrix failure events occur earlier in thick layers compared to thin layers. This example demonstrates that EST can accurately predict the results as long as the fiber failure properties are correct. Similar agreement between the experiments and simulations are seen in this layup for open hole tension/compression [17]. Figure B.5 shows the laminate degradation states corresponding to the three modes of failures at the two piece failure stage predicted by EST. It has to be kept in mind that the model cannot predict the crack paths accurately due to the accumulation of finite element stress calculation errors following element failure events. However the model is able to capture the two piece failure crack path fairly well in this case. While the fiber failure is over a narrow region, matrix failure is spread over a larger region as one would expect.

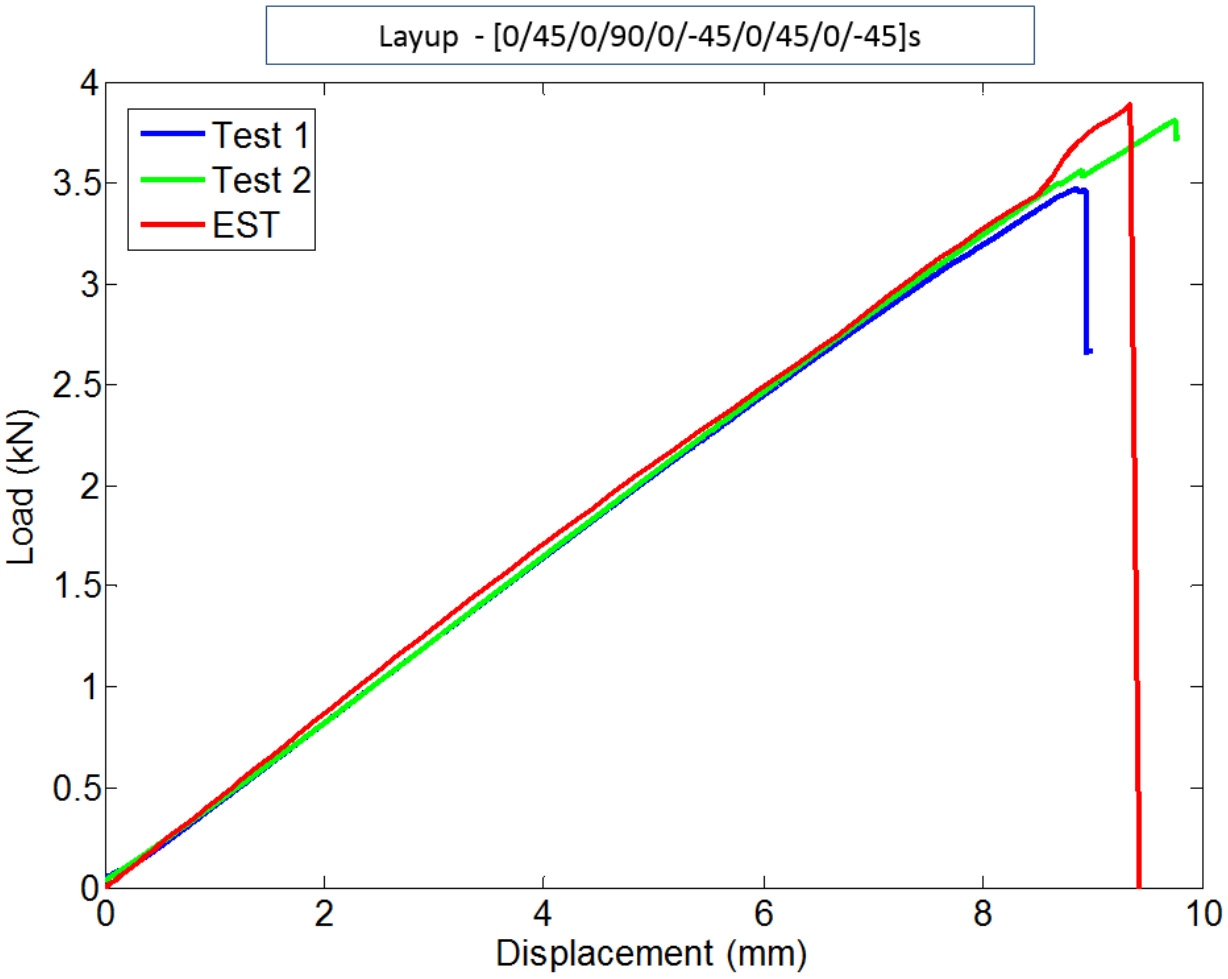

Figure B.4: Load-displacement plot of 50/40/10 laminate coupon

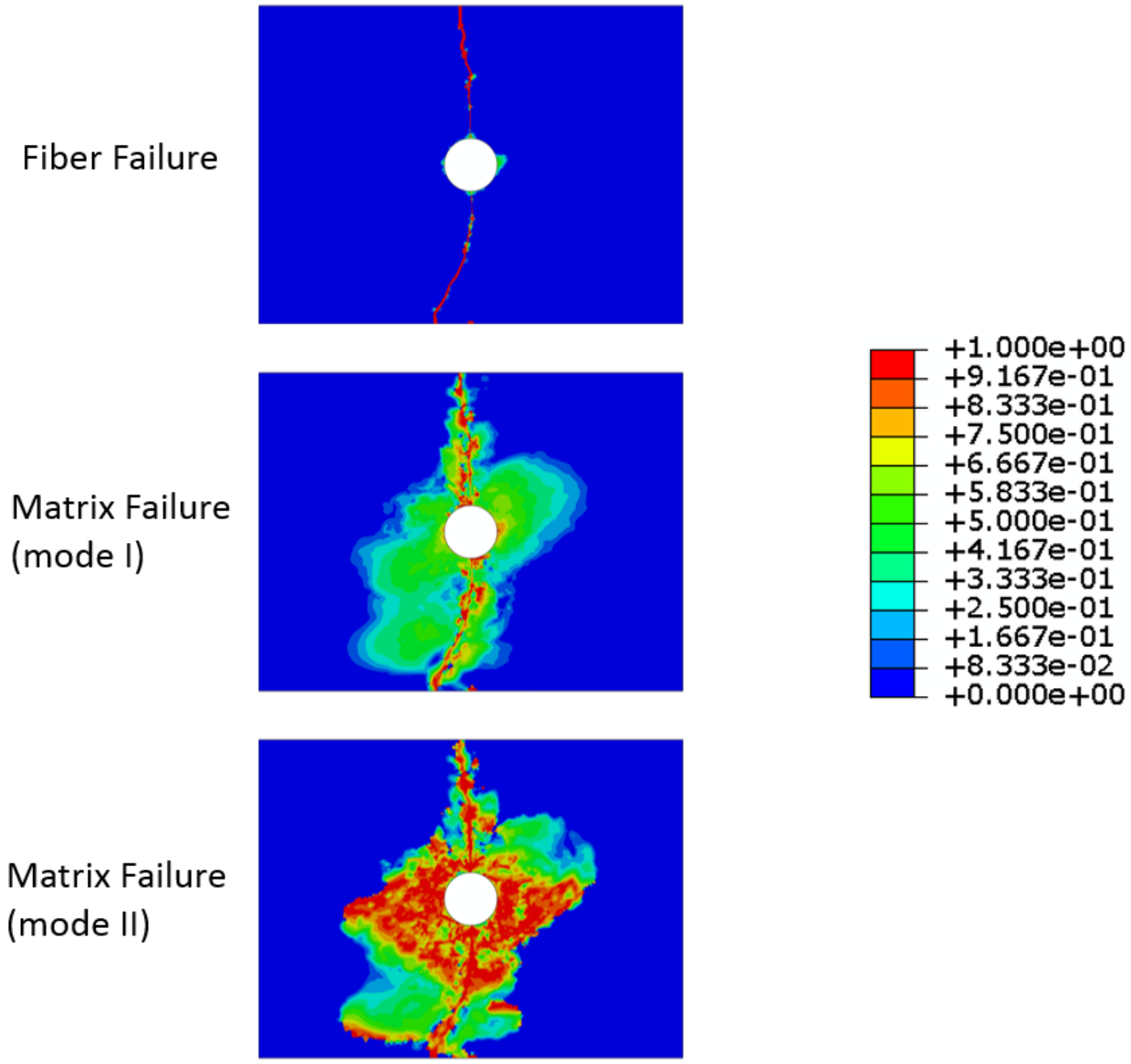

Figure B.5: Failure of 50/40/10 laminate coupon under bending

EST prediction for the 25/50/25 laminate does not agree quite well with the experiments. There is significant variation between the test data itself. More number of tests are to be conducted for this layup to make a better comparison with simulation. However the larger non-linear region close to the peak load in the experimental curves indicate that

delamination is a significant failure mechanism here. Larger peak load predicted by EST can be attributed to it's inability to account for delamination mode of failure. Degradation states shown in figure B.7 indicates very large matrix failure region compared to other layups and suggests that future studies on this layup will have to include delamination interface elements in the model. A similar over-prediction behavior was also observed in the open hole tension/compression study of this layup [17].

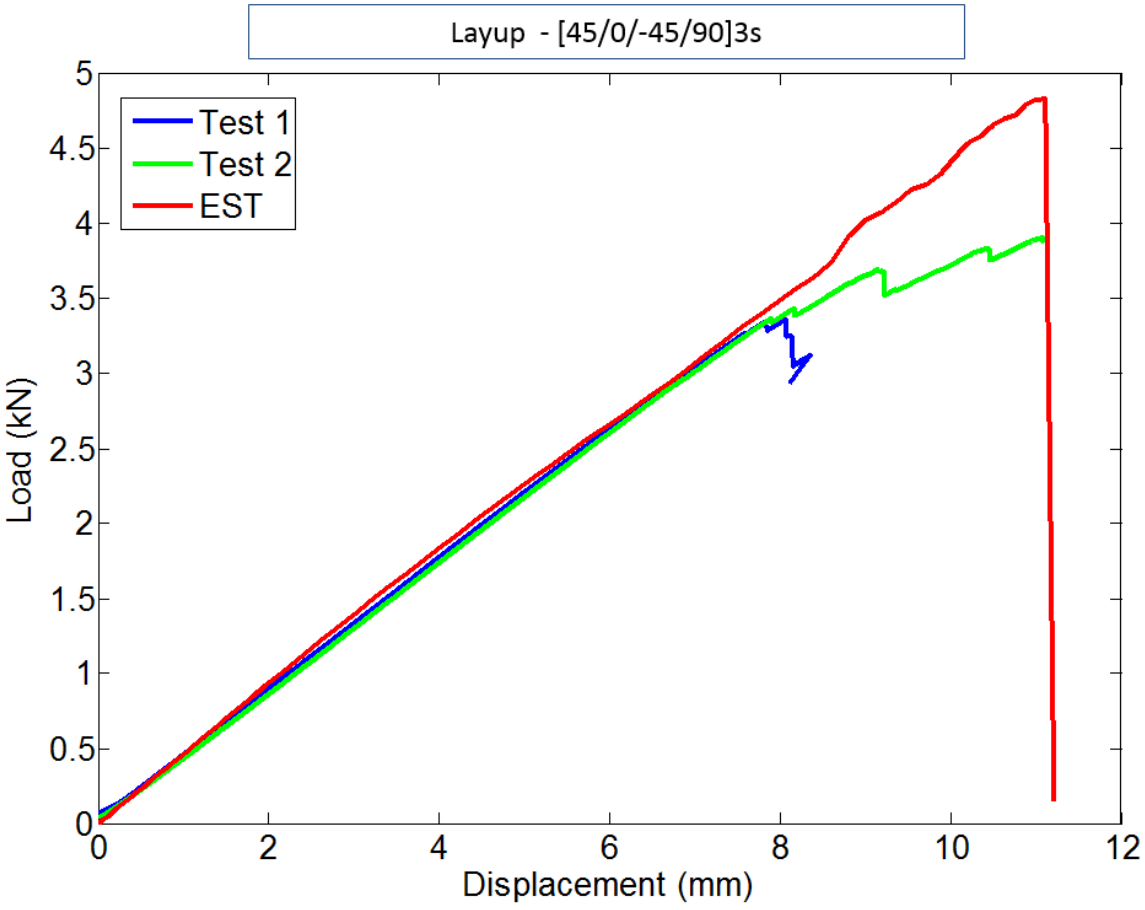

Figure B.6: Load-displacement plot of 25/50/25 laminate coupon

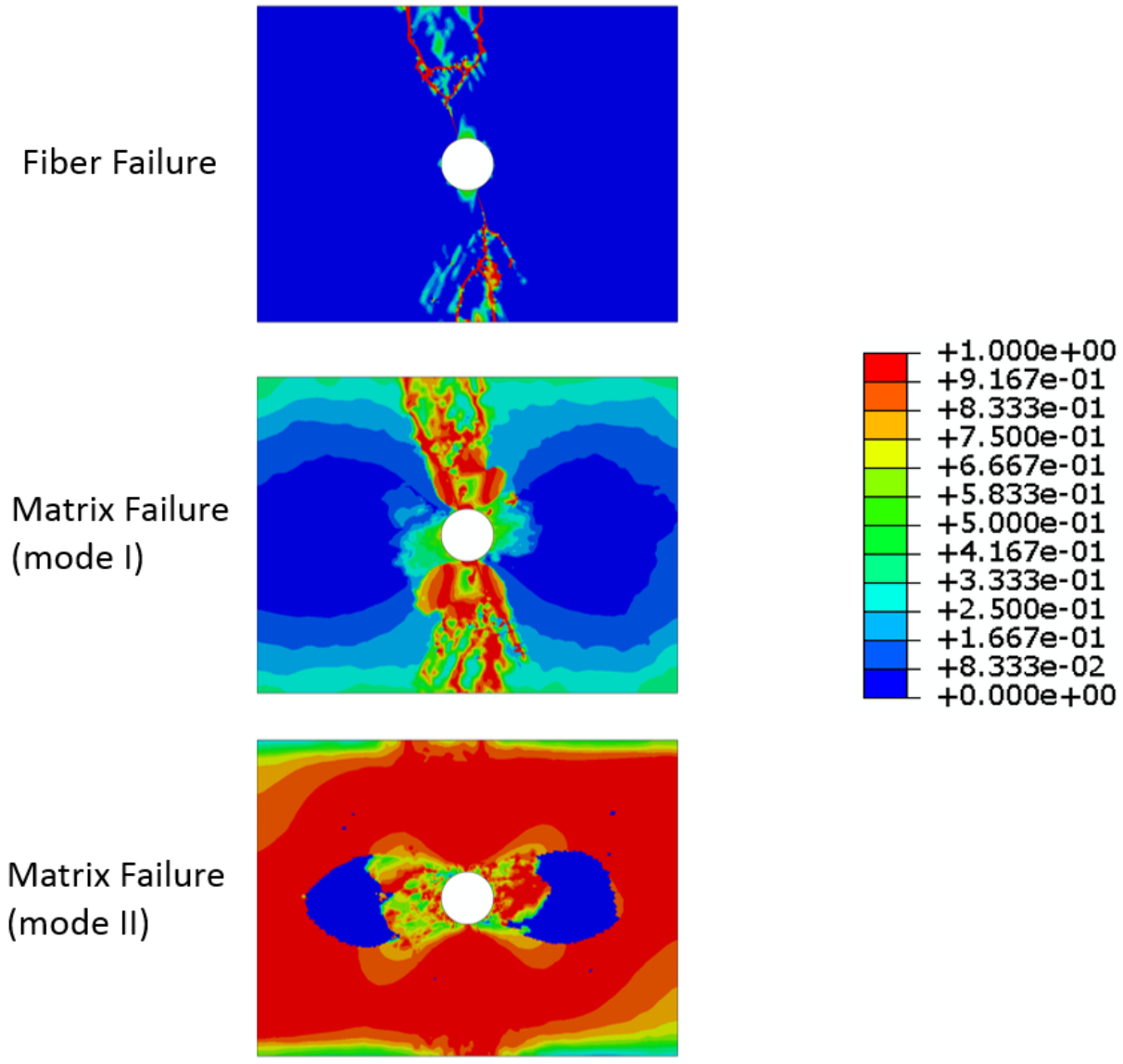

Figure B.7: Failure of 25/50/25 laminate coupon under bending

Experiment-EST agreement is very good for the 10/80/10 laminate as shown in figure B.8. Large number of +45/-45 layers present in this laminate makes matrix failure events to be the main failure mechanism. Laminate fracture toughness of this laminate (table B.3) is much smaller compared to other laminates and hence matrix failure mechanisms has a

big influence on the peak load value. Failure pattern shown in figure B.9 indicate matrix failure patterns aligned along +45 nd -45 angles. Similar failure pattern aligned along the -45 angle was observed in the open hole tension/compression study of this layup [17]. Larger percentage of the +45/-45 layers in this layup makes the single shell model to pick failure paths along the dominant fiber orientations.

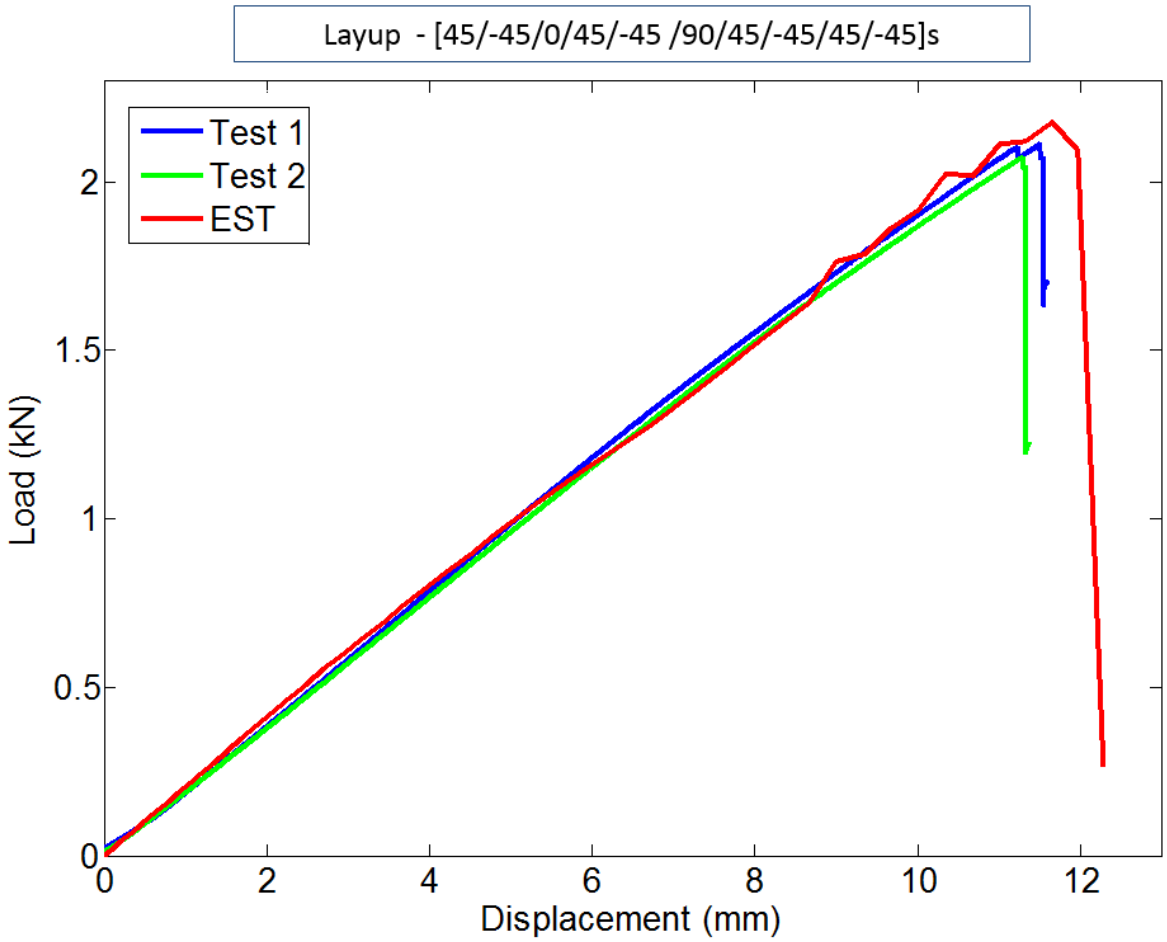

Figure B.8: Load-displacement plot of 10/80/10 laminate coupon

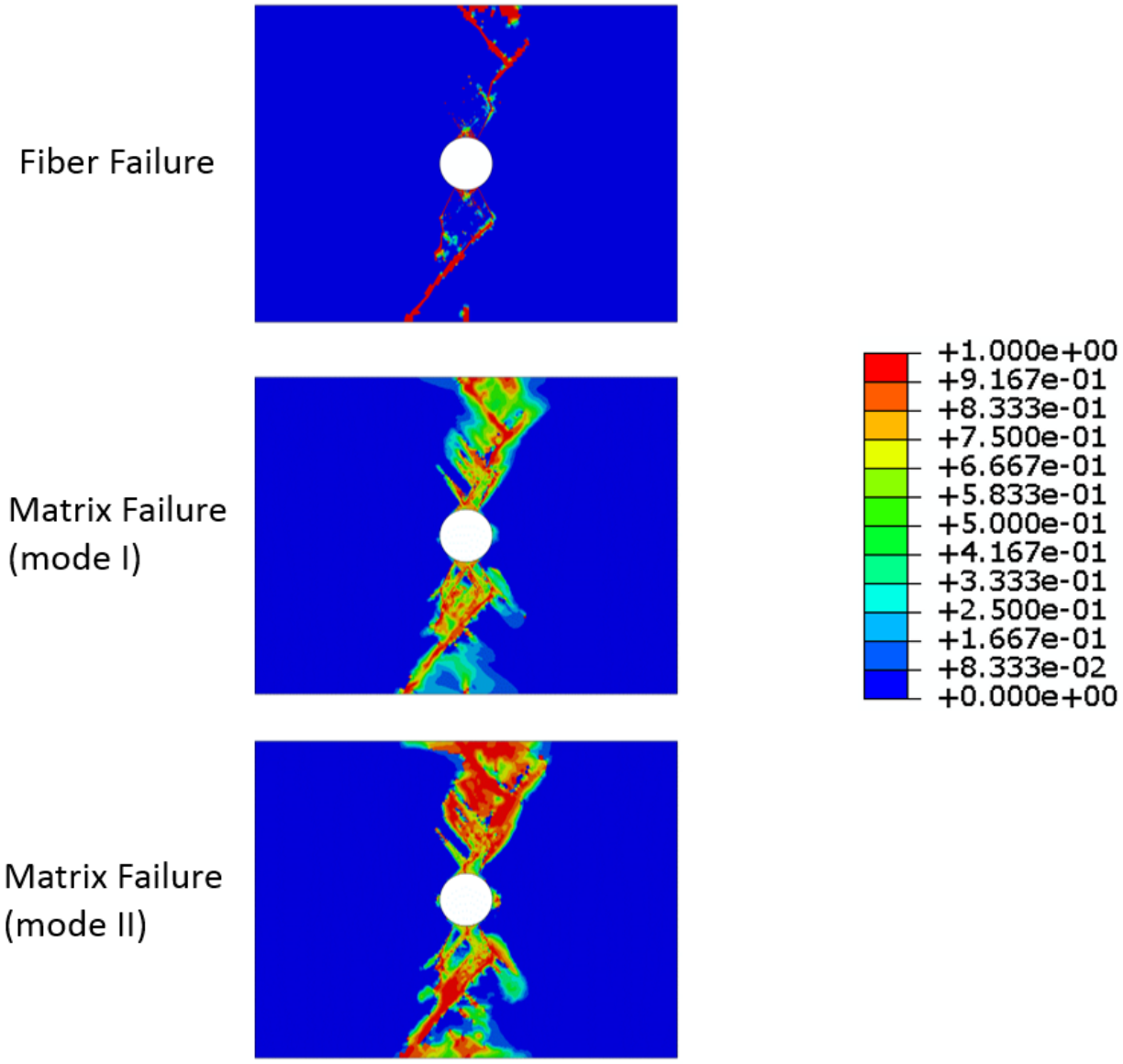

Figure B.9: Failure of 10/80/10 laminate coupon under bending

For all the layups studied, failure events are initiated by the tranvsverse/shear failure initiation in the 90/45 layer on the outer laminae under tension. The final load drop happens when the 0 layers fail in compression. Thus, compressive failure is a strength limiting mechanism. In the 10/80/10 laminate case, fiber failure is more controlled by the matrix

failure in the adjacent layers. Since the failure strain and fracture toughness in the fiber direction are lower in compression than in tension, it is expected that the final failure occurs due to the compressive failure in the top layers. When this happens, instantaneous failure in the other layers due to compression/tension occurs and the specimen loses its load bearing capacity. A remarkable achievement of the present EST model is it's ability to capture the curvature change in the beam through the damage development, peak load attainment and post-peak response. Figure B.10 shows the curvature of the beam just before the peak load and after the two-piece failure.

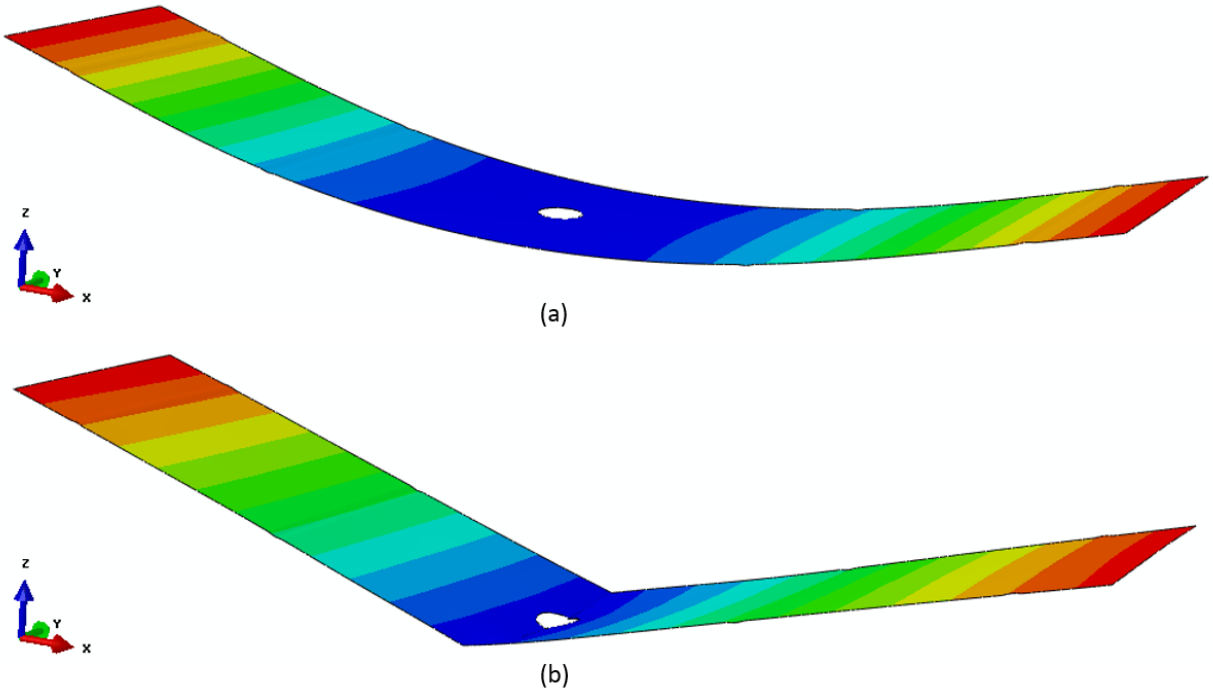

Figure B.10: (a) Curvature of the beam before failure. (b) Curvature of the beam after failure

The laminate fracture toughness scaling used in this study is particularly suited for in-plane problems. More investigation is required to develop a better scaling condition for the bending case. Ideally, this can be achieved through a high-fidelity micromechanics study of

a representative volume element that contains multiple laminae. For simplicity the effect of bending on laminate fracture toughness is ignored here. Even with all the limitations of a single shell model, it is quite remarkable that the EST model agrees very well with experimental data for the laminates studied here.

B.5 Conclusions

The validity of EST as a computationally efficient and accurate model for capturing the in-plane failure in a composite laminate with stress concentrations due to holes/notches has been established in previous studies. More complex loading conditions such as bending is addressed in the present study and the failure events due to that are predicted using EST. Overall, experimental results are found to agree very well with the EST predictions. Comparison shows that the modeling strategy can accurately predict the failure patterns and the change in curvature of the specimen after the catastrophic load drop. The model, as expected, is seen to over-predict the strength for layups and loading conditions when delamination is an important failure mechanism. More study on the laminate fracture toughness scaling is needed to address this issue. Another way of solving this issue is by including delamination interface elements, however this can increase the computational cost. In cases where lay-up rules permit to rule out delamination as an important failure mode (that is, those cases that show compressive peel stresses between layers), EST is a cost-effective predictive tool for virtual testing of composite structures.

B.6 Acknowledgments

The authors are grateful for the sponsorship from the Boeing company. Useful discussions with Salvatore Liguore, Brian Justusson and Joseph Schaefer are gratefully acknowledged.